Eur. Phys. J. Plus (2023) 138:1090
https://doi.org/10.1140/epjp/s13360-023-04737-0

THE EUROPEAN PHYSICAL JOURNAL PLUS

Regular Article

Plasma needle-induced cell cycle arrest of human lung carcinoma cells A549 via p21-dependent pathway

Nenad Selaković[1], Nevenka Gligorijević[2], Milena Čavić[2], Nevena Puač[1], Gordana Malović[1], Siniša Radulović[2], Zoran Lj. Petrović[3,4,a]

[1] Institute of Physics, University of Belgrade, Pregrevica 118, 11080 Belgrade, Serbia
[2] Department of Experimental Oncology, Institute for Oncology and Radiology of Serbia, Pasterova 14, 11000 Belgrade, Serbia
[3] Serbian Academy of Sciences and Arts, Knez Mihailova 35, 11000 Belgrade, Serbia
[4] School of Engineering, Ulster University, Jordanstown, Co., Antrim BT37 0QB, UK

Received: 19 August 2023 / Accepted: 23 November 2023

Abstract Low temperature plasma (LTP) sources, which operate at atmospheric pressure, can produce reactive oxygen and nitrogen species (ROS and RNS) that have a potential to induce cancer cell death. Numerous scientific papers indicate that the cell death mechanisms following LTP treatment vary with both cell type and plasma source used. In this study, we apply plasma needle suitable for direct treatment of biological samples with the power delivered to the plasma precisely controlled. Furthermore, we investigated the effect of our plasma on human cancer cell lines (HeLa and A549) and normal cells (BEAS-2B). The investigation of cytotoxic activity confirmed the cytotoxic potential of our plasma needle, with lower sensitivity toward normal cells, and a higher sensitivity toward cancer cell lines. Further investigation of the effect on cell cycle in resistant A549 cell line showed a decrease in the number of cells in the G0/G1 phase and arrest of cell cycle in the G2/M phase. A significant overexpression of the cyclin-dependent kinase inhibitor 1 (p21) was also observed at the genetic level in a power dependent manner. However, there was no reduction in growth of A549 cells in a 3D cell culture of multicellular tumor spheroids (MCTS) after plasma treatment under investigated experimental conditions. Our results show that the redesigned plasma source has a potential to inhibit proliferation of A549 lung adenocarcinoma cells in vitro, induce their apoptosis and also a combined treatment with PARP (poly(ADP-ribose) polymerase), inhibitor enhanced the effect of LTP.

1 Introduction

Low temperature plasmas have been for decades a useful tool in material processing [1, 2], but in the past 25 years, with the development of the LTPs that operate at the atmospheric pressure, they have become important assets in the now well-established fields of plasma medicine [3–6] and plasma agriculture [7–9]. The main obstacle for the LTPs operating at atmospheric pressure was to achieve non-equilibrium conditions and create gas phase chemical environment that contains ions, metastable, reactive (especially reactive oxygen species ROS and reactive nitrogen species RNS) and exited species, neutrals, weak UV radiation, electromagnetic fields and more. This is achieved by using different electrode configurations and geometries of the device, types of the power supply (pulsed/sine wave) operating at different frequencies, different noble gasses or their mixtures as feeding gases, added molecular species, especially the humidity [10–14] and all other parameters that may affect the plasma.

The most important feature of atmospheric pressure LTPs is that they are rich in reactive oxygen and nitrogen species (RONS) responsible for their biological/therapeutic effects. So far LTPs have been investigated in wound healing [15, 16], dentistry [17–19], stem-cell differentiation [20, 21], blood coagulation [22, 23], as a bactericidal agent [24, 25] and also in induction of cancer cell death [26–30]. In this paper, we shall study the non-equilibrium low-temperature plasma for which we shall also use equivalent briefer terms: low temperature plasma (or LTP), cold plasma, non-thermal plasma. The different terms should be avoided if possible, but those terms will be used here to stress the relevant property of the plasma that is relevant or to add variety and relax the writing style.

Numerous research laboratories reported promising in vitro and in vivo results on anticancer potential of different LTP systems [31, 32]. A major milestone in the development of the LTP-based cancer therapies was the US Food and Drug Administration (FDA)

Nenad Selaković and Nevenka Gligorijević have contributed equally to this work.

[a] e-mails: z.petrovic@ulster.ac.uk; zoran@ipb.ac.rs (corresponding author)

Published online: 07 December 2023

approval of the first clinical trials in the USA in 2019 [33]. These trials have led to positive results that have been published recently [34].

In cancer cell treatment, RONS produced in a gas phase atmospheric pressure LTP can induce cell death due to their sensitivity on overproduction of RONS, while the healthy cells stay less affected [31–34]. Different types of non-thermal plasma systems show a range of cellular responses including DNA damage, decreased cell viability and clonogenicity, reduced proliferation and cell cycle arrest [26, 31, 35–38]. The vast majority of studies indicate that the cell death mechanisms following LTP treatment vary with both cell type and plasma source used reporting apoptosis; however, senescence and non-apoptotic cell death have also been presented [31]. The multitude of RONS generated by LTPs could provide significant advantage over other cancer therapies, e.g. radiotherapy and photodynamic therapy which generally produce only ROS [31].

To determine the potential of our plasma system to interfere with various cellular processes in tumor cells, we investigated its antiproliferative potential in 2D and 3D cell culture models, apoptotic potential, potential of modulating cell cycle and level of ROS in A549 cells. Adequate time and exposure dose of LTP for our plasma system are determined since both are of great importance.

As a combination therapy, a treatment modality that combines two or more therapeutic agents, is considered a cornerstone of cancer therapy [39]. Combined effect of our LTP system on cell survival of cancer cells after pre-treatment with poly(ADP-ribose) polymerase (PARP inhibitor) was investigated. Poly(ADP-ribose) polymerase 1 (PARP-1) is a nuclear enzyme that is activated by DNA damage by binding to DNA breaks [40]. PARP-1 activation among other functions facilitates the repair of single-strand breaks by the base-excision repair pathway (BER) [41, 42]. Tumor cells often have defects in DNA damage repair mechanisms which make them sensitive to combined treatment of DNA damaging agent and inhibitor of repair [43]. It may be inhibited to increase chemosensitivity to a wide spectrum of DNA-damaging agents including alkylating agents (cisplatin and other metal complexes), topoisomerase I inhibitors (etoposide), ionizing radiation, etc. [44].

2 Methods

2.1 Experimental setup for LTP treatments

In this work, we used a plasma needle that operates at atmospheric pressure and is well suited for applications in biology and medicine [45–48].

The schematics of experimental setup is shown in Fig. 1. We have used Kurt J. Lesker R301 RF source, Jefferson Hills, USA, that includes a power supply, matching box and controller unit to powered the plasma needle at 13.56 MHz. The plasma needle comprises a Teflon body that houses a centrally positioned glass tube with an outer diameter of 6 mm and an inner diameter of 4 mm. Inside the glass tube is a ceramic insulator tube (2 mm in diameter) that surrounds a tungsten wire (0.5 mm) that protrudes outside the ceramic tube for few millimeters and acts as the central powered electrode. The discharge occurred solely at the tip of the tungsten wire. The observed emission profile is stationary, centered around the tip of the wire and it has been presented in [49, 50]. The adopted configuration allowed us to achieve precise and localized plasma production and consequently treatment in the experiment.

We have used derivative probes [45] designed and built in our laboratory. Inductive probe is applied to measure current, while capacitive probe is used to record the voltage. Probes, as seen in Fig. 1, were designed and calibrated for precise electrical measurements that allow us to calculate, from the recorded waveforms (using an oscilloscope Agilent DSO 6052a, Santa Clara, California,

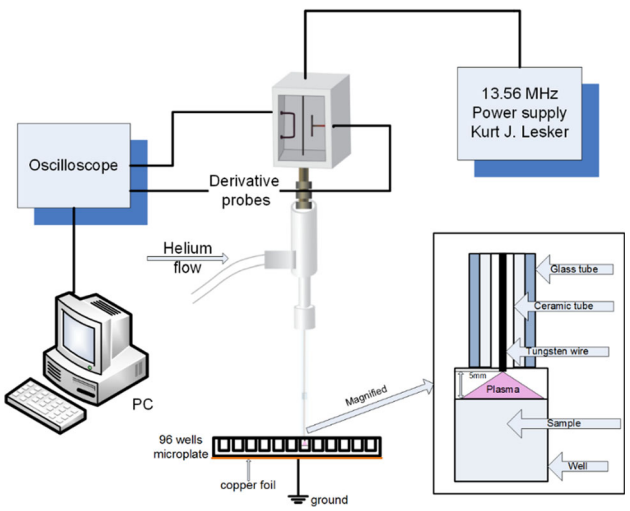

Fig. 1 Schematics of the plasma needle setup

USA), the power delivered to the LTP. Frequency dependent calibration of the system was applied to the signals converted to the frequency domain. The signals were then converted back to the time domain where power was calculated by multiplying voltages and current values as a function of the phase within one period.

High accuracy, reproducibility and sensitivity of better than plus/minus 0.1 W have all been achieved. Accurate and highly sensitive recording and control of the power deposited to the plasma is necessary to ascertain reproducibility and to maintain non-thermal conditions. Under non-equilibrium (low temperature) plasma conditions, background gas is not heated to temperatures that could induce thermal necrosis of the living cells (40 °C and more).

Establishing plasma in rare gases at the edge of the tube is the basis of the technique to avoid excessive ionization and optimize initialization of the plasma chemical reactions. Helium proved to be the best choice in our experiments as it gave us very effective production of radicals and stable operation of the system without formation of the streamers. The flow of the chosen feeding gas He was 1 slm (*standard liters per minute*) controlled by the Bronkhorst flow meter/controller. During the entire experiment, plasma needle was placed in a laminar chamber in order to avoid possible contamination of the cells. The samples were prepared in 96-well microplates and placed on a stand below the LTP. Beneath the microplate, we glued a thin layer of grounded copper foil. Its role was to provide a stable discharge. The plasma needle was positioned perpendicular to the bottom of each well that was being treated. The distance from the tip of the central electrode to the surface of the liquid was maintained at 5 mm. We have filled 100 μl of the prepared nutrient medium liquid on top of the cell cultures placed inside the wells. The 5 mm gap refers to the distance from the surface of the liquid to the tip of the needle.

The following parameters were varied: exposure time (10 s, 30 s and 60 s) and power delivered to the discharge (1.3 W and 2.2 W). Having experimental device placed inside the Laminar Chamber, that has a strictly controlled flow of the gas, we made sure that the possible impurities were kept at a low, constant and reproducible level. Yet the fact that plasma is mixed with the air the level of molecular gases is defined by the act of mixing and not by the impurities in the rare gas. We have used He gas with 5.0 purity.

In addition to the electrical measurements that were constantly made, we have used mass spectrometry, optical emission spectroscopy, ICCD recordings of the plasma profile and other techniques to monitor plasma, assure its reproducibility and operation in the desired conditions [50, 51]. Even after our search for the optimal conditions a more thorough and expansive variations of different operating parameters could perhaps provide even better operating conditions. Nevertheless, what we adopted as a protocol provided solid desired effects (without claiming that some further improvements cannot be achieved) and of the reproducibility of the LTP that was being used.

Measurements of heating of the standard targets proved that no object in the region of interaction with plasma has ever been heated to temperatures more than a couple of degrees higher than the room temperature [46]. In all measurements, the design of the plasma source, the parameters such as power and buffer gas flow and the geometry have been selected to allow only operation when no heating of the treated target may be observed.

2.2 Cell lines and culture conditions

Human lung adenocarcinoma cells (A549), human cervix carcinoma cells (HeLa) and non-cancer human bronchial epithelial cells (BEAS-2B) were maintained as monolayer cultures in the Roswell Park Memorial Institute (RPMI) 1640 nutrient medium (Sigma Chemicals Co, USA). RPMI 1640 nutrient medium was prepared in sterile ionized water, supplemented with penicillin (100 U/mL), gentamicin (50 μg/mL), 4-(2-hydroxyethyl) piperazine-1-ethanesulfonic acid (HEPES) (25 mM), L-glutamine (3 mM) and 10% of heat-inactivated fetal calf serum (FCS) (pH 7.2). The cells were grown at 37 °C in a humidified atmosphere of 95% air and 5% CO_2.

2.2.1 Cytotoxicity assay

Cytotoxic effect of the low temperature plasma treatment was determined by a 3-(4, 5-dimethyl-2-thiazolyl)-2,5-diphenyl-2H-tetrazo-lium bromide (MTT, Sigma) assay as described previously [52]. The cells were seeded into 96-well cell culture plates (Thermo Scientific Nunc™), at an appropriate cell density for each cell line. After 24 h of growth, cells were exposed to the low temperature plasma. Two experimental parameters were varied: exposure time (10 s, 30 s and 60 s) and power delivered to the plasma (1.3 W and 2.2 W), all treatments were done in triplicates. The distance between the plasma needle tip and the sample surface was 5 mm and was kept constant during all experiments. After 24 h, 20 μL of MTT solution (5 mg/mL in phosphate buffer, pH 7.2) was added to each well. Samples were incubated for 4 h at 37 °C in a humidified atmosphere of 5% CO_2, and then 100 μL of 10% sodium dodecyl sulfate (SDS) was added. Absorbance was recorded after 24 h, on an enzyme-linked immunosorbent assay (ELISA) reader (Thermo Labsystems Multiskan EX 200–240 V), at the wavelength of 570 nm.

2.2.2 Morphological analysis

The A549 cells (5.0×10^3 cells/well) were seeded into 96-well plates (ThermoScientific Nunc™) in nutrient medium. After 24 h of growth, the cells were exposed to the low temperature plasma. Following 72 h of treatment, the cells were observed under the inverted microscope for cell culture Olympus CKX53, Tokyo, Japan, equipped with Olympus EP50 camera using 10x/0.5 objective.

2.2.3 Cell cycle analysis

The analysis of cell cycle phase distribution of A549 cells after treatment with low temperature plasma needle in a time and power dependent manner was performed by propidium iodide (PI) staining and flow cytometric analysis [53]. Cells were seeded at a density of 1.5×10^4 cells per well, into 48-well plates (Thermo Fisher Scientific), in the nutrition medium. After treatment, the cells were incubated for 24 h and then harvested by trypsinization and fixed in ice-cold 70% ethanol. Cells were kept at − 20 °C until further analysis. For analysis, the cells were harvested by centrifugation and resuspended in 800 μL PBS. They were then treated with 100 μL of RNase (1 mg/mL) and 100 μL of propidium iodide (400 μg/ml) and incubated at 37 °C for 30 min. The stained cells were analyzed using fluorescence activated cell sorter (FACS) on a Calibur Becton Dickinson flow cytometer, at 488 nm excitation line (Argon-ion laser). The data were analyzed by CellQuest computer software.

2.2.4 Flow cytometric analysis of apoptosis (Annexin-FITC and PI staining)

Flow cytometric analysis of the cell death induced by low temperature plasma treatment was performed using Annexin-V-FITC apoptosis detection kit, according to the manufacturer's instructions (BD Biosciences Cat. No. 65874x, Pharmingen San Diego, CA, USA). The A549 cells (1.5×10^4) were seeded into 48-well plates (Thermo Scientific Nunc™), in 200 μL of RPMI medium. After 24 h of growth, the cells were treated with low temperature plasma, 1 W and 1.5 W for 20 s. After 24 h treatment, cells were washed with ice-cold PBS and then resuspended in 200 μL of binding buffer (10 mM HEPES/NaOH pH 7.4, 140 mM NaCl, 2.5 mM $CaCl_2$). 100 μL of the cell suspension (10^5 cells) was transferred to a 5-mL culture tube and mixed with 5 μL of Annexin-V-FITC and 5 μL of propidium iodide (PI). After incubation for 15 min, at 25 °C in the dark, 400 μL of binding buffer was added to each tube and analyzed using a FACS Calibur Becton–Dickinson flow cytometer and CellQuest computer software. A minimum of 10.000 cells were analyzed per sample.

RNA extraction and cDNA synthesis The A549 cells were seeded into 48-well plates at a density of 1.5×10^4 cells per well. After incubation for 24 h, the cells were treated with low temperature plasma 1 W and 1.5 W for 20 s and analyzed 24 h after treatment. The cells were harvested, washed twice with ice-cold PBS and centrifuged (10 min at 2000 rpm). Total RNA was extracted from pelleted cells by cell lysis using the TRI REAGENT® BD kit (Sigma-Aldrich, St. Louis, USA). The quality and quantity of the obtained RNA were assessed spectrophotometrically using BioSpec-nano (Shimadzu Scientific Instruments). Complementary DNA (cDNA) was prepared using random primers by RT-PCR. 2 μg total RNA was used as a template for MultiScribeTM Reverse Transcriptase (50 U/μL) using a high-capacity cDNA reverse transcription kit (Applied Biosystems). The reaction was conducted in a final volume of 20 μL, using the following program: 25 °C for 10 min, 37 °C for 120 min, and inactivation at 85 °C for 5 min. cDNA was used as a template for quantitative RT-PCR.

Quantitative Real-Time PCR (qRT-PCR) The mRNA levels of Bax (RefSeq. NM_001291428.1), Bcl2 (RefSeq. NM_000633.2), SKP2 (RefSeq. NM_005983.3) and CDKN1A (p21) (RefSeq. NM_000389.4) were detected by quantitative real-time PCR (qRT-PCR) using TaqMan® Gene Expression Assays and TaqMan® Gene Expression Master Mix, (Applied Biosystems). PCR reactions were performed on ABI Prism 7500 Sequence Detection System (Applied Biosystems). Non-template controls were included in each amplification. The thermal cycling conditions comprised an initial denaturation step at 95 °C for 10 min followed by 40 cycles of denaturation (15 s at 95 °C) and annealing/extension (1 min at 60 °C) in a final volume of 20 μL. Three independent experiments were performed, and the fluorescence of the double-stranded products was monitored in real time. To exclude variations arising from different inputs of total mRNA to the reaction, gene expression data were normalized to an internal housekeeping gene, glyceraldehyde-3-phosphate dehydrogenase (GAPDH, RefSeq. NM_002046.5). Data were analyzed using the classical delta-delta-Ct method and results presented as mean fluorescence expressed in relative units, with non-treated cells as a control sample (mean fluorescence 1). GraphPad Prism 9.00 (GraphPad Software, CA, USA) was used to compare means by two-way analysis of variance (ANOVA) and Dunnett's method to adjust the p-value for multiple comparisons. Differences were considered significant if $p < 0.05$.

2.2.5 Measurement of intracellular reactive oxygen species (ROS)

The intracellular ROS levels were measured with a fluorescent dye 2′,7′-dichlorodihydrofluorescein diacetate (DCFH-DA, Sigma-Aldrich Co) [54]. The A549 cells were seeded into 48-well plates at a density of 1.5×10^4 cells per well. After incubation for 24 h, the cells were treated with low temperature plasma 1 W and 1.5 W for 20 s in order to focus on the effects like DNA damage or markers of the early apoptosis time window. We analyzed results 24 h after the treatment. For analysis, cells were harvested, washed twice with ice-cold PBS, re-suspended in 1 mL of 25 μM DCFH-DA and incubated for 30 min at 37 °C in the dark. After incubation, cells were washed with PBS, re-suspended in 500 μL of PBS and immediately analyzed at FL1 channel of FACS Calibur Becton Dickinson flow cytometer using CellQuest computer software (Becton Dickinson, Heidelberg, Germany). Excitation wavelength used in measurements was 485 nm with peak emission measured at 530 nm.

2.2.6 Combined treatment

The sensitivity of A549 tumor cells to a combined treatment of the PARP inhibitor olaparib and low temperature plasma induced by our plasma needle system was determined by MTT assay (according to the procedure already described). The combined treatment was performed by pre-treatment with 10 μM olaparib for 90 min and then treatment with plasma (2 W) for 10, 30 and 60 s. All treatments were carried out in triplicates and results presented as mean ± SD. The absorbances were recorded 24 h after plasma treatment on an enzyme-linked immunosorbent assay (ELISA) reader (ThermoLabsystems Multiskan EX 200–240 V) at the wavelength of 570 nm. Inhibitor olaparib (AZD2281Astra Zeneca) was used.

2.2.7 Growth inhibition investigation in 3D cell culture model

The 3D cell culture model of multicellular tumor spheroids (MCTS) of A549 cells were prepared using the low attachment U96-well plate Thermo Scientific Nunclon Sphera (Nunclon Sphera 96 well U bottom plates). The A549 cells in the exponential growth phase were dissociated by a trypsin/EDTA solution to gain single-cell suspensions. A number of 5000 cells/well were transferred to 96-well plates with 200 μL of RPMI containing 10% serum. The single cells formed MCTS aggregates approximately 400 μm in diameter after three days. The formation and growth of spheroids were examined using the fluorescent microscope Axio Observer Z1, using AxioVision imaging software (Carl Zeiss MicroImaging GmbH). The A549 spheroids pre-selected for homogeneous volume and shape were treated by plasma needle with 1 W for 60 s and 120 s in triplicates. Growth inhibition was monitored by measuring spheroids' diameter after 1 day and 7 days of treatment. Brightfield images obtained using a fluorescent microscope Axio Observer Z1, (10x/0.5 objective) were analysed by AxioVision Rel 4.7 Imaging System by interactive measurement of diameter of MCTSs.

3 Results and discussion

3.1 Results of cytotoxicity assay

Many different low temperature plasma systems have been designed and applied to a range of different cancer cell lines in culture with numerous promising results [31, 55]. Also, some studies indicated that the cell death mechanisms following LTP treatment vary with both cell type and plasma design used [31]. Due to a broad versatility in plasma system designs and problematic direct data comparison [31], every plasma system must be thoroughly examined individually. The effect of our plasma needle system for non-thermal plasma treatment on the viability of cells of different origin was determined and presented in Fig. 2, as cell survival curves determined by MTT assay. Photomicrographs are shown in Fig. 3. Two cancer cell lines A549 (human lung carcinoma cells) and HeLa (human cervix carcinoma cells) and one normal cell line BEAS-2B (human bronchial epithelial cells) were exposed to the low temperature plasma with two different powers 1.3 and 2.2 W and three different exposure times (10, 30, 60 s). Figure 2 shows representative experiment out of at least three independent experiments (for different cell line samples) with each experiment performed in triplicates that were used to obtain the standard deviation.

Results presented in Fig. 2 show that HeLa cells displayed greatest vulnerability to the plasma treatment among the investigated cell lines. The difference between two applied powers was the highest on HeLa cells. The A549 cells as an example of a more resilient cell line of human non-small cell lung cancer (NSCLC) type show less sensitivity to the treatment. Some decrease in cell viability was detected for the normal cell line, BEAS-2B but it did not reach 50% of reduction of cell survival upon treatment. The antiproliferative and cytotoxic potential of many different non-thermal plasma systems were observed and confirmed in many tumor types including cell lines used in our experiments [55]. Our experiments confirmed the potential of our plasma needle system for non-thermal plasma treatment to decrease the viability of cancer cells.

The cause of the decrease in the viability of treated cells with plasma is not determined by this test. We can see only that the number of cells is decreasing and that cells changed their morphology (morphological analysis) and metabolic activity (MTT test). We cannot observe directly what induced those effects, the temperature or other resulting plasma effects like production of ROS. We assumed according to the literature and our experiment measuring the intracellular ROS level that the production of ROS is the cause of the observed effect.

3.2 Morphological analysis of cell death

The morphological characteristics of A549 cells following plasma needle treatment were analyzed by using inverted microscopy (photomicrographs presented in Fig. 3). After 72 h, the number of cells was reduced in time-dependent manner. Cells lost their elongated morphology, become rounded and detached. Power-dependent cytotoxicity was observed with higher power treatment of 2 W being more aggressive than the 1 W treatment.

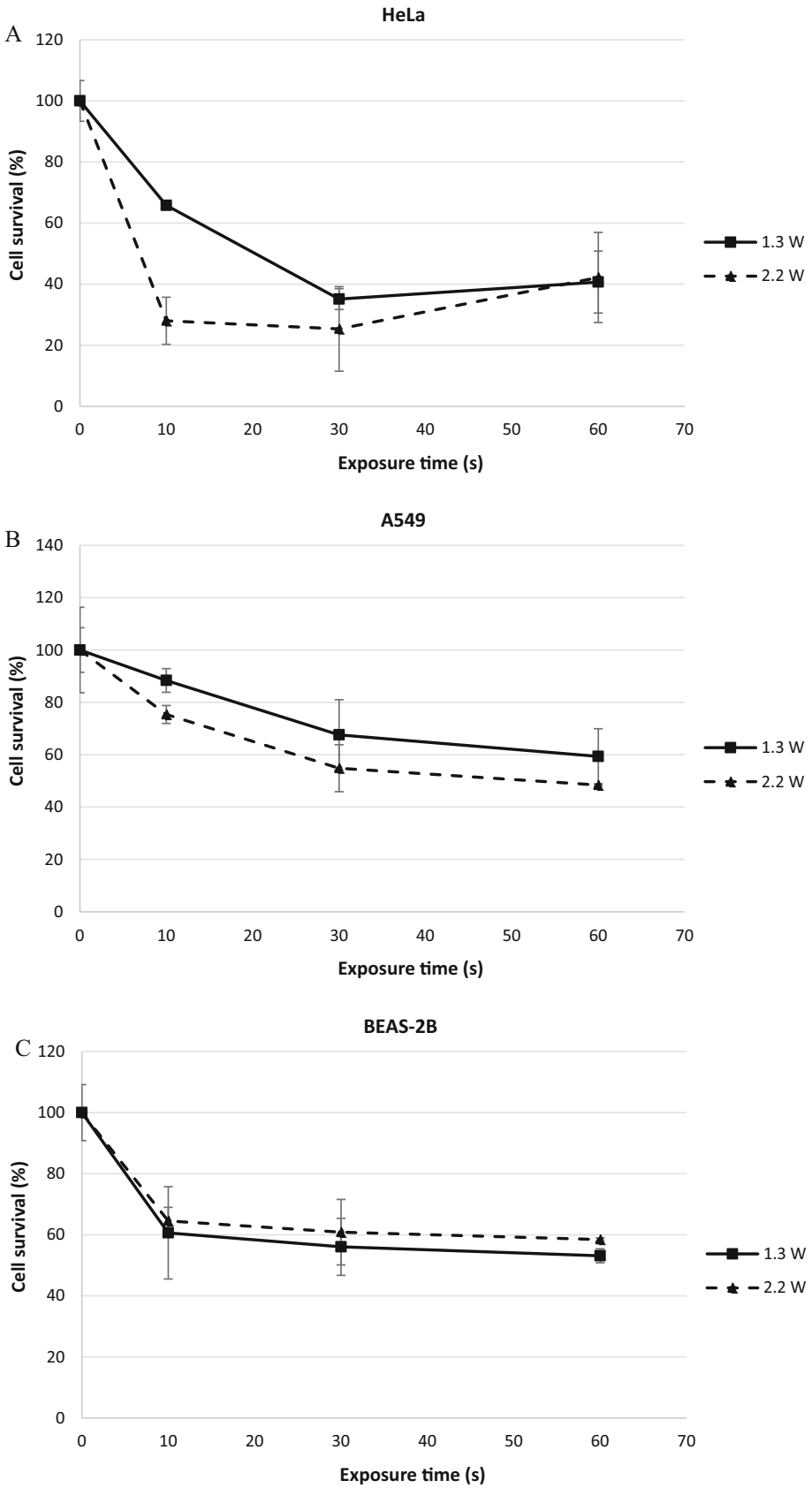

Fig. 2 Representative cell survival curves determined by MTT assay 24 h after treatment of **A** HeLa, **B** A549 and **C** BEAS-2B cell lines with plasma needle treatment. Two different powers were applied, 1.3 and 2.2 W, for three different exposure times (10, 30, 60 s). The distance from the tip of the needle to the surface of the liquid sample was 5 mm

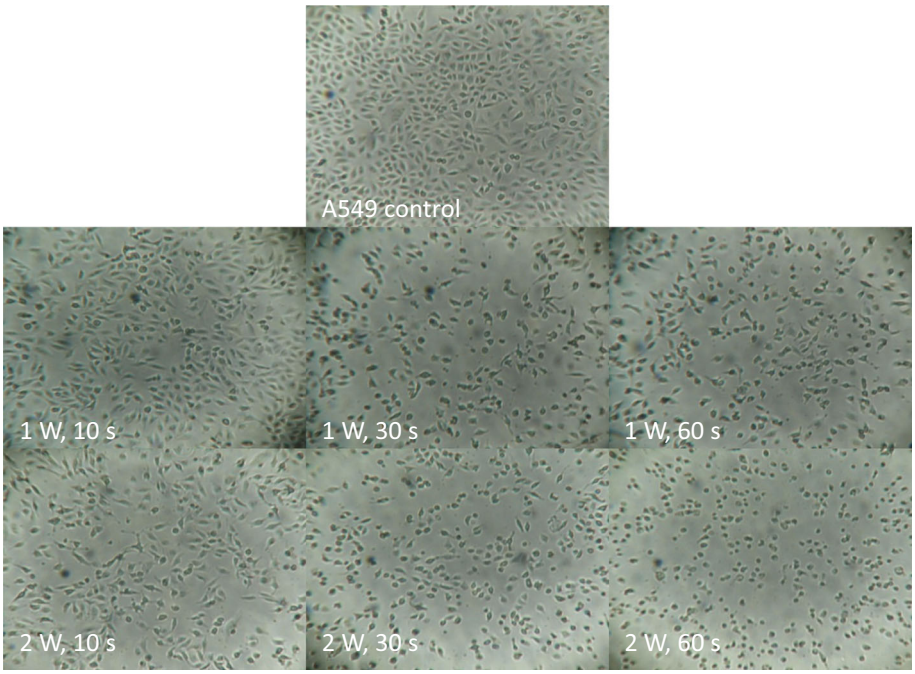

Fig. 3 The photomicrographs of untreated A549 cells (control) and treated A549 cells with LTP for different powers of plasma and exposure times

3.3 Results of cell cycle analysis

Results of the cell cycle analysis presented in Fig. 4 show that treatment with our low temperature plasma needle system has a potential to induce cell cycle perturbations of A549 cells. After the treatment with 1W of power as short as 10 s, the percentage of cells in G0/G1 phase decreases. Prolongation of treatment to 20 s and 30 s induced a more pronounced decrease in cell percentage in G0/G1 phase up to 45% (for 30 s treatment) compared to the control which had 60% of cells in G0/G1 phase. LTP treatment also induced an increase in the percentage of cells in the G2/M phase, while the percentage of Sub-G1 cells (which represents fragmented DNA) increased up to 12%, compared to 2% in the control. However, changes in the cell cycle, that were insignificant, showed the same trend, as the decrease of percentage of cells in G0/G1 phase and the increase in the percentage of cells in G2/M phase dependent on the power used. The occurrence of cell cycle arrest has been confirmed in numerous other cold plasma treated cancer cells [56].

3.4 Results of flow cytometric analysis of apoptosis (Annexin-FITC and PI staining)

The potential of our low temperature plasma needle system to induce apoptosis in A549 cells was investigated by flow cytometric analysis after Annexin-V-FITC and propidium iodide (PI) staining [56–59]. Treatment of A549 cells with plasma did not induce apoptosis after 4 h after treatment (results not shown), while in the samples 24 h after treatment early apoptosis was detected (Figs. 5 and 6). This is in accordance with literature data that indicate that induction of apoptosis by plasma treatment is slow and effects may be expected after 24 h. Also, the time window of detecting apoptosis depends on the cell type and inducer [60]. Results presented in Fig. 5, show that after treatment of A549 cells with low temperature plasma for 20 s with 1 W and 1.5 W and subsequent analysis after 24 h majority of cells are still alive (81%). Only 12% of cells after 1W treatment and 10% cells after 1.5 W treatment were introduced in early apoptosis (detected by staining only with Annexin-V-FITC) compared to 2% cells in control sample. On the basis of dot plot graphs (Fig. 6) we can see that the cells in the treatment with 1 W and 1.5 W of low temperature plasma for 20 s are slightly moving toward lower right (early apoptotic cells) and upper right (late apoptotic cells) quadrants. Having in mind that numerous different plasma designs are being investigated direct data comparison is not easy. In discussion, we assumed that the mechanism leading to the apoptosis is the effect of produced ROS in the medium according to the literature data and our experiment measurement of the intracellular ROS level. The main aim of this research was to determine whether our plasma system has a potential to induce cell deaths and the type of cell deaths. We can only give the conclusion in the based on our experiments with additional input from the literature.

However, by investigating the performances of our in house-made plasma needle system, it was confirmed that it is able to induce apoptosis in A549 cells.

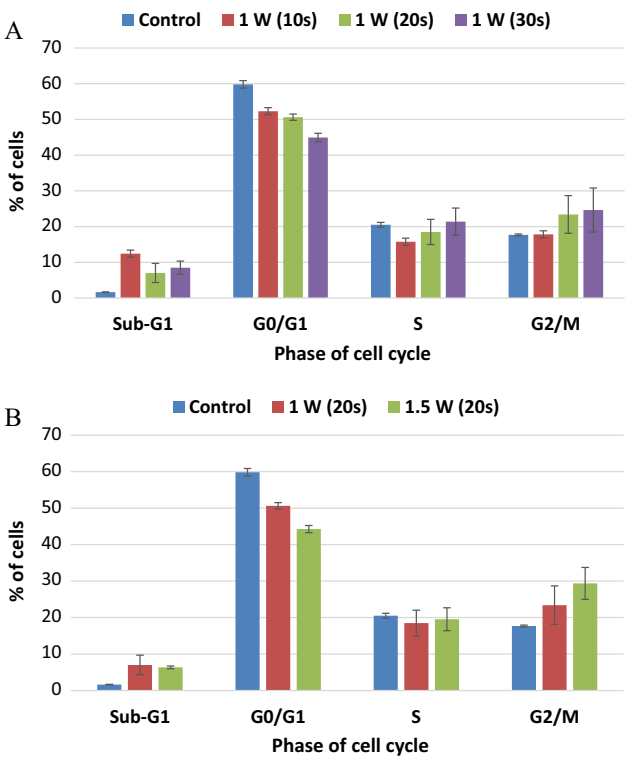

Fig. 4 **A** Time (10, 20, 30 s) and **B** Power (1 and 1.5 W) dependent cell cycle perturbations of cell cycle of A549 cells 24 h after treatment. A representative experiment is shown, each sample analyzed in duplicate

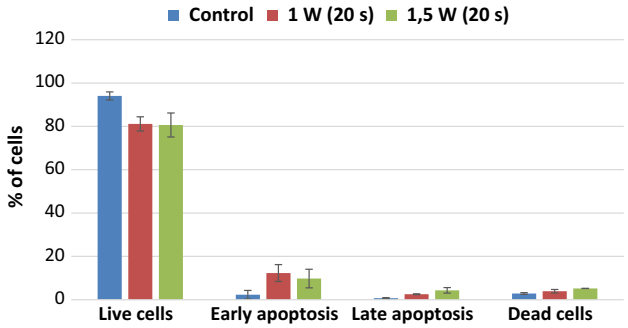

Fig. 5 The detection of externalization of phosphatidylserine (as an early apoptotic change in the plasma membrane) in A549 cells after low temperature plasma treatment and dual staining with Annexin-V-FITC and PI and flow cytometric analysis. Bar graphs represent the percentage of cells in: early apoptosis (Annexin-V-FITC + and PI – cells), late apoptosis (Annexin-V-FITC + and PI + cells), live cells (Annexin-V-FITC—and PI – cells) and already dead cells (Annexin-V-FITC + and PI + cells). Results present a representative experiment out of 3 independent experiments, whereby each experiment was performed in duplicates

3.5 Results of qRT-PCR

In order to elucidate the mechanisms underlying the effect of low temperature plasma treatment, the changes in *Bax*, *Bcl-2*, *TP53*, *SKP2* and *CDKN1A* gene expressions in A549 cells were analyzed by quantitative real-time PCR 24 h after treatment (1W and 1.5W) (Fig. 7). *P* values are indicated in Fig. 7 Legend.

Compared to non-treated cells, the quantitative analysis showed an insignificant upregulation of pro-apoptotic *Bax*, downregulation of anti-apoptotic *Bcl-2* and downregulation of the oncogenic cell cycle regulator *SKP2* mRNA expression. This suggests a cell cycle arrest potential of our low temperature plasma on A549 cells leading to mild apoptosis-inducing effect.

A significant overexpression of the cyclin-dependent kinase inhibitor 1 (CDKN1A) was also observed at the genetic level in a power-dependent manner. Treatment with 1 W induced a 6.1-fold increase, while the 1.5 W treatment induced a 9.3-fold increase in mRNA expression of *CDKN1A*, which encodes for the p21 protein, a known cell cycle arrest promoter [61].

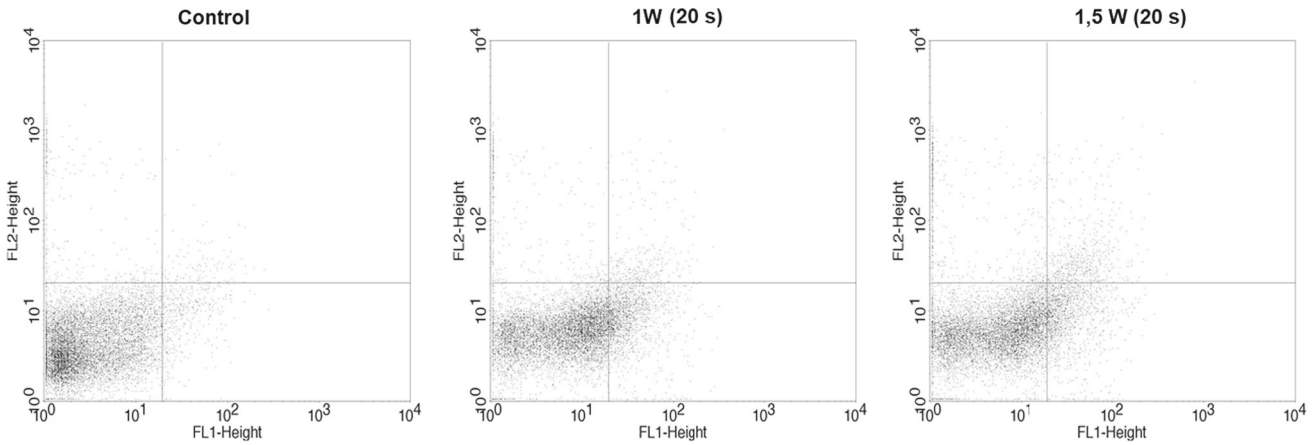

Fig. 6 Detection of apoptotic changes in plasma membrane in A549 cells after treatment with low temperature plasma and dual staining with Annexin-V-FITC and PI and flow cytometric analysis. Bar graphs represent the percentage of cells in early apoptosis (Annexin-V-FITC + and PI – cells) and percent of cells in late apoptosis (Annexin-V-FITC + and PI + cells) and dual parameter dot plot of FL1-Height for Annexin-V-FITC (x axis) and FL2-Height for PI (y axis) are shown. Quadrants: lower left (LL)-live cells, lower right (LR)-early apoptotic cells, upper right (UR)-late apoptotic cells, upper left (UL)-dead cells

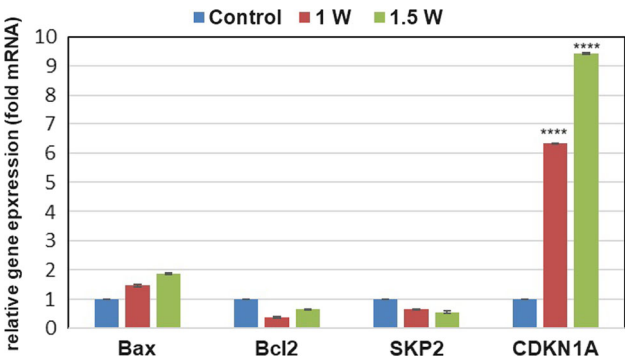

Fig. 7 Analysis of *Bax*, *Bcl-2*, *SKP2 and CDKN1A* mRNA expression 24 h after 20 s plasma treatment. Gene expression levels were determined by qPCR and normalized to *GAPDH*. Data represent mean ± SD of three independent experiments. Asterisks denotes statistical significance compared to control (****$p < 0.0001$)

3.6 Results of measurement of intracellular reactive oxygen species (ROS)

Numerous studies have shown that anticancer therapies that manipulate ROS levels, including immunotherapies, produce promising in vitro as well as in vivo results [62].

A significant rise of intracellular ROS is the well-known response of LTP treated cells [56], also the measured ROS levels in cancer cells is higher than that determined in normal cells after the NTP treatment [56, 63]. One of the models that explain the observed trend proposed that such a different rise of ROS in the normal and cancerous tissue is due to different basal intracellular levels between cancer and normal cells [56]. As a result, selective anti-cancer effect is determined, as cancer cells experience more apoptosis than normal cells upon LTP treatment [56].

The effect of our plasma needle treatment on ROS level in A549 cells was investigated with a fluorescent dye DCFH-DA and subsequent flow cytometric analysis. Results presented in Fig. 8. show a change in ROS level 24 h after 20 s treatment compared with the amount in the untreated cells. The fluorescent signal curves are shifted to the right indicating a fluorescence intensity increase in a power dependent manner (Fig. 8). Results of DCFH-DA fluorescence intensity shown in Fig. 9 confirmed the potential of our plasma needle to induce an increase in intracellular ROS [9].

3.7 Results of combination study

The potential effect of the low temperature plasma treatment induced by our plasma needle system on the level of ROS in A549 cells was determined by a fluorescent dye DCFH-DA and subsequent flow cytometric analysis confirmed an increase in intracellular ROS as one of the most common responses of cells treated with low temperature plasma [45]. Results of combined treatment (Fig. 10) with PARP-1 inhibitor olaparib and low temperature plasma treatment with our plasma needle system showed that olaparib at concentration of 10 μM, potentiated the cytotoxicity of LTP only after applying the treatment for 30 s, while with longer LTP treatment (60 s) the influence of olaparib pre-treatment on cytotoxicity is lost. This may indicate that 30 s LTP-induced single-strand breaks exert an influence on cytotoxicity to a greater extent, while 60 s treatment probably managed to induce a variety of different DNA damages leading to a loss of olaparib's major pre-treatment effect on LTP cytotoxicity. As previously reported, the prolonged

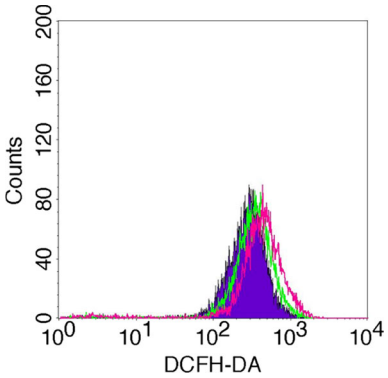

Fig. 8 Histograms showing detection of ROS using the DCFH-DA assay 24 h after 20 s treatment of A549 cells with low temperature plasma 1W (green line) and 1.5 W (pink line). The enhancement of the intracellular ROS accumulation can be observed via the shift of the signal curve obtained for the treated cells to the right, compared with control cells (purple fill)

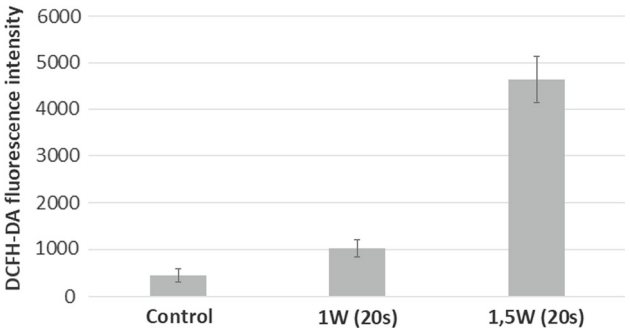

Fig. 9 Bar graph presenting mean fluorescence intensity of DCFH-DA. A representative experiment is shown with each sample analyzed in duplicate

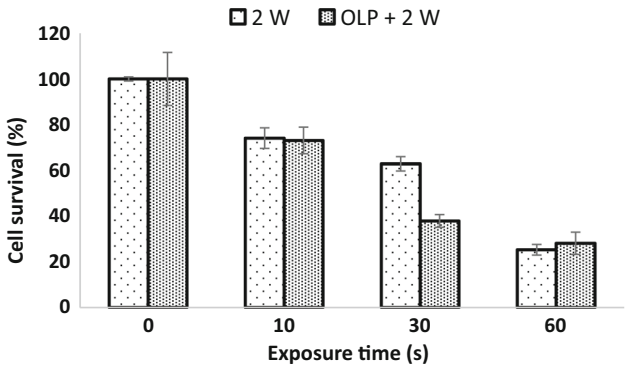

Fig. 10 Comparison of cell survival of A549 cells after plasma treatment (2 W) alone and combined treatment with PARP inhibitor olaparib (OLP. For combined treatment, cells were pre-treated for 90 min with PARP inhibitor OLP in 10 μM concentration and then treated with plasma (2 W). Cell survival was determined with MTT test and results presented as mean ± SD. Results for the representative experiment out of 3 independent experiments, each performed in triplicates

treatment probably produced a variety of ROS and RNS (reactive nitrogen species) in different amounts, compared to the shorter treatment [57, 58]. These species might trigger numerous responses which have different importance on cell survival [57, 58].

Similar more comprehensive research of Ji Ye Choi et al. investigating a combinatorial regimen targeting PARP-1 pathways during LTP treatment has also shown that inhibition of PARP-1 augments apoptosis in human lung carcinoma A549 and melanoma SK-MEL2 cells during LTP and LTP combined with oxygen flow treatment using their plasma jet device [64]. The increasing number of studies of combined action of different types of drugs and LTP indicate that LTP might have the potential for development as an enhanced cancer therapy with favorable therapeutic responses [65].

3.8 Results of investigation of growth inhibition in 3D cell culture model

Finally, 3D cell culture model of multicellular tumor spheroids (MCTS) was employed to predict the in vivo antitumor effects of our system for low temperature plasma treatment in A549 cells. The MCTSs provide insight into metabolic properties similar to solid tumor profiles such as nutrient and oxygen gradients, hypoxic/necrotic regions, cell–cell matrix interactions and gene expression [66].

The results shown in Fig. 11 indicate that there was no reduction in growth of A549 cells MCTS after 60 s and 120 s plasma treatment for investigated experimental conditions. The majority of published studies concerning spheroid treatment by the LTP jet showed that plasma induced cell damage was limited to surface [31]. Because of the complexity of the 3D model, further extensive investigations are needed, varying duration, power as well as other experimental conditions, for a more comprehensive study of the effect of our LTP system.

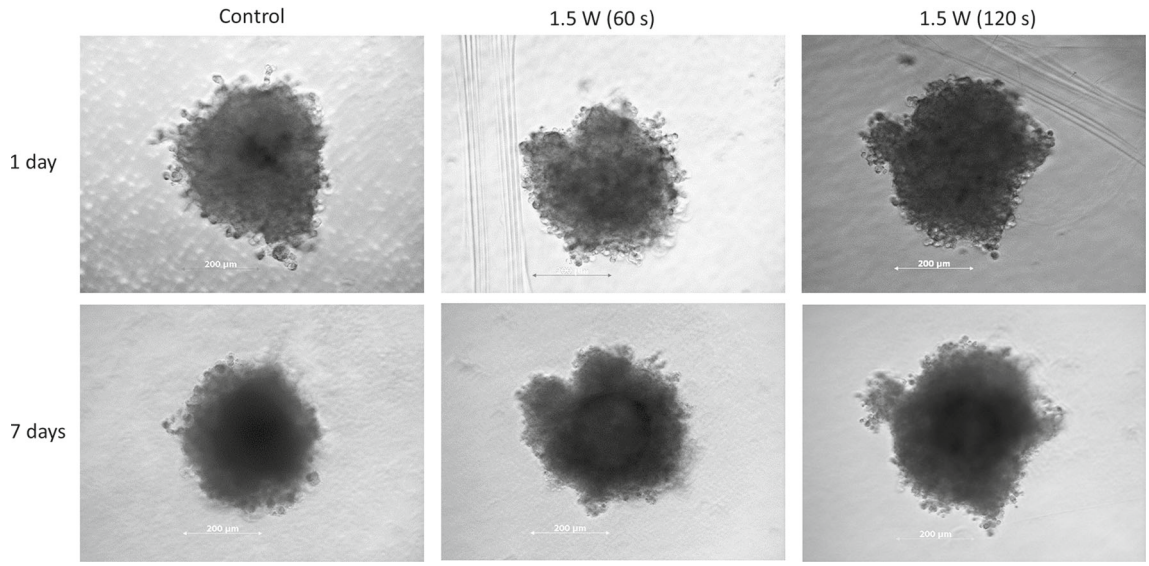

Fig. 11 Growth inhibition monitoring of low temperature plasma treated A549 MCTSs

4 Conclusion

LTP as emerging technology has numerous outstanding potentials in pharmaceutical field as future treatment modality. A wide range of plasma sources that have been developed and applied for biomedicine give us an opportunity to seek numerous different approaches to specific applications. This variety also means that it is difficult to compare results from one platform to another [31–33]. Our group developed plasma generating device that induces cell cycle arrest in A549, lung cancer cells, leading to apoptosis in direct treatment in 2D cell culture model. However, further extensive investigations are needed, varying treatment conditions, for more comprehensive study of the effect of our LTP system on 3D cell culture model and for finding most adequate application in anticancer combat. Our results with combined treatment with PARP inhibitor direct us to the conclusion that the LTP will probably have the greatest potential in combined treatment with chemotherapeutic drugs in agreement with conclusions of Robert et al. [67].

Acknowledgements The authors gratefully acknowledge financial support from the Ministry of Science, Technological Development and Innovation of the Republic of Serbia (Agreements No. 451-03-47/2023-01/200043). This work was supported by MSTDI Republic of Serbia under the Grant Number 451-03-47/2023-01/200024. Z. Lj. P. is grateful to the SANU Project F155 for partial support. The inhibitor olaparib (AZD2281) was obtained as a gift from AstraZeneca. Authors are grateful to the anonymous referees for investing a lot of effort toward improvement of this manuscript.

Author contributions NS and NG contributed to conception and design, data acquisition, data analysis, data interpretation, writing—original draft, preparation—final draft; MC helped in data acquisition, data analysis, data interpretation, writing—original draft, approval—final draft; NP: contributed to conception and design, data analysis, data interpretation, supervision, writing—critical revision, preparation—final draft; GM helped in data interpretation, supervision, writing—critical revision, approval—final \draft; SR done resources, funding, supervision, writing—critical revision, approval—final draft; Z.Lj.P. contributed to conception and design, resources, funding, supervision, writing—critical revision, preparation—final draft.

Data Availability Statement This manuscript has associated data in a data repository. [Authors' comment: The data will be available after publication of the paper upon a reasonable request to the authors. All the data obtained for this paper are presented here in graphs, text and tables.]

Declarations

Conflict of interest The authors have no competing interests to declare that are relevant to the content of this article.

References

1. T. Makabe, Z.L. Petrovic, *Plasma Electronics: Applications in Microelectronic Device Fabrication*, 2nd edn. (CRC Press, Cambridge, 2014)
2. M. Laroussi, Plasma Process. Polym. **2**, 91 (2005)
3. E. Stoffels, Y. Sakiyama, D.B. Graves, IEEE Trans. Plasma Sci. **36**, 1441 (2008)
4. D.B. Graves, J. Phys. D Appl. Phys. **45**, 263001 (2012)
5. M.G. Kong, G. Kroesen, G. Morfill, T. Nosenko, T. Shimizu, J. Van Dijk, J.L. Zimmermann, New J. Phys. **11**, 115012 (2009)
6. G. Fridman, G. Friedman, A. Gutsol, A.B. Shekhter, V.N. Vasilets, A. Fridman, Plasma Process. Polym. **5**, 503 (2008)
7. N. Puač, M. Gherardi, M. Shiratani, Plasma Process. Polym. **15**, 1700174 (2018)
8. P. Ranieri, N. Sponsel, J. Kizer, M. Rojas-Pierce, R. Hernández, L. Gatiboni, A. Grunden, K. Stapelmann, Plasma Process. Polym. **18**, 2000162 (2021)

9. M. Ito, T. Ohta, M. Hori, J. Korean Phys. Soc. **60**, 937 (2012)
10. Q. Xiong, X.P. Lu, K. Ostrikov, Y. Xian, C. Zou, Z. Xiong, Y. Pan, Phys. Plasmas **17**, 043506 (2010)
11. D. Maletić, N. Puač, G. Malović, A. Đorđević, Z.L. Petrović, J. Phys. D Appl. Phys. **50**, 145202 (2017)
12. A. Stancampiano, N. Selaković, M. Gherardi, N. Puač, Z.L. Petrović, V. Colombo, J. Phys. D Appl. Phys. **51**, 484004 (2018)
13. J.S. Oh, H. Furuta, A. Hatta, J.W. Bradley, Jpn. J. Appl. Phys. **54**, 01AA03 (2014)
14. G.Y. Park, S.J. Park, M.Y. Choi, I.G. Koo, J.H. Byun, J.W. Hong, J.Y. Sim, G.J. Collins, J.K. Lee, Plasma Sources Sci. Technol. **21**, 043001 (2012)
15. O. Assadian, K.J. Ousey, G. Daeschlein, A. Kramer, C. Parker, J. Tanner, D.J. Leaper, Int. Wound J. **16**, 103 (2019)
16. K. Miyamoto, S. Ikehara, H. Sakakita, Y. Ikehara, J. Clin. Biochem. Nutr. **60**, 25 (2017)
17. G.B. McCombs, M.L. Darby, Int. J. Dent. Hyg. **8**, 10 (2010)
18. S. Cha, Y.S. Park, Clin. Plasma Med. **2**, 4 (2014)
19. J.N. Stasić, N. Selaković, N. Puač, M. Miletić, G. Malović, Z.Lj. Petrović, D.N. Veljović, V. Miletić, Clin. Oral Investig. **23**, 1383 (2019)
20. M. Miletić, S. Mojsilović, I.O. Đorđević, D. Maletić, N. Puač, S. Lazović, G. Malović, P. Milenković, Z.Lj. Petrović, D. Bugarski, J. Phys. D Appl. Phys. **46**, 345401 (2013)
21. S. Lazović, N. Puač, M. Miletić, D. Pavlica, M. Jovanović, D. Bugarski, S. Mojsilović, D. Maletić, G. Malović, P. Milenković, Z.Lj. Petrović, New J. Phys. **12**, 083037 (2010)
22. S.U. Kalghatgi, G. Fridman, M. Cooper, G. Nagaraj, M. Peddinghaus, M. Balasubramanian, V.N. Vasilets, A.F. Gutsol, A. Fridman, G. Friedman, IEEE Trans. Plasma Sci. **35**, 1559 (2007)
23. G. Fridman, M. Peddinghaus, A. Fridman, M. Balasubramanian, A. Gutsol, G. Friedman, in: *32nd IEEE International Conference on Plasma Science* (p. 257) (2005).
24. M. Miletić, D. Vuković, I. Živanović, I. Dakić, I. Soldatović, D. Maletić, S. Lazović, G. Malović, Z.Lj. Petrović, N. Puač, Cent. Eur. J. Phys. **12**, 160 (2014)
25. G. Fridman, A.D. Brooks, M. Balasubramanian, A. Fridman, A. Gutsol, V.N. Vasilets, H. Ayan, G. Friedman, Plasma Process. Polym. **4**, 370 (2007)
26. S. Tomić, A. Petrović, N. Puač, N. Škoro, M. Bekić, Z.Lj. Petrović, M. Čolić, Cancers **13**, 1626 (2021)
27. S. Iseki, K. Nakamura, M. Hayashi, H. Tanaka, H. Kondo, H. Kajiyama, H. Kano, F. Kikkawa, M. Hori, Appl. Phys. Lett. **100**, 113702 (2012)
28. H.M. Joh, S.J. Kim, T.H. Chung, S.H. Leem, AIP Adv. **3**, 092128 (2013)
29. S.J. Kim, T.H. Chung, S.H. Bae, S.H. Leem, Appl. Phys. Lett. **97**, 023702 (2010)
30. H. Tanaka, M. Mizuno, K. Ishikawa, K. Takeda, K. Nakamura, F. Utsumi, H. Kajiyama, H. Kano, Y. Okazaki, S. Toyokuni, S. Maruyama, IEEE Trans. Plasma Sci. **42**, 3760 (2014)
31. A.M. Hirst, F.M. Frame, M. Arya, N.J. Maitland, D. O'Connell, Tumor Biol. **37**, 7021 (2016). https://doi.org/10.1007/s13277-016-4911-7
32. M. Laroussi, Plasma Process. Polym. **11**, 1138 (2014). https://doi.org/10.1002/ppap.201400152
33. M. Laroussi, Front. Phys. **8**, 74 (2020). https://doi.org/10.3389/fphy.2020.00074
34. J. Canady et al., Cancers **15**, 3688 (2023). https://doi.org/10.3390/cancers15143688
35. S. Lazović, D. Maletić, A. Leskovac, J. Filipović, N. Puač, G. Malović, G. Joksić, Z. Lj. Petrović, Appl. Phys. Lett. **105**, 12 (2014). https://doi.org/10.1063/1.4896626
36. L. I. Partecke, K. Evert, J. Haugk, F. Doering, L. Normann, S. Diedrich, F.-U. Weiss, M. Evert, N. O. Huebner, C. Guenther, C. D. Heidecke, A. Kramer, R. Bussiahn, K.-D. Weltmann, O. Pati, C. Bender, W. von Bernstorff, BMC Cancer **12**, 1 (2012)
37. M. Ishaq, S. Kumar, H. Varinli, Z. J. Han, A. E. Rider, M. D. M. Evans, A. B. Murphy, K. Ostrikov, MBoC **25**, 1523 (2014). https://doi.org/10.1091/mbc.e13-10-0590
38. O. Volotskova, T. S. Hawley, M. A. Stepp and M. Keidar, Sci. Rep. **2**, 636 (2012)
39. R.B. Mokhtari, T.S. Homayouni, N. Baluch, E. Morgatskaya, S. Kumar, B. Das, H. Yeger, Oncotarget **8**, 38022 (2017). https://doi.org/10.18632/oncotarget.16723
40. N.J. Curtin, E. Rev, Mol. Med. **7**, 1 (2005)
41. F. Dantzer, V. Schreiber, C. Niedergang, C. Trucco, E. Flatter, G. De La Rubia, J. Oliver, V. Rolli, M.J. Ménissier-de, G. de Murcia, Biochimie **81**, 69 (1999)
42. F. Dantzer, G. de La Rubia, M.J. Ménissier-De, Z. Hostomsky, G. de Murcia, V. Schreiber, Biochemistry **39**, 7559 (2000)
43. J.F. Alhmoud, J.F. Woolley, A.-E. AlMoustafa, M.I. Malki, Cancers **12**, 1050 (2020). https://doi.org/10.3390/cancers12041050
44. N. Gligorijević, S. Aranđelović, L. Filipović, K. Jakovljević, R. Janković, S. Grgurić-Šipka, I. Ivanović, S. Radulović, ŽL. Tešić, J. Inorg. Biochem. **108**, 53 (2012)
45. N. Puač, Z. Lj. Petrović, G. Malović, A. Dordević, S. Živković, Z. Giba, D Grubišić, J. Phys. D Appl. Phys. **39**, 3514 (2006)
46. S. Lazović, N. Puač, M. Miletić, D. Pavlica, M. Jovanović, D. Bugarski, S. Mojsilović, D. Maletić, G. Malović, P. Milenković, Z. Petrović, New J. Phys. **12**, 083037 (2010)
47. E. Stoefels, A J Flikweert, W. W. Stoffels, G M W Kroesen, Plasma Sources Sci. Technol. **11**, 383 (2002)
48. R. E. J. Sladek, E. Stoffels, R. Walraven, P. J. A. Tielbeek, R. A. Koolhoven, IEEE Trans. Plasma Sci. **32**, 1540–1543 (2004)
49. M. Gherardi, N. Puač, D. Marić, A. Stancampiano, G. Malović, V. Colombo, Z. Lj. Petrović, PSST **24**, 064004 (2015)
50. N. Puač, J. Phys. Conf. Ser. Vol. 133. No. 1. IOP Publishing, (2008).
51. G. Malović, N. Puač, S. Lazović, Z. Petrović, Plasma Sources Sci. Technol. **19**, 034014 (2010)
52. R. Supino, *Methods in Molecular Biology*, in: S. O'Hare, C.K. Atterwill (Eds.), (Humana Press, New Jersey, 1995) pp. 137–149
53. M.G. Ormerod, Analysis of DNA—general methods, in *Flow Cytometry, a Practical Approach*. ed. by M.G. Ormerod (Oxford University Press, New York, 1994), pp.119–125
54. E. Eruslanov, S. Kusmartsev, Methods Mol. Biol. **594**, 57 (2010)
55. K.P. Arjunan, V.K. Sharma, S. Ptasinska, Effects of atmospheric pressure plasmas on isolated and cellular DNA: a review. Int. J. Mol. Sci. **16**, 2971 (2015)
56. D. Yan, J.H. Sherman, M. Keidar, Oncotarget **8**(9), 15977 (2017)
57. N. Kaushik, N. Uddin, G.B. Sim, Y.J. Hong, K.Y. Baik, C.H. Kim, S.J. Lee, N.K. Kaushik, E.H. Choi, Sci. Rep. **5**, 8587 (2015)
58. T. Adachi, H. Tanaka, S. Nonomura, H. Hara, S.-I. Kondo, M. Hori, Free Radical Biol. Med. **79**, 28 (2015)
59. D. Wlodkowic, W. Telford, J. Skommer, Z. Darzynkiewicz, Methods Cell Biol. **103**, 55 (2011)
60. I.E. Kieft, M. Kurdi, E. Stoffels, IEEE Trans. Plasma Sci. **34**, 1331 (2006)
61. A. Parveen, M.S. Akash, K. Rehman, W.W. Kyunn, Dual, role of p21 in the progression of cancer and its treatment. Crit. Rev. Eukaryot. Gene Exp. **26**, 49 (2016)
62. H. Nakamura, K. Takada, Cancer Sci. **112**, 3945 (2021)
63. S.B. Karki, T.T. Gupta, E. Yildirim-Ayan, K.M. Eisenmann, H. Ayan, Plasma Chem. Plasma Process. **40**, 99 (2020)

64. J.Y. Choi, H.M. Joh, J.-M. Park, M.J. Kim, T.H. Chung, T.-H. Kang, Oncotarget **7**, 32980 (2016)
65. L. Gao, X. Shi, X. Wu, J. Pharm. Anal. **11**, 28e36 (2021). https://doi.org/10.1016/j.jpha.2020.05.001
66. S. Nath, G.R. Devi, Pharmacol. Ther. **163**, 94 (2016)
67. E. Robert, M. Vandamme, L. Brullé, S. Lerondel, A. Le Pape, V. Sarron, D. Riès, T. Darny, S. Dozias, G. Collet, C. Kieda, J.M. Pouvesle, Clin. Plasma Med. **1**, 8 (2013)

foods

MDPI

Article

Modeling and Investigation of Deoxynivalenol Reduction in Wheat Flour After Cold Atmospheric Plasma Treatment Using Artificial Neural Networks

Elizabet Janić Hajnal [1,*], Milan Vukić [2], Lato Pezo [3], Nenad Selaković [4], Nikola Škoro [4] and Nevena Puač [4]

[1] Institute of Food Technology, University of Novi Sad, 21000 Novi Sad, Serbia
[2] Faculty of Technology Zvornik, University of East Sarajevo, 75400 Zvornik, Bosnia and Herzegovina; milan.vukic@tfzv.ues.rs.ba
[3] Institute of General and Physical Chemistry, University of Belgrade, 11000 Belgrade, Serbia; latopezo@yahoo.co.uk
[4] Institute of Physics, University of Belgrade, 11080 Belgrade, Serbia; nele@ipb.ac.rs (N.S.); nskoro@ipb.ac.rs (N.Š.); nevena@ipb.ac.rs (N.P.)
* Correspondence: elizabet.janich@fins.uns.ac.rs

Abstract

The aim of this study was to explore the effectiveness of cold atmospheric plasma (CAP) treatments for reducing the deoxynivalenol (DON) content in spiked white wheat flour samples containing 750 μg kg^{-1} DON. The flour samples were treated with plasma generated in air for durations of 30 s, 60 s, 90 s, 120 s, 150 s, and 180 s and at four distances from the cold plasma source: 6 mm, 21 mm, 36 mm, and 51 mm. An artificial neural network (ANN) model with three layers utilizing the Broyden–Fletcher–Goldfarb-Shanno (BFGS) iterative algorithm was developed to predict the reduction in deoxynivalenol (DON) content, moisture content, and temperature in wheat flour samples following cold atmospheric plasma (CAP) treatment. The model accounted for two key variables: the distance from the plasma source and the treatment duration. The ANN model exhibited excellent predictive performance, achieving coefficient of determination (r^2) values of 0.999, 0.996, and 0.996 for DON reduction, moisture content, and temperature, respectively, during the training phase. The ANN model successfully identified the experimental optimal CAP conditions (51 mm distance and 150 s treatment), resulting in a 71% reduction in DON content. Multi-objective optimization (MOO) using the ANN further predicted the same level of reduction but at 168 s while maintaining acceptable moisture and temperature levels, representing the model-derived optimal treatment within the investigated design space. The study highlights the potential of ANNs to model complex relationships and optimize CAP treatment for efficient mycotoxin reduction in wheat flour.

Keywords: wheat flour; cold atmospheric plasma; deoxynivalenol reduction; HPLC-DAD; mathematical modelling

Academic Editors: Ana Cristina De Aguiar Saldanha Pinheiro, Junior Bernardo Molina-Hernández and Silvia Tappi

Received: 15 January 2026
Revised: 31 January 2026
Accepted: 3 February 2026
Published: 5 February 2026

1. Introduction

The most commonly found mycotoxin in wheat and wheat-based products worldwide is deoxynivalenol (DON), categorized as a type B trichothecene. DON, as a secondary metabolite mainly of *Fusarium culmorum* and *Fusarium graminearum*, represents a significant hazard to the food and feed processing chain, causing economic losses as well. Spoilage fungi in cereal crops can produce mycotoxins (secondary metabolites) under optimum conditions in the field or during storage, which can be toxic to humans and animals.

Consumption of mycotoxin-contaminated food can cause hepatic, gastrointestinal, and carcinogenic diseases [1]. With over 140 identified fungal metabolites, *Fusarium* mycotoxins are the biggest class of mycotoxins. Numerous fungal species, primarily *Fusarium* (*F. graminearum* and *F. culmorum*), synthesize them [2]. Trichothecenes, especially DON, are prevalent in cereal crops and their concentrations very often exceed permissible levels [3]. DON contamination of wheat is widespread and frequently detected in the majority of samples tested globally [3]. Since wheat (*Triticum aestivum* L.) ranks as the second most produced grain crop worldwide, with about 800.79 million metric tons in 2024/25, its safety is of particular urgency [4].

DON is resistant to standard processes like milling, baking, and heating. Chemical reagents like ammonia, calcium hydroxide, chlorine, hydrochloric acid, ozone, sodium bisulfite, and sodium hydroxide can degrade DON, but none have been applied due to interference with standard grain processing or health hazards [2]. At the cellular level, DON has been found to have immunosuppressant or immune stimulatory effects depending on the dose and duration of exposure. DON is less toxic than other toxins, like T-2, but high doses can cause shock-like death [5–7]. Stimulatory effects are observed depending on the dose and duration of exposure. Symptoms include abdominal distress, increased salivation, malaise, diarrhea, emesis, and anorexia in sensitive species [6,8]. Chronic toxicity studies in experimental animals show decreased weight gain, anorexia, and altered nutritional efficiency. Animal species are sensitive to DON, with pigs being more sensitive than mice, poultry, and ruminants. In vivo, DON suppresses the immune response to pathogens and induces autoimmune-like effects similar to human immunoglobulin A (IgA) nephropathy [6,8].

In 1993, DON was placed in Group 3 (not classifiable as to its carcinogenicity to humans) of the International Agency for Research on Cancer [9]. Until July 2024, according to EU Commission Regulation No. 2023/915 [10], the maximum level for DON in cereals placed on the market for the final consumer, cereal flour, and semolina, bran, and germ as final products placed on the market for the final consumer was limited to 750 μg kg^{-1}. The most recent Commission Regulation (EU) No. 2024/1022 [11] changed Regulation (EU) No. 2023/915 related to the maximum level of DON in certain foods. Now, in milling products of cereal, except for milling products of maize, its content is limited to 600 μg kg^{-1} [11]. Traditional technological processes for DON reduction may lead to food quality decline, but biodegradation and innovative processes and/or techniques offer mild conditions and high efficiency [12], which ensure the preservation of product quality with a significant reduction in DON content.

Among novel decontamination approaches, cold atmospheric plasma (CAP) has gained significant attention due to its ability to generate a broad range of reactive oxygen and nitrogen species (RONS) under mild, non-thermal conditions. CAP operates at atmospheric pressure, without any pumping facilities for pressure reduction, does not require chemical additives, and leaves no harmful residues, making it suitable for direct application to food products and simple integration into existing food processing systems. Unlike thermal, chemical, or UV-based treatments—which may compromise nutritional or sensory quality—CAP offers a residue-free and energy-efficient alternative that preserves the functional integrity of food matrices [13–15]. Furthermore, several recent studies have demonstrated its ability to effectively degrade DON and other mycotoxins in cereal-based systems through oxidation and structural disruption of toxic moieties [16,17].

Chemical processes induced by cold plasma have been studied extensively for many years in a wide range of applications, including recently established applications in plasma agriculture field and food technology [13–15,18]. Given these advantages, CAP has emerged as a promising tool for mycotoxin mitigation, particularly in food matrices where thermal or

chemical treatments may be unsuitable. This is especially relevant for dry food powders like wheat flour, which presents a challenging matrix due to its heat-sensitive nutrients, the risk of denaturing functional gluten proteins, and the practical difficulty of treating a flowing, particulate material in vacuum. The underlying mechanism involves the interaction of plasma-generated reactive species—such as ozone (O_3), nitric oxide (NO), and hydroxyl radicals (·OH)—with target contaminants, often resulting in molecular breakdown or functional group disruption. Due to their light mass, electrons in the gas are accelerated, gain high energies (1–10 eV), and are not in thermal equilibrium with other particles (ions, neutrals). The collisions of high-energy electrons with bulk gas molecules (N_2, O_2, and H_2O) result in the formation of highly reactive short-lived (e.g., ·O, ·N, and ·OH) and long-lived species (O_3, H_2O_2, NO, N_2*, O_2*, etc.) that can react with samples, performing processes of oxidation or reduction [19]. Considering the types of plasma sources, DBD sources are particularly convenient with respect to other atmospheric-pressure cold plasma sources as they can create large effective surfaces of active plasma, enabling treatment of larger areas. Electrode geometry in the case of surface DBD (SDBD) allows for the creation of a stable discharge close to the surface of the dielectric, which is not influenced much by the target type. Moreover, the source is modular, so many sources can be stacked together, increasing the effective surface for treatment.

The gas-phase plasma chemistry and reaction pathways that result in the formation of plasma-generated chemical species depend on various parameters, such as input power, gas mixture, sample distance, etc. The species created in CP operating at atmospheric pressure have very short mean free paths between collisions (order of μm); therefore, the plasma chemistry varies with the distance from the CP source. Determination of the precise plasma chemistry is a crucial input parameter for studying interaction processes and revealing the plasma mechanisms against particular pathogens. Mass spectrometry is a straightforward plasma diagnostic technique that can provide information on the created neutral and ionic species in plasma [20,21].

As many plasma decontamination studies have demonstrated that reactive oxygen and nitrogen species (RONS) generated by cold plasma sources play a crucial role in the interaction with pathogens [22], plasma diagnostics using mass spectrometry have focused on characterizing these species. As plasma technology begins to enter the food sector, this study presents findings on a promising new technique for mitigating mycotoxins. Although cold atmospheric plasma shows considerable potential as an innovative and effective approach for mycotoxin reduction, this technology is still under investigation and requires further validation and standardization before it can be considered ready for industrial application. To our knowledge, so far, there is no specific, universally established regulatory pathway for the use of plasma technology by food producers to reduce the mycotoxin content in food in most major jurisdictions, such as the United States (FDA), the European Union (EFSA), or other countries.

In years with severe DON contamination, conventional wheat processing steps may not be adequate to reduce toxin levels in white flour below the maximum allowed limit. Therefore, they may not ensure compliance under severe contamination. In a previous study, low-pressure RF helium and oxygen plasma for homologous wheat flour was studied, and the results indicated considerable reduction in DON content after 90 s and 150 s [23].

Artificial neural networks (ANNs) are increasingly used in food processing to model complex, nonlinear relationships between processing conditions and product responses [24,25]. For non-thermal technologies such as cold atmospheric plasma, where the treatment time and plasma–sample distance simultaneously affect reactive species generation, energy transfer, and mass and heat exchange, conventional modeling approaches are often inadequate [26]. ANN models provide an effective data-driven framework for

capturing these interconnected effects and reliably predicting multiple responses, including contaminant degradation, moisture changes, and temperature variation [27–29].

In this study, we precisely determined the reactive species formed in plasma employing mass spectrometry and used ANN modeling for the first time to identify the CAP conditions that yielded the highest reduction in DON content. Therefore, the objective of this study was to investigate the possibility of predicting the reduction in DON content, moisture content, and temperature of wheat flour samples after cold atmospheric plasma treatment using a DBD source operating in air, based on the distance of the cold plasma source to the sample and process time. The study was performed using an artificial neural network (ANN) model with three layers and data obtained from mass spectrometry measurements. Various network topologies with 5 to 20 hidden neurons were evaluated over 100,000 training iterations, and the optimal configuration was selected by minimizing the validation error.

This study presents significant progress in mycotoxin mitigation for cereal processing, primarily through the first application of an artificial neural network (ANN) in modeling cold atmospheric plasma (CAP) treatment of deoxynivalenol (DON) in wheat flour. It addresses a significant gap in the literature by focusing directly on wheat flour, rather than on whole grains or liquid matrices. The research also includes a unique mechanistic analysis of reactive oxygen and nitrogen species using mass spectrometry, providing insights into the efficacy of plasma treatments. Furthermore, a genetic algorithm-based multi-objective optimization framework is utilized to enhance CAP treatment conditions, maximizing DON reduction while maintaining flour quality, thereby facilitating safer food processing practices.

To our knowledge, this is the first study to integrate predictive modeling, mechanistic diagnostics, and multi-objective optimization in the context of CAP-mediated mycotoxin (DON) reduction in wheat flour.

2. Materials and Methods

2.1. Material and Chemicals

For this study, white wheat flour was purchased at the market. The initial moisture content of white wheat flour was 14.1%. Before further procedures, a white wheat flour sample was analyzed to confirm that it was a blank sample without DON. To investigate the effect of atmospheric cold plasma on DON content, 10 g of white wheat flour was artificially contaminated, spiked, with DON standard solution (750 μg kg^{-1} in flour). This value was chosen to represent the maximum regulatory limit for DON in wheat flour as set by the European Union prior to July 2024 (Commission Regulation (EU) No. 2023/915) [10], and to reflect contamination levels commonly encountered in naturally contaminated samples. After spiking, the wheat flour sample was thoroughly mixed and then allowed to equilibrate at room temperature overnight to ensure homogenous distribution of DON within the matrix and to better mimic natural contamination scenarios. Subsequently, the spiked flour sample was stored at −20 °C until CAP treatment. The DON standard (10 mg) was purchased from Supelco^{TM} (Bellefonte, PA, USA). The stock solution was prepared by diluting the DON standard (100.1 μg mL^{-1}) to a concentration of 10 μg mL^{-1} in a normal 10 mL vessel, from which further dilution series were made. Acetonitrile and methanol (all HPLC grade) were purchased from Merck (Darmstadt, Germany). Deionized water (Millipore, Bedford, MA, USA) was used for HPLC analysis.

2.2. Treating Spiked Samples with SDBD

2.2.1. Plasma System for Treatment

A schematic of the DBD plasma system for wheat flour treatment is shown in Figure 1. The DON-spiked wheat flour samples were kept in the sample holder during the treatments. The sample holder was positioned at four different distances from the plasma region.

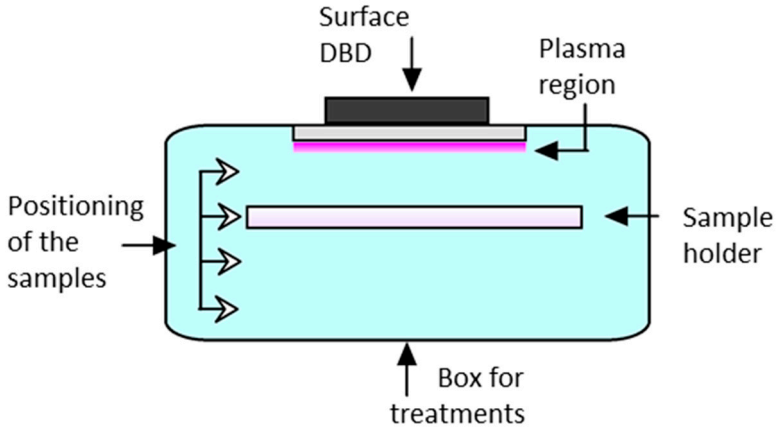

Figure 1. Schematic of the DBD plasma system for wheat flour treatment.

The SDBD source was based on a 2 mm ceramic dielectric plate (length 70 mm × width 40 mm). The ceramic dielectric plate consisted of nine comb-like stripe electrodes (~1 mm width), with a 4 mm inter-stripe spacing on the bottom side and a conductive layer on the top side of the plate. Electrodes on both sides were connected to the HV transformer. We used a commercial HV transformer with a maximum output power of 85 W and floating signal output, so direct measurement of the voltage supplied to generate the plasma was not possible. A Variac regulator was used to control the input voltage to the transformer, and it was powered through the standard electrical grid at a frequency of 50 Hz. The output signal, supplied to the electrodes, was a high-frequency signal with several peaks 4–5 kV (peak-to-peak) modulated in continuous pulses at around 100 Hz. This enabled discharge ignition and stable operation. The detailed characteristics of the DBD system are described in more detail in ref. [30]. For the treatments, the SDBD source with an active cooler on the top side was mounted on the box lid. Spiked flour for treatment was weighed (10 g) in a Petri dish of 100 mm in diameter and placed in the box for treatment. The samples were spread in a thin layer (3 mm thickness) so that the screening effect and possible temperature gradients were minimized. For each plasma treatment, the distance between the flat dielectric surface of the SDBD emitter was precisely set to the required distance from the top surface of the flour layer inside the Petri dish. This was made possible by the compact dimensions of the plasma plate (70 mm × 40 mm), which fit within the Petri dish opening. Moreover, for further analysis, a complete amount of treated sample was homogenized and used to effectively average the effects of the treatment. The two-factor design assessed distance, which governed reactive species flux, and time, which determined the treatment dose, as key parameters for a scalable process. Specifically, 4 combinations of distances, (6 mm, 21 mm, 36 mm, and 51 mm) and 6 time points (30, 60, 90, 120, 150, and 180 s) resulted in 24 experimental conditions. Distances were selected to cover the operational range of our plasma source, from the point of near contact (6 mm) to a distance where significant plasma effluent dissipation was observed (~51 mm). The range of treatment times from 30 s to 180 s was chosen based on preliminary trials to identify the optimal treatment window. Shorter times (<30 s) showed negligible decontamination, while times exceeding 180 s risked inducing undesirable physical changes due to the observed temperature rise and

moisture loss in the flour. Our preliminary trials also showed that 30 s intervals provided sufficient resolution to capture kinetic trends.

Plasma was formed on the lower side of the SDBD source in air, uniformly covering the surface of the SDBD source for an input voltage of 200 V, which was controlled by the Variac. The plasma thickness was around 1 mm, and it was checked visually that the operating regime was the same for all treatments. All plasma treatments were carried out under laboratory conditions, with a stable relative humidity of 45 ± 1%. Although the same humidity conditions were maintained for all experiments, minor fluctuations could not be entirely excluded. Since relative humidity may influence the plasma chemistry and the formation of reactive oxygen and nitrogen species, its potential impact represents a limitation of the present study and should be addressed in future investigations using controlled gas environments. However, as the humidity conditions were identical for all treatments, relative differences in the plasma chemistry and reactive species reaching the contaminated samples can be attributed primarily to the treatment distance and exposure time. After the treatments, the spiked samples were transferred from the box to sealed bags and stored at 4 °C until mycotoxin analysis.

2.2.2. Mass Spectrometry

In this study, we employed mass spectrometry to investigate RONS formation in a cold atmospheric plasma system used for flour treatment. Specifically, the analysis of neutral species was performed using a commercial HIDEN Molecular Beam Mass Spectrometer (MBMS) HPR60 (Hiden Analytical Ltd., Warrington, UK). The unique design of this instrument enables direct sampling from atmospheric conditions, making it particularly suitable for the investigation of gas-phase plasma discharges and the identification of neutral species produced by DBD sources, as previously shown by Čech et al. [31]. To ensure accurate representation of the conditions used for plasma treatment process, the sampling orifice of the mass spectrometer was positioned at the same distance from the plasma source as the treated sample (6 mm, 21 mm, 36 mm, and 51 mm). The difference in the longest distance was because of experimental capabilities. Since we were not measuring absolute concentrations of the species but their time-resolved creation and development, this did not influence the results a great detail. Additionally, the discharge conditions during mass spectrometric measurements were maintained identical to those used during the plasma treatment of the sample—the input voltage on the voltage regulator was 200 V, while the total consumed power from the power grid was determined to be 76 W. RONS identification was carried out using the residual gas analyzer (RGA) mode of the MBMS in two different operational settings: (1) recording the integral spectrum of the plasma discharge to obtain a comprehensive overview of species present, and (2) the MID scan mode, which enabled real-time monitoring of radical evolution under both active and inactive discharge conditions. A shutter (swagelock-SL) in the inner side of the sampling orifice of the MBMS enabled closing the influx of particles from the surroundings and allowed us to measure the contribution of the signal from the species present only in the device itself. This distinguished the foreground and the background signals measured by the mass spectrometer. To ensure the reliability of the MS measurements, the instrument was tuned according to the manufacturer's procedure prior to the beginning of the experimental series. Background spectra were recorded with the internal shutter closed and subtracted from all foreground signals to remove the signals of species from the unit itself. As the aim of the MS analysis was to follow the relative evolution of plasma-generated species rather than determine absolute concentrations, we did not perform absolute calibration. Measurements were repeated at least 3 times and they generated reproducible signals with

sufficient signal-to-noise ratios. Signal intensities expressed in counts per second (c/s) correspond to the particular m/z value count rate registered by the detector.

In this study, mass spectrometry was employed as a diagnostic tool to qualitatively characterize plasma-generated reactive oxygen and nitrogen species and to monitor their relative evolution as a function of distance from the plasma source. The MS results were used to support the mechanistic interpretation of the observed DON reduction trends by identifying dominant long-lived reactive species and their relative changes under different treatment conditions. The MS analysis was not intended to provide absolute quantitative concentrations of species or to establish direct kinetic correlations with DON degradation.

2.3. Moisture Content

Moisture content in white wheat flour samples before and after the applied treatments was determined using an IM 9500 NIR instrument with the optional flour module (Perten Instruments, Hagersten, Sweden) and is expressed on a dry basis.

2.4. Quantification of DON Content Before and After Cold Atmospheric Plasma Treatment

2.4.1. Sample Preparation

Sample preparation involved utilizing using MycoSep®225Trich SPE columns (Romer Lab, Inc., Union, MO, USA) for clean-up. Briefly, subsamples of spiked white wheat flour (5 g) underwent extraction with 20 mL of acetonitrile/deionized water (84:16, v/v) and were shaken for 30 min in a laboratory Griffin flask shaker (Griffin and George, Wembley, UK). The extracts were filtered through Whatman No. 4 filter paper (Whatman International Ltd., Maidstone, UK), and 5.0 mL of the filtrate was collected in the glass tube. The MycoSep clean-up column was employed to filter the extract upward, followed by transferring 2.0 mL of the upper layer into a glass cuvette for nitrogen evaporation (Reacti-Therm I#18821, Thermo Scientific, Bellefonte, PA, USA). The dry residue was dissolved in 0.40 mL of mobile phase and transferred to an HPLC vial through a regenerated cellulose (RC, 4 mm, 0.2 µm) premium syringe filter (Agilent Technologies, Strathaven, Lanarkshire, Scotland, UK).

2.4.2. Instrumental Conditions and Method Performance

The DON content was determined using an Agilent 1260 Infinity HPLC system (Agilent Technologies Inc., Böblingen, Germany) consisting of a solvent degassing unit, a quaternary pump, an autosampler, a thermostated column, and a diode array detector (DAD). The DAD was set to 220 nm. Water/methanol/acetronitrile (90:5:5 $v/v/v$) at a flow rate of 0.60 mL min^{-1} under isocratic conditions were used as the mobile phase. The total run time was 25 min (15 min run, 10 min post-run). Separation was achieved using a Poroshell 120 EC-C18 column (4.6 × 100 mm, i.d. 2.57 µm) (Agilent Technologies Inc., Santa Clara, CA, USA) at 25 °C, and 15.0 µL standards and samples were injected into the duplicate. The retention time of DON was 3.80 min. The chromatograms were analyzed using Chemstation LC software ver. C.01.06 (Agilent Technologies Inc., Santa Clara, CA, USA). European Commission Regulation (EC) No. 401 [32] and Technical Report CEN/TR 16059 [33] from the European Committee for Standardization were utilized to establish and express validation parameters for the HPLC-DAD method. The method was validated concerning linearity, limit of quantification (LOQ), recovery, repeatability, and reproducibility with a standard curve obtained from duplicate injections at 5 concentrations ranging from 100 to 1000 ng mL^{-1} DON. The squared correlation coefficient (r^2) was above 0.9990 for the calibration curve. For analytical methods to determine contaminants with prescribed maximum permitted concentrations, the LOQ should be well below the regulatory threshold. As per Technical Report CEN/TR16059 [33], the LOQ for deoxynivalenol (DON) must be 100 µg kg^{-1}, which was confirmed by accuracy and repeatability tests on white wheat flour samples spiked to this level. The analytical method's quality was

evaluated using spiked white wheat flour samples, focusing on recovery, repeatability, and reproducibility. Recovery studies indicated high trueness, with values of 109.6%, 108.1%, and 107.8% for concentrations of 500, 750, and 1000 μg kg^{-1} DON, respectively. The relative standard deviation (%*RSDr*) was used to measure repeatability, and the results were 4.43%, 1.48%, and 1.36% at 500, 750, and 1000 μg kg^{-1} DON, respectively. The within-laboratory reproducibility (%*RSDR*) over three days yielded values of 8.38%, 7.69%, and 4.43%. The method met the criteria set by the European Official Decision procedure for confirmatory methods [32] and CEN/TR 16059 [33] from the European Committee for Standardization.

All flour samples were prepared and analyzed twice. The obtained results, i.e., concentration of DON before and after treatments, are expressed on a dry matter basis. The reduction in DON content was calculated as follows:

$$Reduction\ of\ DON\ content\ (\%) = 100 - \left(C_x \cdot \frac{100}{C_0}\right) \quad (1)$$

where C_x is the concentration of DON in the wheat flour sample after treatment, and C_0 is the initial concentration of DON in the spiked wheat flour sample before treatment.

2.5. Mathematical Modelling

2.5.1. Kinetics Modeling

To evaluate the deoxynivalenol reduction rate during cold atmospheric plasma treatment in wheat flour, kinetic modeling was performed. The temporal kinetics of the DON reduction rate, tested with different distances of the cold plasma source to the sample, were described using a four-parameter sigmoidal mathematical model (Equation (2)), which is highly suitable for biological systems. This model was used due to the complexity of the treated matrix (flour) and it was not related to plasma chemistry.

$$y(t) = d_1 + \frac{a_1 - d_1}{1 + \left(\frac{t}{c_1}\right)^{b_1}} \quad (2)$$

In Equation (1), the DON reduction rate (%) is represented as $y(t)$, whereas the regression coefficients are denoted as follows: a_1—minimum of the experimentally obtained values (at t = 0); d_1—the maximally acquired value; c_1—the inflection point (the point between a_1 and d_1); and b_1—the Hill's slope (the steepness of the inflection point c_1).

2.5.2. ANN Modeling

A three-layer multilayer perceptron (MLP) model—comprising input, hidden, and output layers—was used to develop an artificial neural network (ANN) for predicting the reduction in DON content, as well as the moisture content and temperature of wheat flour after treatment, based on the distance of the cold plasma source and process time. The ANN approach has been shown to effectively approximate nonlinear functions [34–37]. Prior to modeling, all input and output data were normalized to improve network performance. The input data were iteratively presented to the network [38,39], and the Broyden–Fletcher–Goldfarb–Shanno (BFGS) algorithm was applied to solve the unconstrained nonlinear optimization problem during ANN training.

The experimental database (72 data points from 24 plasma treatment conditions, each in duplicate) was randomly divided into training (60%), validation (20%), and testing (20%) sets. During model development, the number of hidden neurons (5–20) and the corresponding weight coefficients were optimized. To reduce dependence on random initialization, network training was repeated 100,000 times with different randomly assigned initial weights and biases, and the model with the lowest validation error was selected. The optimized ANN architecture consisted of a multi-layer perception with 8 input neurons,

11 hidden neurons, and 3 output neurons, resulting in 157 adjustable parameters (weights and biases). Although the dataset comprised 72 data points, overfitting was controlled through data normalization, early stopping, and independent testing. Model performance metrics and residual analysis confirmed adequate generalization within the studied experimental domain. Model robustness was assessed by 10-fold cross-validation and learning curves constructed from data subsets. Successful training was achieved when learning and validation errors converged toward zero, ensuring a conservative data-to-parameter ratio and minimizing overfitting.

Data acquisition for studying DON reduction in wheat flour after cold atmospheric plasma treatment was limited by the complexity, cost, and time required for each controlled experiment and chemical analysis. Despite the small dataset, the applied modeling strategy—with optimized network topology, extensive training, and cross-validation—ensured stable convergence and minimized overfitting.

Coefficients associated with the hidden layer (weights and biases) were grouped in matrices W_1 and B_1. Similarly, coefficients associated with the output layer were grouped in matrices W_2 and B_2. It was possible to represent the neural network by using matrix notation (Y is the matrix of the output variables, f_1 and f_2 are transfer functions in the hidden and output layers, respectively, and X is the matrix of input variables [40]:

$$Y = f_1(W_2 \cdot f_2(W_1 \cdot X + B_1) + B_2) \quad (3)$$

Weight coefficients (elements of matrices W_1 and W_2) were determined during the ANN learning cycle, which updated them using optimization procedures to minimize the error between the network and experimental outputs [38,41,42], according to the sum of squares (SOS) and BFGS algorithm, and were used to speed up and stabilize convergence [43]. The coefficients of determination were used as parameters to check the performance of the obtained ANN model.

2.5.3. Global Sensitivity Analysis

Yoon's interpretation method was used to determine the relative influences of the reduction in DON content, moisture content of wheat flour samples after treatment, and temperature of wheat flour samples after treatment, based on the distance of the cold plasma source to the sample and process time [44]. This method was applied on the basis of the weight coefficients of the developed ANN:

$$RI_{ij}(\%) = \frac{\sum_{k=0}^{n}\left(w_{ik} \cdot w_{kj}\right)}{\sum_{i=0}^{m}\left|\sum_{k=0}^{n}\left(w_{ik} \cdot w_{kj}\right)\right|} \quad (4)$$

Global sensitivity analysis was performed using Yoon's interpretation method to assess the relative influence of the input factors, such as the distance of the plasma source (d) and treatment time (t), on the predicted outputs: DON reduction, moisture content (MC), and sample temperature (T). The method, based on ANN weight coefficients, provided a global measure of the contribution of each input parameter to the outputs, aiding in identifying the most influential variables for process optimization.

2.5.4. Standard Score Calculation

Normal scores were calculated for each variable and were used for complex comparison of the observed samples, regarding the technological and chemical properties of the samples listed in Table 1. The ranking procedure between different samples was performed

based on the ratio of raw data and extreme values for each applied assay [45], according to these equations:

$$\overline{x_i} = 1 - \frac{\max\limits_i x_i - x_i}{\max\limits_i x_i - \min\limits_i x_i}, \ \forall i \quad (5)$$

in the case of "the higher, the better" criteria, or

$$\overline{x_i} = \frac{\max\limits_i x_i - x_i}{\max\limits_i x_i - \min\limits_i x_i}, \ \forall i \quad (6)$$

in the case of "the lower, the better" criteria, where x_i represents the raw data.

Table 1. The results of cold atmospheric plasma treatments on reduction in DON content in wheat flour.

Inputs			Outputs			
Run	***d* (mm)**	***t* (s)**	**DON_{red} (%) ***	***MC* (%)**	***T* (°C)**	**Standard Score**
1	6	30	61.0 ± 1.6^{ijk}	13.6 ± 0.2^{ab}	37.4 ± 2.4^{ij}	0.477
2	6	60	56.6 ± 2.3^{hi}	14.1 ± 0.4^{b}	29.0 ± 1.2^{bcdef}	0.506
3	6	90	59.7 ± 3.1^{ij}	13.8 ± 0.4^{ab}	33.2 ± 1.0^{fghi}	0.500
4	6	120	65.4 ± 1.1^{jkl}	13.0 ± 0.5^{ab}	41.6 ± 3.1^{jk}	0.596
5	6	150	48.0 ± 1.6^{efg}	12.6 ± 0.5^{ab}	45.9 ± 0.6^{kl}	0.463
6	6	180	51.5 ± 0.7^{gh}	12.3 ± 0.2^{a}	50.0 ± 3.0^{l}	0.497
7	21	30	49.3 ± 3.5^{fg}	14.1 ± 0.8^{b}	27.0 ± 1.7^{abc}	0.439
8	21	60	47.0 ± 0.7^{defg}	14.0 ± 0.3^{ab}	27.9 ± 1.2^{abcde}	0.426
9	21	90	50.0 ± 2.1^{fg}	14.0 ± 0.5^{ab}	30.0 ± 1.2^{bcdefg}	0.425
10	21	120	41.1 ± 1.6^{bcd}	13.8 ± 0.4^{ab}	32.0 ± 0.6^{defgh}	0.359
11	21	150	42.2 ± 0.9^{cde}	13.8 ± 0.5^{ab}	34.1 ± 1.0^{ghi}	0.342
12	21	180	43.9 ± 0.8^{def}	13.5 ± 0.5^{ab}	36.0 ± 0.8^{hi}	0.388
13	36	30	47.7 ± 1.5^{efg}	14.1 ± 0.7^{b}	25.7 ± 0.8^{ab}	0.441
14	36	60	67.5 ± 3.7^{l}	14.1 ± 0.6^{b}	26.9 ± 0.7^{abc}	0.599
15	36	90	48.2 ± 1.1^{efg}	14.1 ± 0.6^{b}	28.7 ± 1.1^{bcdef}	0.408
16	36	120	37.4 ± 0.5^{abc}	14.1 ± 0.4^{b}	30.5 ± 1.1^{cdefg}	0.291
17	36	150	35.3 ± 1.1^{ab}	13.9 ± 0.6^{ab}	32.2 ± 1.9^{efgh}	0.287
18	36	180	32.8 ± 0.6^{a}	13.5 ± 0.9^{ab}	34.0 ± 1.1^{ghi}	0.316
19	51	30	33.1 ± 1.2^{a}	14.1 ± 1.0^{b}	24.0 ± 0.3^{a}	0.336
20	51	60	51.9 ± 2.1^{gh}	14.1 ± 0.6^{b}	25.9 ± 0.6^{ab}	0.476
21	51	90	66.2 ± 2.2^{kl}	14.0 ± 0.4^{ab}	27.5 ± 1.5^{abcd}	0.598
22	51	120	51.4 ± 1.2^{gh}	14.0 ± 0.1^{ab}	29.1 ± 0.9^{bcdef}	0.449
23	51	150	71.0 ± 4.4^{l}	13.9 ± 1.1^{ab}	30.8 ± 1.3^{cdefg}	0.617
24	51	180	51.6 ± 1.7^{gh}	13.9 ± 0.6^{ab}	32.5 ± 1.2^{fgh}	0.425
	Polarity		+	-	-	

d—distance of the cold plasma source to the sample; *t*—treatment duration; *MC*—moisture content of wheat flour samples after treatment; *T*—temperature of wheat flour samples after treatment; DONred *—reduction in deoxynivalenol content; polarity—negative sign is associated with "the lower the better" criteria, while positive sign is associated with "the higher the better" criteria, as explained in Section 2.5.4. Values are calculated (see Section 2.5.4). Values designated by the same letter in a row are not significantly different ($p > 0.05$).

2.5.5. The Accuracy of the Model

The numerical verification of the developed model was tested using the coefficient of determination (r^2), reduced chi-square (χ^2), mean bias error (*MBE*), root mean square

error (*RMSE*), and mean percentage error (*MPE*). These commonly used parameters can be calculated as follows [46]:

$$\chi^2 = \frac{\sum_{i=1}^{N} (x_{\exp,i} - x_{pre,i})^2}{N-n},\ RMSE = \left[\frac{1}{N} \cdot \sum_{i=1}^{N} (x_{pre,i} - x_{\exp,i})^2\right]^{1/2},$$
$$MBE = \frac{1}{N} \cdot \sum_{i=1}^{N} (x_{pre,i} - x_{\exp,i}),\ MPE = \frac{100}{N} \cdot \sum_{i=1}^{N} \left(\frac{\left|x_{pre,i} - x_{\exp,i}\right|}{x_{\exp,i}}\right) \quad (7)$$

where $x_{exp,i}$ denotes the experimental values; $x_{pre,i}$ indicates the predicted values calculated by the model; and N and n represent the number of observations and constants, respectively.

2.5.6. Multi-Objective Optimization (MOO)

The developed ANN model was employed as a surrogate model in a multi-objective optimization (MOO) framework to determine the cold atmospheric plasma (CAP) operating conditions. The optimization problem was formulated to maximize the reduction in DON content while simultaneously minimizing moisture content and process temperature. Mathematically, the MOO problem can be expressed as follows:

- maximize $f_1(x)$ = DON reduction,
- minimize $f_2(x)$ = moisture,
- minimize $f_3(x)$ = temperature,

where x represents the vector of CAP process variables. The solution of the MOO problem is a Pareto front consisting of non-dominated solutions, where improvement in one objective cannot be achieved without deterioration in at least one other objective [47].

A genetic algorithm (GA) was applied to solve the MOO problem using a stochastic evolutionary approach based on selection, crossover, mutation, and inheritance operators [48]. The optimization was performed in MATLAB, ver. R2018b using the gamultiobj function. The initial population was randomly generated within the defined design space, and successive generations were obtained using non-dominated sorting and distance-based diversity preservation [47,49,50].

2.6. Statistical Analysis

The normality of the data distribution was evaluated using the Shapiro–Wilk test. Results showed that most variables did not significantly deviate from normality ($p > 0.05$). Data are expressed as mean values ($n = 3$). Differences between sample means were analyzed using Tukey's HSD test. The statistical analysis was conducted using the STATISTICA V14.0.0.15 software package [51].

3. Results and Discussion

3.1. Mass Spectrometry of Plasma Source

In Figure 2, we present the integral mass spectrum recorded at a 6 mm distance from the plasma source. This spectrum, obtained using the RGA mode of the MBMS, provides an overview of all neutral species detected during operation of the plasma source in ambient air at 200 V input voltage controlled by the Variac. Apart from the species coming from the surrounding air, distinct alterations in RONS peaks were noticed in the rich spectrum of neutrals, e.g., NO (nitric oxide), NO_2 (nitrogen dioxide), O_3 (ozone), etc. When plasma is ignited, nitrous oxide is created in the plasma through the reaction $\cdot NO_2 + \cdot N \rightarrow N_2O + O\cdot$ [52]. At $m/z = 44$, the detected signal corresponded to the combined contribution of N_2O and CO_2, as these species share the same molecular mass and cannot be distinguished by quadrupole mass spectrometry. Such overlap at

m/z = 44 is a well-known limitation of residual gas and molecular beam mass spectrometry in atmospheric-pressure plasma diagnostics and has been reported in previous plasma chemistry studies [52–54]. Therefore, the recorded intensity at this mass-to-charge ratio represented the cumulative signal of both species rather than a single compound.

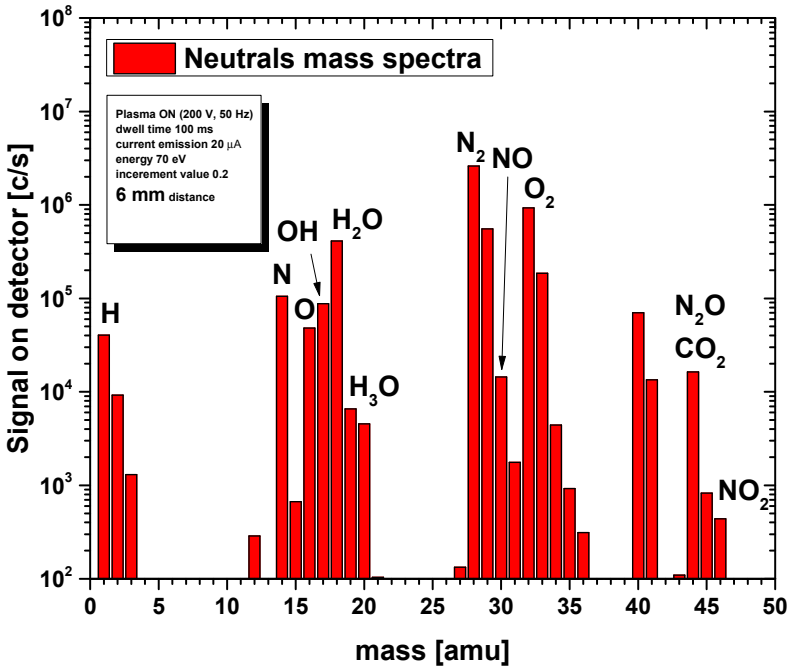

Figure 2. Complete neutral mass spectrum for 6 mm distance. Measurement was performed with the energy of electrons set to 70 eV in the ionization chamber. Data represent the averaged result of three independent measurements recorded under identical discharge conditions (n = 3).

Although atomic species such as H, N, and O were detected in the mass spectrum, their presence was mainly attributed to fragmentation in the ionization chamber of the mass spectrometer. Due to their extremely short lifetimes and limited transport distances at atmospheric pressure, it was hypothesized that these short-lived species play a minor role in DON degradation under the applied treatment conditions. Instead, longer-lived reactive species were more likely to contribute to the observed effects. Therefore, further analysis focused on longer-lived, oxidizing species such as NO, NO_2, and O_3, which were more likely to contribute to chemical interactions with the wheat flour matrix. Figures 3–5 illustrate the real-time evolution of NO, NO_2, and O_3 concentrations at different distances (6 mm, 21 mm, 36 mm, and 51 mm) between the plasma source and the mass spectrometer's sampling orifice. The y-axis is given as counts per second (c/s), which is proportional to the concentration of particular species and enables relative comparison between concentrations. The black vertical lines on the graphs separate the different operating conditions under which the signals were recorded. In the graphs, one can distinguish between plasma-off (0 V) and plasma-on (200 V) conditions. Also, the mass spectrometer was operated in 2 regimes: SL open—when it recorded the sum of both foreground (outside the mass spectrometer) and background (inside the mass spectrometer) signals, and SL closed—when only the background signal was acquired. The duration of recording of the mass spectrometer for each operating condition was set to 3 min to allow enough time to stabilize after changing the conditions.

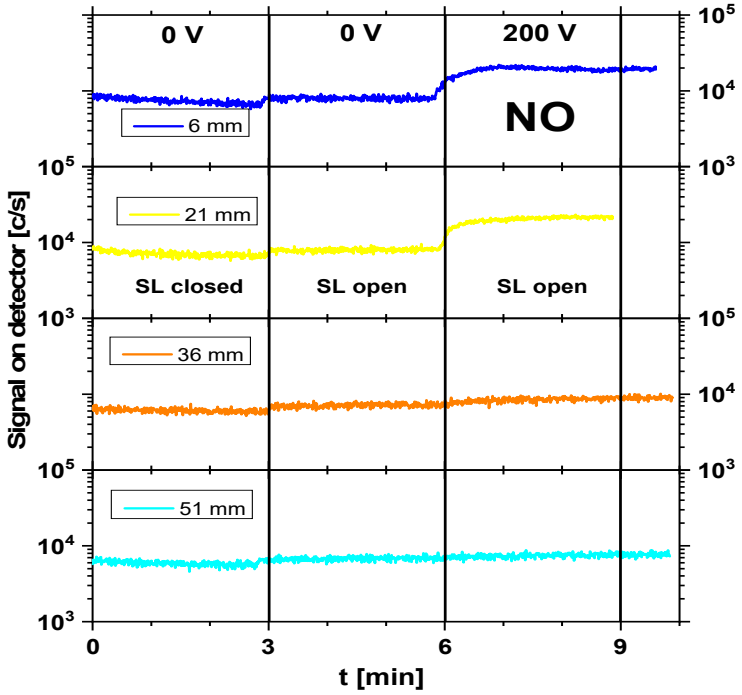

Figure 3. NO time evolution in cases of plasma-off (0 V) and plasma-on (200 V) conditions for different distances (6 mm, 21 mm, 36 mm, and 51 mm) from the plasma source to the mass spectrometer's sampling orifice. SDBD was operating at 200 V input voltage. SL = internal shutter of the MBMS (open/closed).

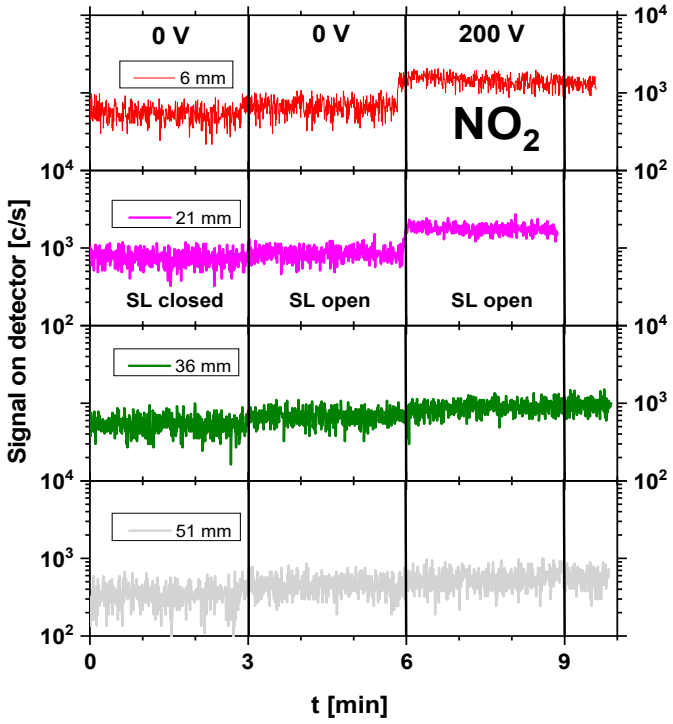

Figure 4. NO_2 time evolution in cases of plasma-off (0 V) and plasma-on (200 V) conditions for different distances (6 mm, 21 mm, 36 mm, and 51 mm) from the plasma source to the mass spectrometer's sampling orifice. SDBD was operating at 200 V input voltage. SL = internal shutter of the MBMS (open/closed).

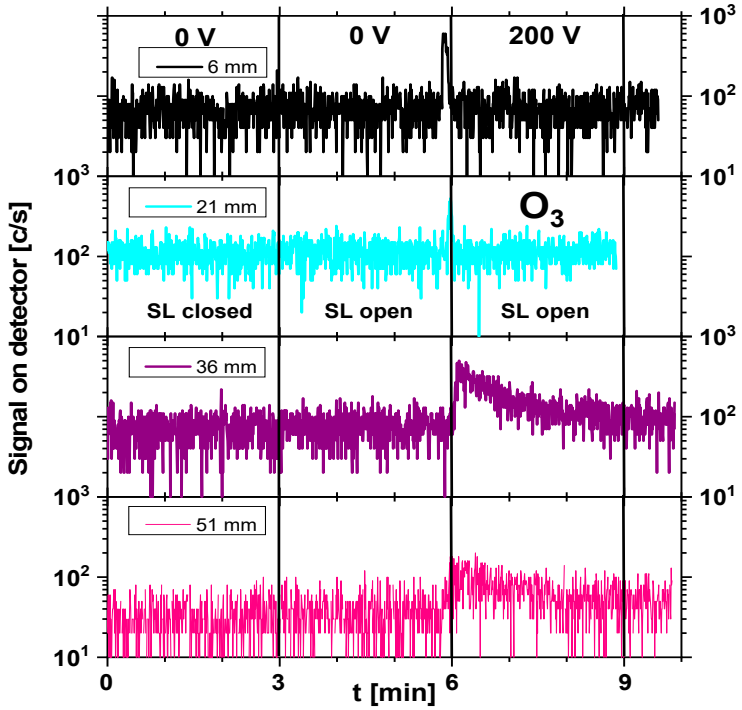

Figure 5. O_3 time evolution in cases of plasma-off (0 V) and plasma-on (200 V) conditions for different distances (6 mm, 21 mm, 36 mm, and 51 mm) from the plasma source to the mass spectrometer's sampling orifice. SDBD was operating at 200 V input voltage. SL = internal shutter of the MBMS (open/closed).

The NO signal (Figure 3) exhibited a strong dependence on the distance and plasma conditions. At 6 mm, the NO concentration was the highest, with an average value of around 19,000 c/s, indicating its primary formation near the plasma region. At 21 mm, the NO concentration reached its peak at around 20,100 c/s, suggesting a region of high NO stability before dilution began. As the distance increased, NO levels gradually decreased (8400 c/s at 36 mm and 7400 c/s at 51 mm), indicating dilution and oxidation into NO_2. Under plasma-on conditions (200 V), the NO signal was significantly stronger compared to that under plasma-off conditions (0 V), confirming its production in the discharge.

The NO_2 concentration followed an inverse trend to NO, increasing with distance (shown in Figure 4). At 6 mm, NO_2 was present at 1500 c/s, while at 21 mm, its concentration increased to 1800 c/s, showing active oxidation of NO. At 36 mm, NO_2 levels slightly decreased to 890 c/s, and at 51 mm, they further dropped to 560 c/s, likely due to secondary reactions reducing the NO_2 concentration in the sampled region. The difference between SL open and SL closed signals confirmed that NO_2 was actively formed in the plasma and not a background contaminant inside the spectrometer, particularly for the two shorter distances, which was apparent.

As shown in Figure 5, the O_3 concentration in all cases exhibited a significant peak at the moment of plasma inception (point at 6 min after start of the recording). At that moment, there was a gradual increase in the voltage by using a potentiometer on the power supply, and within 10 s, plasma covered the whole surface of the SDBD source. This behavior suggested that ozone formation was initially enhanced at a lower plasma power, while increasing the voltage up to 200 V led to a stabilization effect. At larger distances (36 mm and 51 mm), the ozone levels were the highest, indicating that its formation was favored further from the plasma source, where three-body recombination reactions stabilized O_3. Compared to Figure 3, which presents the NO signal, the measured intensities presented in Figures 4 and 5 were of the same order or lower than the NO signal intensity. To be able to

compare signals obtained for all three compounds, the settings of MS had to be the same. This led to a lower signal-to-noise ratio in the cases of NO_2 and O_3 molecules.

3.2. Reduction in DON Content by Atmospheric Cold Plasma Treatments

The results obtained through the analysis of DON content are presented in Table 1. Depending on the treatment applied, the reduction in DON content in wheat flour samples ranged from 33.1 ± 1.2% to 70 ± 4.4%. It can be observed that, by decreasing the distance of the plasma source from the flour sample and increasing the duration of treatment, the temperature increased while the moisture content in the flour decreased. The evaporated water present in the plasma-treated environment may theoretically participate in plasma-induced reactions, potentially leading to the formation of reactive species such as ·OH and H_2O_2, as suggested by established plasma chemistry mechanisms. In the present study, these species were not directly measured and are discussed here solely to support the theoretical interpretation of plasma–water interactions. Wheat kernels with optimal moisture content experienced more effective decreases in deoxynivalenol (DON) compared to drier kernels, demonstrating a factor that influences the degradation mechanism of DON [53].

Larger standard score (SS) values were assigned to more efficient DON reduction. SS analysis showed that the maximum reduction in DON content (71.0%) in wheat flour was obtained with the treatment performed at 51 mm for 150 s (Table 1). From the point of view of economic viability, the obtained optimal treatment that provided a satisfactory reduction rate (67.5%) of DON was achieved when wheat flour was treated for 60 s at a 36 mm distance from the plasma source.

The two main degradation pathways of mycotoxins induced by plasma are outlined in the literature. The double C=C bond undergoes addition reactions or it is reduced, and the lactone ring mainly undergoes ring opening and reduction of the carbonyl group. Additionally, reactions of oxidation, side chain shedding, and skeleton structure breaking are among the complex degradation mechanisms [54].

The specific formation pathways of DON degradation products and the mechanisms of each reaction site revealed that RONS mainly react with the C9=C10 double bond, the C12–C13 epoxy ring, and hydroxyl groups [55,56]. More specifically, O_3 attacks the C9–C10 double bond and oxidizes the allylic carbon at C8 [57]. This is in agreement with the results of O_3 concentrations in our study. At larger distances, ozone levels were the highest, and the treatment with the greatest DON reduction was at the distance of 51 mm. This effectively indicated that O_3 exhibited a considerable effect on DON reduction, as the results of mass spectrometry of the plasma source indicated that its formation was favored further from the plasma source.

This study achieved a 71% reduction rate of DON after just 2.5 min at a distance of 51 mm from the cold plasma source. As previously noted, O_3 levels were the highest at larger distances (36 mm and 51 mm), suggesting that its creation was more favorable farther away from the plasma source, where O_3 was stabilized by three-body recombination processes. Based on the above, we assume that the degradation of DON at a 51 mm distance from the cold plasma source from the sample was favored by the oxidation process, since O_3 is a strong oxidizing medium that can also cause the structure of DON to be destroyed [12]. Furthermore, Zhang et al. [54] identified ozone as a key oxidizing agent in their proposed degradation mechanism during DBD plasma treatment, confirming its role in disrupting the molecular structure of DON. These findings align with our results, where an increase in ozone levels corresponded to an increase in DON reduction.

The complex mixture of RONS generated by CAP, including hydroxyl radicals and ozone, leads to non-selective oxidation. Insights about the toxicity of the produced oxy-

genated compounds can be drawn from other advanced oxidation processes. For instance, a study on DON degradation by saturated aqueous ozone found that the resulting degradation products did not exhibit a significant change in overall toxicity compared to the parent DON molecule when assessed via in vitro cytotoxicity assays [58]. This suggests that the chemical structure of DON can be broken down by CAP, but also that the overall toxicological profile after CAP treatment may not be immediately exacerbated.

It is well-established that the reactive oxygen and nitrogen species (RONS) central to the degradation of deoxynivalenol (DON) can also initiate and propagate lipid oxidation in foods [59]. These effects of CAP also occur in wheat flour, leading to the oxidation of free fatty acids and phospholipids. However, it is noteworthy that at lower intensities of treatments, no significant lipid changes were detected [60]. CAP also can inactivate lipase and lipoxygenase in wheat flour, which can have beneficial effects [61]. All stated underscores the importance of process modulation to control changes in lipids in an intended direction.

Given that during this study neither the degradation products of DON nor the toxicity of the degradation products or changes in lipids were analyzed, future research should focus on these aspects.

3.3. Kinetics Model

The diagrams in Figure 6 depict the deoxynivalenol reduction rate during cold atmospheric plasma treatment in wheat flour using different distances of the cold plasma source to the sample, with data points representing sample treatment times from 30 to 180 s. The results demonstrate (Table 1, Figure 6) that both electrode distance (d) and treatment time (t) strongly influenced the efficiency of DON reduction in wheat flour subjected to cold atmospheric plasma treatment, with trends indicating a complex and nonlinear interaction between the two factors. At short distances (d = 6 mm), the plasma intensity was the highest and DON reduction generally improved with increasing treatment time, reaching a maximum at around 120 s (65.4%), after which efficiency declined, most likely due to the recombination of reactive species, energy saturation, or structural changes in the flour matrix that hindered further degradation.

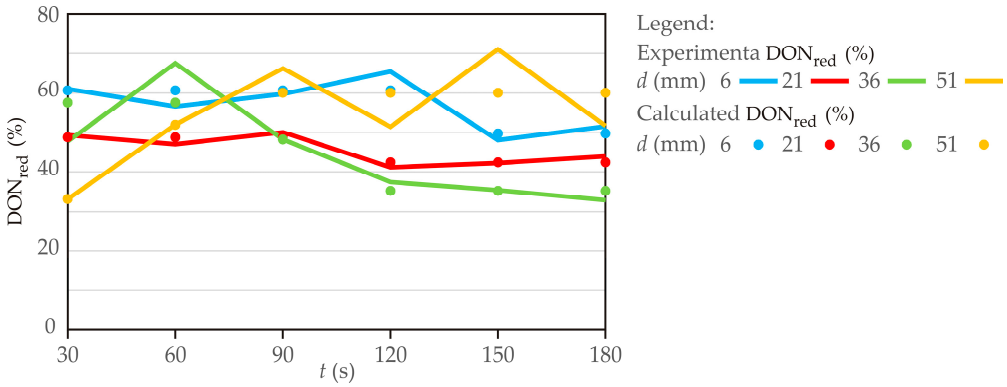

Figure 6. Kinetic modeling of deoxynivalenol reduction rate during cold atmospheric plasma treatment in wheat flour using different distances of the cold plasma source to the sample (points indicate calculated results, while lines represent experimentally obtained results).

At intermediate distances (21–36 mm), the reduction effect was noticeably lower (32–50%) and tended to decrease further with longer treatments, reflecting the weakening of plasma intensity as the distance increased. By contrast, at the largest electrode distance (d = 51 mm), the plasma effect became less predictable, with reductions ranging from only 33% at 30 s to the highest recorded value of 71% at 150 s, suggesting that extended

exposure was necessary to compensate for reduced plasma density, although treatment efficiency became less stable. These findings emphasized that both underexposure (short time or large distance) and overexposure (excessive treatment times) can lead to suboptimal performance, and that an optimal treatment window exists. Overall, the data highlighted that effective DON degradation can be achieved through a balance of plasma intensity and duration, with the most favorable outcomes observed at moderate treatment times (90–150 s) combined with either short or long electrode distances, while intermediate distances appeared less effective. This behavior underscores the importance of carefully optimizing cold plasma parameters, as excessive treatment may compromise efficiency while unnecessarily increasing processing time and energy consumption.

Table 2 presents the kinetic parameters (a_1, b_1, c_1, and d_1) of a four-parameter sigmoidal model (Equation (2)) describing DON reduction as a function of the cold plasma source to the sample in millimeters. The upper asymptote a_1, which denotes the highest predicted response level prior to the sigmoidal transition, decreased with increasing d_1 parameter, indicating a reduction in DON content at greater distances, with the lowest value observed at d_1 = 51 mm (33.1%). The inflection point c_1, representing the midpoint of the transition, also declined (134.5 to 59.5), suggesting that the transition occurred earlier as the distance increased. Furthermore, the slope parameter b_1 exhibited a decreasing trend (162.5 to 93.5), indicating a more gradual sigmoidal transition at greater distances. These findings suggested that DONred (%) was influenced by distance, potentially due to diffusion, degradation, or other spatial factors affecting its reduction.

Table 2. Kinetics model parameters for a four-parameter sigmoidal mathematical model of deoxynivalenol reduction rate during cold atmospheric plasma treatment.

d (mm)	6	21	36	51
d_1	49.7	42.4	35.2	60.0
a_1	60.7	48.8	57.6	33.1
c_1	134.5	103.9	90.3	59.5
b_1	162.5	100.4	98.2	93.5
r^2	0.775	0.872	0.749	0.659

The coefficient of determination (r^2) was used to assess the goodness of fit of the four-parameter sigmoidal model in describing the temporal kinetics of DON reduction. At d = 21 mm, the highest r^2 value (0.872) indicated the strongest agreement between the experimental data and the model predictions. By contrast, the lower r^2 value observed at d = 51 mm (0.659) reflected a reduced ability of the model to capture the observed variability in the data. Intermediate r^2 values at d = 6 mm (0.775) and d = 36 mm (0.749) indicated moderate model performance. The variation in r^2 values across treatment distances suggested distance-dependent differences in model fit, without implying specific underlying mechanisms.

3.4. ANN Model Results

The number of neurons in the hidden layer has a critical effect on model performance. To reduce the influence of random correlations caused by initial weight assumptions, each network topology was trained 100,000 times with different randomly initialized weights and biases, and the model with the lowest validation error was selected. This repetition was distinct from the number of training epochs in a single run. Among the tested configurations, the highest coefficient of determination (r^2) during training was obtained with nine hidden neurons (Figure 7a). The model was trained for 100 epochs, and the corresponding performance metrics—training accuracy and error (loss)—are presented

in Figure 7b. Accuracy consistently improved with increasing epochs and began to plateau between the 70th and 80th epoch, where the highest accuracy and lowest loss were recorded. After this point, only marginal gains in accuracy and minimal decreases in loss were observed, suggesting that extending training further would provide little benefit and could increase the risk of overfitting. Consequently, limiting training to approximately 70 epochs was considered optimal for achieving high accuracy while maintaining model generalizability (Figure 7b). After this point, only marginal gains in accuracy and further decreases in loss were observed, indicating the onset of overfitting. Consequently, limiting training to approximately 70 epochs was considered optimal for achieving high accuracy while minimizing the risk of overfitting (Figure 7b).

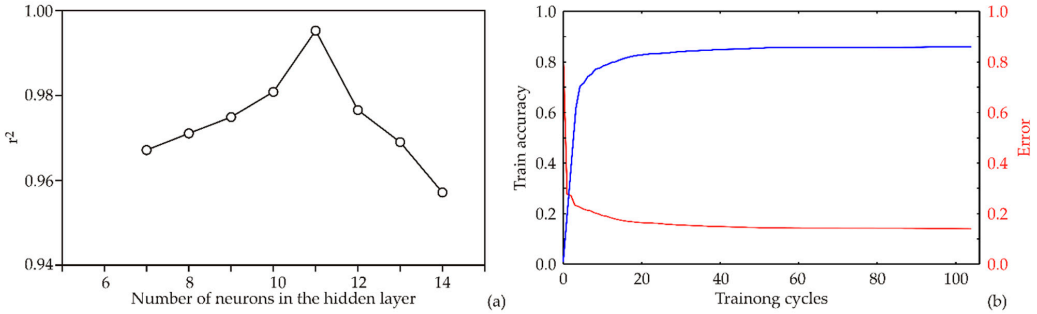

Figure 7. ANN calculation: (**a**) The dependence of the r^2 value of the number of neurons in the hidden layer in the ANN model, (**b**) Training results per epoch.

The acquired optimal neural network model showed a good generalization capability for the experimental data and could be used to accurately predict the reduction in DON content, moisture content of wheat flour samples after treatment, and temperature of wheat flour samples after treatment based on the distance of the cold plasma source to the sample and process time. Network MLP 8-11-3 obtained the highest values of r^2 during the training cycle. The r^2 values for the output variables were 0.999, 0.996, and 0.996, respectively (Table 3).

Table 3. Artificial neural network model summary (performance and errors), for training, testing, and validation cycles.

Network Name	Performance			Error			Training Algorithm	Error Function	Hidden Activation	Output Activation
	Train	Test	Valid	Train	Test	Valid				
MLP 8-11-3	0.997	0.998	0.999	0.275	0.189	0.203	BFGS 4179	SOS	Logistic	Identity

The performance term represents the coefficient of determination (r^2), indicating the goodness of fit between experimental and predicted values. The error terms correspond to prediction error metrics (SOS), which quantify the deviation between model outputs and measured data and thus reflect the predictive accuracy of the ANN model.

The obtained ANN model for the prediction of output variables was complex (157 weights–biases) because of the high nonlinearity of the observed system [62,63]. The slight inconsistency in r^2 values among the predicted parameters likely reflected differences in the complexity of underlying relationships between input variables and each output. DON reduction, for instance, may be more directly influenced by distance and time than moisture content or temperature, which can be affected by additional uncontrolled factors (e.g., ambient humidity and sample variability). All r^2 values exceeded 0.95, indicating excellent predictive performance of the ANN model across the evaluated datasets.

The goodness of fit between experimental measurements and model-calculated outputs, represented as ANN performance (sum of r^2 between measured and calculated output variables), during the training, testing, and validation steps are shown in Table 4.

Table 4. The "goodness of fit" tests for the developed ANN model.

Output Variable	χ^2	RMSE	MBE	MPE	SSE	AARD	r^2
DON_{red}	0.304	0.515	2.9×10^{-5}	0.703	6.376	8.103	0.998
MC	0.002	0.040	2.9×10^{-6}	0.231	0.039	1.660	0.993
T	0.324	0.533	-3.9×10^{-5}	1.372	6.806	10.336	0.993

DON_{red}—reduction of deoxynivalenol; MC—moisture content of wheat flour samples after treatment; T—temperature of wheat flour samples after treatment.

Artificial neural network (ANN) models demonstrate clear advantages over traditional kinetic models due to their ability to capture complex, nonlinear relationships between multiple input variables (treatment time and distance from plasma source) and output responses (DON reduction, moisture content, and temperature). Unlike kinetic models, which require predefined mathematical equations based on assumptions of reaction order or rate-limiting steps, ANN models learn directly from experimental data without assuming a specific functional form. The ANN model predicted the experimental variables reasonably well for a broad range of process variables. For the ANN model, the predicted values were very close to the measured values in most cases in terms of r^2 values. The performance of the ANN model was evaluated using multiple goodness-of-fit metrics, including RMSE, MBE, MPE, SSE, AARD, and r^2 (Table 4). These metrics quantify the deviation between predicted and experimental values and provide a statistically valid assessment of model accuracy and predictive performance. Comparisons to experimental error were removed, as SSE and other model-dependent metrics cannot be directly interpreted as experimental uncertainty. The ANN model had insignificant lack of fit tests, which meant that the model satisfactorily predicted output variables. A high r^2 value was indicative that the variation was accounted for and that the data fit the proposed model satisfactorily [64,65].

The residuals from a fitted model were observed and the corresponding prediction of the response was computed using the ANN regression model. Residuals represent the differences between predicted and experimental values. Their random distribution around zero indicates that the unexplained variance behaves randomly and that no systematic patterns remain, confirming that the ANN model adequately captures the underlying relationship between the explanatory and response variables. The residuals appeared to behave randomly, which suggested that the model fit the data well (Table 5).

Table 5. The residual analysis tests for the developed ANN model.

Output Variable	Skew	Kurt	StDev	Var
DON_{red}	−1.039	2.962	0.527	0.277
MC	0.665	1.069	0.041	0.002
T	0.237	−0.329	0.544	0.296

DONred—reduction in deoxynivalenol content; MC—moisture content of wheat flour samples after treatment; T—temperature of wheat flour samples after treatment.

Residual analysis of the developed model was also performed. Skewness measures the deviation of the distribution from normal symmetry. If the skewness is clearly different from zero, then the distribution is asymmetrical, while normal distributions are perfectly symmetrical. Kurtosis measures the "peakedness" of a distribution. If the Kurtosis is clearly different from zero, then the distribution is either flatter or more peaked than normal; the Kurtosis of a normal distribution is zero. A high r^2 value indicates that a large proportion of the variance in the experimental data is explained by the model; however, satisfactory model performance also requires randomly distributed residuals, low RMSE, and unbiased MBE. Together, these metrics confirmed that the ANN model adequately

captured the relationship between input and output variables [62,66]. The ANN model predicted experimental variables reasonably well for a broad range of process variables, as shown in Figure 8.

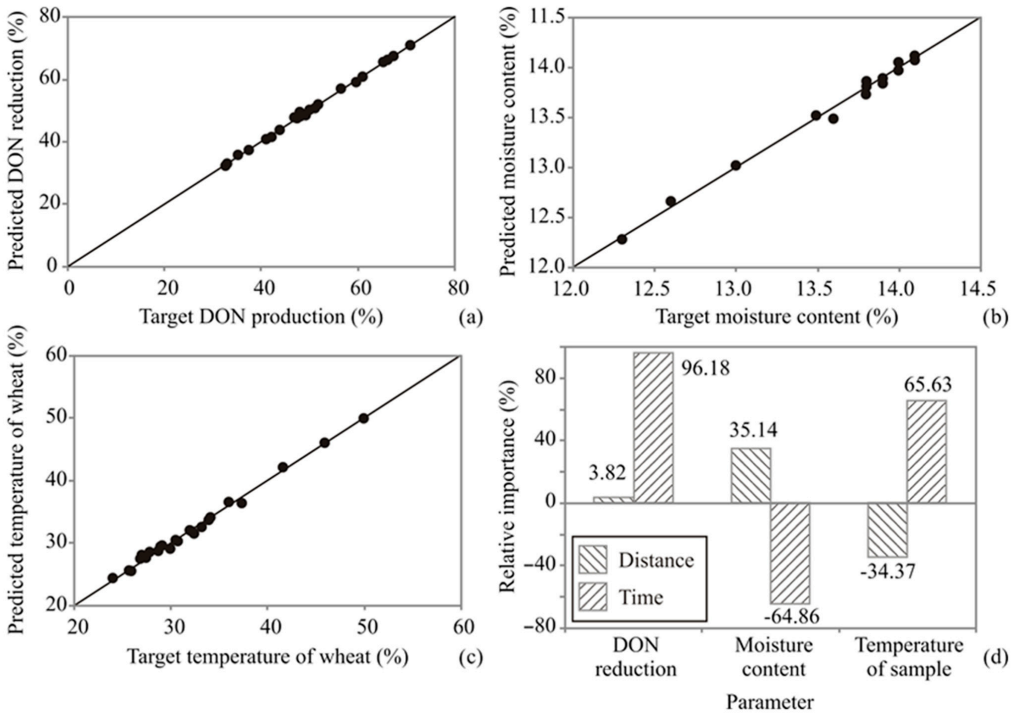

Figure 8. Experimentally measured and ANN model-predicted values of (**a**) reduction in DON content, (**b**) moisture of wheat flour samples after treatment, (**c**) temperature of wheat flour samples after treatment, and (**d**) the relative importance of input variables on outputs, determined using Yoon's interpretation method.

For the ANN model, the predicted values were very close to the measured values in most cases, in terms of r^2 values. The SOS values obtained with the ANN model were of the same order of magnitude as experimental errors for output variables reported in the literature [38,42]. The ANN model had insignificant lack of fit tests, which meant that the model satisfactorily predicted output variables. A high r^2 value was indicative that the variation was accounted for and that the data fit the proposed model satisfactorily [62,63].

In practical, real-world settings, however, several factors can affect the success the ANN prediction rate. While the ANN model provided accurate predictions under controlled experimental conditions, variations in the grain matrix (such as homogeneity of the sample, wheat variety, and initial DON levels), ambient environmental factors (relative humidity and temperature), and plasma treatment system stability (plasma intensity or uniformity) may lead to fluctuations in the effectiveness of CAP treatment. The ANN model can be expanded in future studies to predict reductions in the levels of various mycotoxins across different grains or food matrices, offering a generalized tool for optimizing plasma treatment. It could also be integrated into industrial-scale CAP treatments to ensure precise control over factors like plasma source distance and exposure time while maintaining effective mycotoxin degradation and product quality. Additionally, the model could be used in real-time monitoring systems for dynamic adjustments during production. Future research may incorporate variables like relative humidity or flour composition to improve the ANN model's predictive accuracy and broaden its applicability. The ANN model could help identify optimal treatment conditions for different agricultural products, enhancing the versatility of CAP as a decontamination method.

3.4.1. Global Sensitivity Analysis—Yoon's Interpretation Method

In this section, the influence of input variables on the reduction in DON content, moisture content of wheat flour samples after treatment, and temperature of wheat flour samples after treatment, based on the distance of the cold plasma source to the sample and process time, was studied. The sensitivity analysis revealed that time was the predominant factor influencing all observed parameters, exerting a profound positive effect on DON reduction (96.18%) and sample temperature (65.63%), while showing a strong negative correlation with moisture content (−64.86%). Conversely, distance demonstrated a relatively minor influence, contributing most significantly to moisture content (35.14%) and temperature regulation (−34.37%) but remaining negligible (3.82%) in the context of DON degradation. These results indicated that while increasing processing duration is the most effective strategy for maximizing toxin reduction and thermal energy transfer, it simultaneously drives significant dehydration; meanwhile, adjusting the distance serves as a secondary control mechanism for modulating the sample's physical state (moisture and heat) without substantially altering the efficacy of chemical reduction.

3.4.2. Multi-Objective Optimization of the Outputs of the ANN

One of the main goals in this investigation was to maximize results, and these numerical tasks were solved using the MOO calculation in Matlab. The MOO procedure was defined by simultaneously maximizing reduction in DON content and minimizing moisture content and temperature in the ANN model.

The reduction in DON content is critical for improving flour safety, as high DON levels pose health risks. However, changes in moisture content and temperature during CAP treatment can influence flour quality parameters such as color and baking performance. Excessive drying or heating may negatively affect protein functionality or starch behavior. Thus, while maximizing DON reduction is desirable, it is essential to optimize CAP parameters to maintain desirable flour quality characteristics. Constraints used in the optimization procedure were applied within the experimental range of parameters. The number of generations reached 569 for the ANN model, while the size of the population was set to 200 for each input variable. The number of points on the Pareto front was 49 for the ANN model. The calculated maximum reduction in DON content during the plasma treatment was 71.0%, and the minimal moisture content and temperature were 12.5% and 30.7 °C, respectively. The distance was 51 mm, while the process time reached 168.4 s.

4. Conclusions

This study presents a novel application of CAP treatment of wheat flour, demonstrating significant DON reduction in the direct and static treatment of wheat flour as a powder matrix. The highest observed reduction in DON content (71%) occurred at a treatment distance of 51 mm from the plasma source, with a duration of 150 s. Under these conditions, the moisture content and the temperature of wheat flour samples after treatment were 13.9% and 30.8 °C, respectively. Mass spectrometry measurements of the plasma showed the presence of RONS in plasma. In particular, the creation and existence of O_3, NO, and NO_2 species at different distances between the active plasma zone (SDBD surface) and the flour sample were analyzed. As expected, increasing the distance between the plasma source and the sample reduced the concentration of RONS. However, the relative decrease was more pronounced for NO and NO_2 species in comparison to O_3. Additionally, O_3 production rose during the transition period, when the input voltage is increased from zero to the operation voltage, thus resulting in higher overall production of ozone. The observed variability in reduction efficiency across different treatment times and distances suggests that matrix-related factors, such as moisture content and relative humidity, may also influ-

ence plasma efficacy. Additionally, since all samples in this study were spiked with a single DON concentration, further research is needed to determine whether the initial toxin level in naturally contaminated wheat flour affects reduction efficiency under plasma treatment. The artificial neural network model was shown to be adequate for the prediction of output variables (the r^2 values during the training cycle for these variables were: 0.999, 0.996, and 0.996, respectively). By utilizing the ANN model, we were able to identify optimal conditions for maximizing DON reduction (71%) while maintaining acceptable flour quality. This highlights the advantages of ANNs in guiding experimental design and optimizing treatment parameters, which would be difficult to achieve using traditional experimental methods alone. While these findings are promising, the path to industrial application requires addressing clear limitations identified in this study. Future work must validate the treatment's efficacy on naturally contaminated wheat flour, moving beyond the controlled model of artificially spiked samples used in this study. Although we monitored key RONS, a mechanistic validation of their role in the detoxification process and a comprehensive toxicological assessment of any resulting degradation products are needed to guarantee food safety. Finally, the influence of humidity, a factor not fully controlled in this study, must be taken into account and characterized, as it is an important factor affecting plasma chemistry. Therefore, for successful industrial-scale adoption of CAP technology, resolving these scientific questions is a prerequisite for tackling the broader regulatory and technical challenges in scaling CAP technology for the wheat processing industry.

Author Contributions: Conceptualization, E.J.H., L.P. and M.V.; validation, M.V. and E.J.H.; formal analysis, L.P. and E.J.H.; investigation, M.V., E.J.H., N.S., N.Š. and N.P.; resources, E.J.H., M.V., N.P. and N.Š.; data curation, M.V. and E.J.H.; writing—original draft preparation, E.J.H., M.V., N.S., N.Š. and L.P.; writing—review and editing, M.V., E.J.H., L.P., N.S., N.P. and N.Š.; project administration, E.J.H.; supervision, E.J.H.; funding acquisition, E.J.H., N.P. and M.V. All authors have read and agreed to the published version of the manuscript.

Funding: This research was funded by Provincial Secretariat for Higher Education and Scientific Research Activities, Autonomous Province of Vojvodina, Republic of Serbia (grant number No. 000636705 2024 09418 003 000 000 001/2) and by the Ministry of Science, Technological Development and Innovation of the Republic of Serbia (grant number No. 451-03-68/2025-14/200024 and No. 451-03-136/2025-03/200222).

Institutional Review Board Statement: Not applicable.

Informed Consent Statement: Not applicable.

Data Availability Statement: The original contributions presented in the study are included in the article; further inquiries can be directed to the corresponding author.

Conflicts of Interest: The authors declare no conflicts of interest.

Abbreviations

The following abbreviations are used in this manuscript:

DON	Deoxynivalenol
ANN	Artificial neural network
HPLC	High-performance liquid chromatography
DAD	Diode array detector
MOO	Multi-objective optimization
MLP	Multi-layer perceptron

References

1. Fung, F.; Clark, R.F. Health effects of mycotoxins: A toxicological overview. *J. Toxicol. Clin. Toxicol.* **2004**, *42*, 217–234. [CrossRef] [PubMed]
2. Yazar, S.; Omurtag, G.Z. Fumonisins, trichothecenes and zearalenone in cereals. *Int. J. Mol. Sci.* **2008**, *9*, 2062–2090. [CrossRef]
3. Mishra, S.; Srivastava, S.; Dewangan, J.; Divakar, A.; Kumar Rath, S. Global occurrence of deoxynivalenol in food commodities and exposure risk assessment in humans in the last decade: A survey. *Rev. Food Sci. Nutr.* **2019**, *60*, 1346–1374. [CrossRef]
4. Foreign Agricultural Service, USDA. Production—Wheat. 2025. Available online: https://www.fas.usda.gov/data/production/commodity/0410000 (accessed on 23 November 2025).
5. Pestka, J.J.; Zhou, H.R.; Moon, Y.; Chung, Y.J. Cellular and molecular mechanisms for immune modulation by deoxynivalenol and other trichothecenes: Unraveling a paradox. *Toxicol. Lett.* **2004**, *153*, 61–73. [CrossRef]
6. Pestka, J.J.; Smolinski, A.T. Deoxynivalenol: Toxicology and potential effects on humans. *J. Toxicol. Environ. Health—B* **2005**, *8*, 39–69. [CrossRef]
7. Pestka, J.J. Deoxynivalenol: Toxicity, mechanisms and animal health risks. *Anim. Feed Sci. Technol.* **2007**, *137*, 283–298. [CrossRef]
8. Hou, S.; Ma, J.; Cheng, Y.; Wang, H.; Sun, J.; Yan, Y. The toxicity mechanisms of DON to humans and animals and potential biological treatment strategies. *Crit. Rev. Food Sci. Nutr.* **2023**, *63*, 790–812. [CrossRef]
9. IARC. Some naturally occurring substances: Food items and constituents, heterocyclic aromatic amines and mycotoxins. In *Monographs on the Evaluation of Carcinogenic Risks to Humans*; International Agency for Research on Cancer: Lyon, France, 1993; Volume 56, pp. 1–599.
10. *EC 2023/915*; Commission Regulation (EU) 2023/915 of 25 April 2023 on Maximum Levels for Certain Contaminants in Food and Repealing Regulation (EC) No 1881/2006. European Commission: Luxembourg, 2023.
11. *EC 2024/1022*; Commission Regulation (EU) 2024/1022 of 8 April 2024 Amending Regulation (EU) 2023/915 as Regards Maximum Levels of Deoxynivalenol in Food. European Commission: Luxembourg, 2024. Available online: http://data.europa.eu/eli/reg/2024/1022/oj (accessed on 23 November 2025).
12. Zhang, Y.; Ouyang, B.; Zhang, W.; Guang, C.; Xu, W.; Mu, W. Deoxynivalenol: Occurrence, toxicity, and degradation. *Food Control* **2024**, *155*, 110027. [CrossRef]
13. Harikrishna, S.; Anil, P.P.; Shams, R.; Dash, K.K. Cold plasma as an emerging nonthermal technology for food processing: A comprehensive review. *J. Agric. Food Res.* **2023**, *14*, 100747. [CrossRef]
14. Capelli, F.; Laghi, G.; Laurita, R.; Puač, N.; Gherardi, M. Recommendations and guidelines for the description of cold atmospheric plasma devices in studies of their application in food processing. *Innov. Food Sci. Emerg.* **2024**, *97*, 103818. [CrossRef]
15. Zhang, M.; Ye, Z.; Xing, C.; Chen, H.; Zhang, J.; Yan, W. Degradation of deoxynivalenol in wheat by double dielectric barrier discharge cold plasma: Identification and pathway of degradation products. *J. Sci. Food Agric.* **2023**, *103*, 2347–2356. [CrossRef]
16. Chen, X.; Qiu, Y.; Zhang, J.; Guo, Y.; Ding, Y.; Lyu, F. Degradation efficiency and products of deoxynivalenol treated by cold plasma and its application in wheat. *Food Control* **2022**, *136*, 108874. [CrossRef]
17. Huang, S.; Li, L.; Zhou, G.; Liu, X.; Guo, J. Decontamination of deoxynivalenol in Indica rice by cold plasma and the determination of major degradation products. *Food Control* **2025**, *173*, 111180. [CrossRef]
18. Bilea, F.; Garcia-Vaquero, M.; Magureanu, M.; Mihaila, I.; Mildažienė, V.; Mozetič, M.; Pawłat, J.; Primc, G.; Puač, N.; Robert, E.; et al. Non-thermal plasma as environmentally-friendly technology for agriculture: A review and roadmap. *Crit. Rev. Plant Sci.* **2024**, *43*, 428–486. [CrossRef]
19. Bhullar, M.; Gavahian, M.; Misra, N.N. Cold plasma processing: Methods and applications in study of food decontamination. In *Emerging Food Processing Technologies*; Springer: New York, NY, USA, 2022; pp. 31–45.
20. Benedikt, J.; Kersten, H.; Piel, A. Foundations of measurement of electrons, ions and species fluxes toward surfaces in low-temperature plasmas. *Plasma Sources Sci. Technol.* **2021**, *30*, 033001. [CrossRef]
21. Maletić, D.; Puač, N.; Lazović, S.; Malović, G.; Gans, T.; Schulz-Von Der Gathen, V.; Petrović, Z.L. Detection of atomic oxygen and nitrogen created in a radio-frequency-driven micro-scale atmospheric pressure plasma jet using mass spectrometry. *Plasma Phys. Control. Fusion* **2012**, *54*, 124046. [CrossRef]
22. Domonkos, M.; Tichá, P.; Trejbal, J.; Demo, P. Applications of cold atmospheric pressure plasma technology in medicine, agriculture and food industry. *Appl. Sci.* **2021**, *11*, 4809. [CrossRef]
23. Gao, G.; Wu, J.; Wei, Z.; Li, X. Effects of low-pressure radio-frequency cold plasma on the biochemical parameters and fatty acid profile of wheat flours. *Cereal Chem.* **2023**, *100*, 393–413. [CrossRef]
24. Khan, M.I.H.; Sablani, S.S.; Nayak, R.; Gu, Y. Machine learning-based modeling in food processing applications: State of the art. *Compr. Rev. Food Sci. Food Saf.* **2022**, *21*, 1409–1438. [CrossRef] [PubMed]
25. He, M.; Bai, R.; Tan, S.; Liu, D.; Zhang, Y. Data-driven plasma science: A new perspective on modeling, diagnostics, and applications through machine learning. *Plasma Process. Polym.* **2024**, *21*, 2400020. [CrossRef]

26. Boateng, I.D. Recent processing of fruits and vegetables using emerging thermal and non-thermal technologies. A critical review of their potentialities and limitations on bioactives, structure, and drying performance. *Crit. Rev. Food Sci. Nutr.* **2024**, *64*, 4240–4274. [CrossRef]
27. Lin, L.; Gershman, S.; Raitses, Y.; Keidar, M. Data-driven prediction of the output composition of an atmospheric pressure plasma jet. *J. Phys. D Appl. Phys.* **2023**, *57*, 015203. [CrossRef]
28. Ahmed, A.R.; Aleid, S.M.; Mohammed, M. Impact of modified atmosphere packaging conditions on quality of dates: Experimental study and predictive analysis using artificial neural networks. *Foods* **2023**, *12*, 3811. [CrossRef]
29. Mateo, F.; Mateo, E.M.; Tarazona, A.; García-Esparza, M.Á.; Soria, J.M.; Jiménez, M. New Strategies and Artificial Intelligence Methods for the Mitigation of Toxigenic Fungi and Mycotoxins in Foods. *Toxins* **2025**, *17*, 231. [CrossRef]
30. Janić Hajnal, E.; Vukić, M.; Pezo, L.; Orčić, D.; Puač, N.; Škoro, N.; Milidrag, A.; Šoronja Simović, D. Effect of atmospheric cold plasma treatments on reduction of *Alternaria* toxins content in wheat flour. *Toxins* **2019**, *11*, 704. [CrossRef] [PubMed]
31. Čech, J.; Brablec, A.; Černák, M.; Puač, N.; Selaković, N.; Petrović, Z.L. Mass spectrometry of diffuse coplanar surface barrier discharge: Influence of discharge frequency and oxygen content in N_2/O_2 mixture. *Eur. Phys. J. D* **2017**, *71*, 27. [CrossRef]
32. *EC 401/2006*; Commission Regulation (EC) No 401/2006 of 23 February 2006, Laying Down the Methods of Sampling and Analysis for the Official Control of the Levels of Mycotoxins in Foodstuffs. European Commission: Luxembourg, 2006.
33. *CEN/TR 16059*; Technical Report of 19 June 2010, Food Analysis-Performance Criteria for Single Laboratory Vali-Dated Methods of Analysis for the Determination of Mycotoxins. Menagmente Centre, European Committee for Standardization: Brussels, Belgium, 2010.
34. Johnson, D.P.; Stanforth, A.; Lulla, V.; Luber, G. Developing an applied extreme heat vulnerability index utilizing socioeconomic and environmental data. *Appl. Geogr.* **2012**, *35*, 23–31. [CrossRef]
35. Yun, T.S.; Jeong, Y.J.; Han, T.S.; Youm, K.S. Evaluation of thermal conductivity for thermally insulated concretes. *Energy Build.* **2013**, *61*, 125–132. [CrossRef]
36. Kleijnen, J.P.C. Design and Analysis of Simulation Experiments. In *Statistics and Simulation*; Pilz, J., Rasch, D., Melas, V., Moder, K., Eds.; IWS 2015; Springer Proceedings in Mathematics & Statistics; Springer International Publishing: Cham, Switzerland, 2018; Volume 231, pp. 3–22.
37. Pavlić, B.; Pezo, L.; Marić, B.; Tukuljac, L.P.; Zeković, Z.; Solarov, M.B.; Teslić, N. Supercritical fluid extraction of raspberry seed oil: Experiments and modelling. *J. Supercrit. Fluids* **2020**, *157*, 104687. [CrossRef]
38. Kollo, T.; von Rosen, D. *Advanced Multivariate Statistics with Matrices*; Springer: Dordrecht, The Netherlands, 2005.
39. Pezo, L.L.; Ćurčić, B.L.; Filipović, V.S.; Nićetin, M.R.; Koprivica, G.B.; Mišljenović, N.M.; Lević, L.B. Artificial neural network model of pork meat cubes osmotic dehydratation. *Hem. Ind.* **2013**, *67*, 465–475. [CrossRef]
40. Ochoa-Martínez, C.I.; Ayala-Aponte, A.A. Prediction of mass transfer kinetics during osmotic dehydration of apples using neural networks. *LWT-Food Sci. Technol.* **2007**, *40*, 638–645. [CrossRef]
41. Berrueta, L.A.; Alonso-Salces, R.M.; Héberger, K. Supervised pattern recognition in food analysis. *J. Chromatogr. A* **2007**, *1158*, 196–214. [CrossRef]
42. Doumpos, M.; Zopounidis, C. Preference disaggregation and statistical learning for multicriteria decision support: A review. *Eur. J. Oper. Res.* **2011**, *209*, 203–214. [CrossRef]
43. Taylor, B.J. *Methods and Procedures for the Verification and Validation of Artificial Neural Networks*; Springer Science & Business Media: New York, NY, USA, 2006.
44. Yoon, Y.; Swales, G., Jr.; Margavio, T.M. A comparison of discriminant analysis versus artificial neural networks. *J. Oper. Res. Soc.* **1993**, *44*, 51–60. [CrossRef]
45. Brlek, T.; Pezo, L.; Voća, N.; Krička, T.; Vukmirović, Đ.; Čolović, R.; Bodroža-Solarov, M. Chemometric approach for assessing the quality of olive cake pellets. *Fuel Process. Technol.* **2013**, *116*, 250–256. [CrossRef]
46. Aćimović, M.; Pezo, L.; Tešević, V.; Čabarkapa, I.; Todosijević, M. QSRR Model for predicting retention indices of Satureja kitaibelii Wierzb. ex Heuff. essential oil composition. *Ind. Crop. Prod.* **2020**, *154*, 112752. [CrossRef]
47. Kojić, P.; Omorjan, R. Predicting hydrodynamic parameters and volumetric gas–liquid mass transfer coefficient in an external-loop airlift reactor by support vector regression. *Chem. Eng. Res. Des.* **2017**, *125*, 398–407. [CrossRef]
48. Goldberg, D.E. *Genetic Algorithms in Search, Optimisation and Machine Learning*; Addison-Wesley: Boston, MA, USA, 1989.
49. Dharma, S.M.H.H.; Masjuki, H.H.; Ong, H.C.; Sebayang, A.H.; Silitonga, A.S.; Kusumo, F.; Mahlia, T.M.I. Optimization of biodiesel production process for mixed Jatropha curcas–Ceiba pentandra biodiesel using response surface methodology. *Energy Convers. Manag.* **2016**, *115*, 178–190. [CrossRef]
50. Silitonga, A.S.; Mahlia, T.M.I.; Shamsuddin, A.H.; Ong, H.C.; Milano, J.; Kusumo, F.; Sebayang, A.H.; Dharma, S.; Ibrahim, H.; Husin, H.; et al. Optimization of *Cerbera manghas* biodiesel production using artificial neural networks integrated with ant colony optimization. *Energies* **2019**, *12*, 3811. [CrossRef]
51. *STATISTICA (Data Analysis Software System)*, version 14.0.0.15; TIBCO Stat-Soft Inc.: Tulsa, OK, USA, 2020.

52. Bradu, C.; Kutasi, K.; Magureanu, M.; Puač, N.; Živković, S. Reactive nitrogen species in plasma-activated water: Generation, chemistry and application in agriculture. *J. Phys. D Appl. Phys.* **2020**, *53*, 223001. [CrossRef]
53. Rashid, M.T.; Muzaffar, N.; Jatoi, M.A.; Usman, H.; Liu, K. Cold Plasma for Mycotoxin Mitigation in Cereals and Pseudocereals: Mechanisms, Safety, and Processing Aspects. *Food Rev. Int.* **2025**, 1–27. [CrossRef]
54. Wang, X.; Li, S.; Li, L.; Ding, Y.; Xu, T.; Liu, J.; Li, Q.; Zhao, T.; Zhang, Y. Mycotoxins degradation by reactive oxygen species in plasma: Reactive molecular dynamics insights. *LWT-Food Sci. Technol.* **2023**, *184*, 115058. [CrossRef]
55. Li, S.; Wang, X.; Li, L.; Liu, J.; Ding, Y.; Zhao, T.; Zhang, Y. Atomic-scale simulations of the deoxynivalenol degradation induced by reactive oxygen plasma species. *Food Res. Int.* **2022**, *162*, 111939. [CrossRef] [PubMed]
56. Zhu, S.; Shen, F.; Zhang, Y.; Hu, Q.; Yuan, J.; Ji, K.; Jiang, X.; Chen, J. Unraveling the degradation of deoxynivalenol in wheat by sodium bicarbonate assisted cold plasma: A combined reactive molecular dynamics simulation and experimental validation. *Food Chem.* **2025**, *487*, 144785. [CrossRef]
57. Molina-Hernandez, J.B.; Grande-Tovar, C.D.; Neri, L.; Delgado-Ospina, J.; Rinaldi, M.; Cordero-Bueso, G.A.; Chaves-López, C. Enhancing postharvest food safety: The essential role of non-thermal technologies in combating fungal contamination and mycotoxins. *Front. Microbiol.* **2025**, *16*, 1543716. [CrossRef]
58. Yang, Y.; Xu, Y.; Wu, S.; Qiu, T.; Blaženović, I.; Sun, J.; Zhang, Y.; Sun, X.; Ji, J. Evaluation of the toxicity and chemical alterations of deoxynivalenol degradation products under ozone treatment. *Food Control* **2021**, *124*, 107937. [CrossRef]
59. Gavahian, M.; Chu, Y.H.; Khaneghah, A.M.; Barba, F.J.; Misra, N.N. A critical analysis of the cold plasma induced lipid oxidation in foods. *Trends Food Sci. Technol.* **2018**, *77*, 32–41. [CrossRef]
60. Bahrami, N.; Bayliss, D.; Chope, G.; Penson, S.; Perehinec, T.; Fisk, I.D. Cold plasma: A new technology to modify wheat flour functionality. *Food Chem.* **2016**, *202*, 247–253. [CrossRef]
61. Chakraborty, S.; Pulivarthi, M.K.; Raj, A.S.; Prakash, S.D.; Bommina, H.; Siliveru, K. Inactivation of lipase and lipoxygenase in whole wheat flour using atmospheric cold plasma and steam treatments: Kinetics, mechanism, and impact on its compositional properties. *J. Cereal Sci.* **2024**, *117*, 103889. [CrossRef]
62. Montgomery, D.C. *Design and Analysis of Experiments*, 2nd ed.; John Wiley and Sons: New York, NY, USA, 1984.
63. Chattopadhyay, P.B.; Rangarajan, R. Application of ANN in sketching spatial nonlinearity of unconfined aquifer in agricultural basin. *Agric. Water Manag.* **2014**, *133*, 81–91. [CrossRef]
64. Erbay, Z.; Icier, F. Optimization of hot air drying of olive leaves using response surface methodology. *J. Food Eng.* **2009**, *91*, 533–541. [CrossRef]
65. Turanyi, T.; Tomlin, A.S. *Analysis of Kinetics Reaction Mechanisms*; Springer: Berlin/Heidelberg, Germany, 2014.
66. Madamba, P.S. The response surface methodology: An application to optimize dehydration operations of selected agricultural crops. *LWT-Food Sci. Technol.* **2002**, *35*, 584–592. [CrossRef]

Book of abstracts

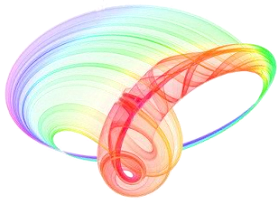

PHOTONICA2021

VIII International School and Conference on Photonics

& HEMMAGINERO workshop

23 - 27 August 2021,

Belgrade, Serbia

Editors

Mihailo Rabasović, Marina Lekić and Aleksandar Krmpot

Institute of Physics Belgrade, Serbia

Belgrade, 2021

ABSTRACTS OF TUTORIAL, KEYNOTE, INVITED LECTURES, PROGRESS REPORTS AND CONTRIBUTED PAPERS

of

VIII International School and Conference on Photonics PHOTONICA2021

23 - 27 August 2021

Belgrade Serbia

Editors
Mihailo Rabasović, Marina Lekić and Aleksandar Krmpot

Publisher
Institute of Physics Belgrade
Pregrevica 118
11080 Belgrade, Serbia

Printed by
Serbian Academy of Sciences and Arts

Number of copies
200

ISBN 978-86-82441-53-3

CIP - Каталогизација у публикацији - Народна библиотека Србије, Београд

535(048)

621.37/.39:535(048)

621.37/.39:535]:61(048)

66.017/.018(048)

INTERNATIONAL School and Conference on Photonic (8; 2021; Beograd)

Book of abstracts / VIII International School and Conference on Photonics PHOTONICA2021 & HEMMAGINERO workshop, 23 - 27 August 2021, Belgrade, Serbia; editors Mihailo Rabasović, Marina Lekić and Aleksandar Krmpot. - Belgrade: Institute of Physics, 2021 (Belgrade: SASA). - V, 192 str.: ilustr.; 30 cm

Tiraž 200. - Bibliografija uz većinu apstrakata. - Registar.

ISBN 978-86-82441-53-3

1. Hemmaginero Workshop (2021; Beograd)

а) Оптика -- Апстракти б) Оптички материјали -- Апстракти в) Оптоелектроника -- Апстракти г) Оптоелектроника -- Биомедицина -- Апстракти д) Телекомуникације -- Апстракти

COBISS.SR-ID 44290057

PHOTONICA 2021 (VIII International School and Conference on Photonics - www.photonica.ac.rs) is organized by Institute of Physics Belgrade, University of Belgrade (www.ipb.ac.rs), Serbian Academy of Sciences and Arts (www.sanu.ac.rs), and Optical Society of Serbia (www.ods.org.rs).

PHOTONICA 2021 is organized under auspices and with support of the Ministry of Education, Science and Technological Development, Serbia (www.mpn.gov.rs).

The support of the sponsors of PHOTONICA 2021 is gratefully acknowledged:

Nonlinear Imaging of Dentin-Adhesive Interface Treated by Cold Atmospheric Plasma

T. Lainović[1], A. Krmpot[2], M. D. Rabasović, N. Selaković, I. Pleštić[1], L. Blažić[1,3], N. Škoro[2], N. Puač[2]
[1]*Faculty of Medicine, School of Dental Medicine, University of Novi Sad, Novi Sad, Serbia*
[2]*Institute of Physics, University of Belgrade, Belgrade, Serbia*
[3]*Dental Clinic of Vojvodina, Novi Sad, Serbia*
e-mail: tijana.lainovic@mf.uns.ac.rs

The Nonlinear Laser Scanning Microscopy (NLSM) could be considered as a useful tool for the analysis of hard dental tissues, and tissue-material interfaces in dental medicine. Two-photon excitation fluorescence microscopy (TPEF) is able to detect the two-photon excited autofluorescence of dental tissues, and the second harmonic generation (SHG) can detect second-order nonlinear susceptibility of collagen type I, the most abundant dentinal organic substance [1,2].

The objective of this study was to microscopically test the effect of Cold Atmospheric Plasma (CAP) [3,4] on the morphology of the dentin-adhesive interface, using NLSM.

Human molar teeth were cut in half for the CAP-treated and control samples. The influence of CAP on standard etch-and-rinse (ER) or self-etch (SE) procedures was investigated. The following CAP configurations were used: feeding gas He, gas flow 1 slm, deposited power in the plasma power input 1 W or 2 W, and tip-to-surface distance 2 mm or 4 mm. The CAP-treated ER group was firstly etched and treated by CAP, before adhesive application. The SE group was treated by CAP before the adhesive placement. The control groups underwent the same process omitting the CAP phase. NLSM was used to image the morphology of hybrid layers.

The results demonstrated that the CAP causes the removal of the smear layer and opens the tubules. The tubules are not only more open but changed by CAP regarding their surface properties so that the permeation of the adhesive is highly favored. Compared to the control groups of around 20-30 μm hybrid layers, the length of resin tags in the CAP treated ER group was measured to even up to 600 μm, and in the CAP-treated SE group they were extended up to 100 μm.

CAP treatment of dentin drastically changes the morphology of the hybrid layer and the extension of resin tags. There is a need for additional analysis in the field to examine the influence of these changes on the quality of the dentin-adhesive interface.

Acknowledgment: Supported by the Ministry of Education, Science and Technological Development of Republic of Serbia (under contract No. NIO 200114 and No. 451-03-68/2021-14/200024), Project HEMMAGINERO, No. 6066079 from Program PROMIS, Science Fund of the Republic of Serbia and by the program “Start up for science. Explore. Make a change.", Funded by Leadership Development Center, Phillip Morris for Serbia, 2019.

REFERENCES

[1] T. Lainović, J. Margueritat, Q. Martinet, X. Dagany, L. Blažić, D. Pantelić, M.D. Rabasović, A.J. Krmpot and T. Dehoux, Acta Biomater 105, 214-222 (2020).
[2] T. Cloitre, I.V. Panayotov, H. Tassery, C. Gergely, B. Levallois and F.J.G. Cuisinier, J Biophotonics 6, 330-337 (2013)
[3] J.N. Stašić, N. Selaković, N. Puač, M. Miletić, G. Malović, Z.Lj. Petrović, D.N. Veljović and V. Miletić, Clin Oral Invest 23**,** 1383–1396 (2019).
[4] A. Stancampiano, D. Forgione, E. Simoncelli, R. Laurita, R. Tonini, M. Gherardi and V. Colombo, J Adhes Dent 21, 229-237 (2019).

Book of Abstracts

EGAS52 Virtual Conference
organized by the EGAS Board and the Institute of Physics in Zagreb, Croatia

July 06-08, 2021

Editor: Danijel Buhin

11:25 **J. Keller** (276)
Precision spectroscopy with In^+ / Yb^+ Coulomb crystals
11:35 **D. Charczun** (291)
Dual-comb spectroscopy based on measurements of cavity resonances
11:45 **M. Tamanis** (124)
Extended Spectroscopic Data and Deperturbative Analysis of $A^1\Sigma_u^+$ and $b^3\Pi_u$ States in K_2
11:55 **T.-L. Chen** (284)
Mid-Infrared Mode-Resolved Cavity Ring-Down Vernier Spectrometer using an Interband Cascade Laser Based Chip-Scale Optical Frequency Comb
12:05 **S. Dickopf** (288)
Determination of the hyperfine structure constant and the g-factors of $^3He^+$
12:15 **F. L. Constantin** (279)
Terahertz Electrometry using Precision Spectroscopy of the Hydrogen Deuteride Molecular Ions

Room 4: Applications to astrophysics, plasma physics, biophysics, clusters & Atom-like systems
Chair: **Nikša Krstulović**, Institute of Physics, Zagreb, Croatia

10:45 **N. Vujičić** (227)
Excitonic effects in CVD grown mono- and bilayer MoS_2 in the low-temeprature limit
10:55 **S. Gamrath** (104)
A new set of oscillator strengths in moderately charged indium ions for the spectral analysis of hot white dwarfs
11:05 **J. Car** (238)
A model for determination of diameter and concentration of metal nanoparticles synthesized by laser ablation in water
11:15 **H. Wei** (250)
Radiative cooling of cationic carbon clusters, C_N^+
11:25 **M. A. Mermigki** (181)
Electronic structure and Bonding Properties of Diatomic Molecule FeS
11:35 **S. Kühn** (266)
High-precision laser spectroscopy measurements of the prominent 3C/3D oscillator-strength ratio in Fe XVII
11:45 **V. Jadriško** (272)
Novel method for preparing nanoscale atomically thin heterostructure devices
11:55 **N. Selaković** (275)
Mass spectrometry and ICCD imaging of atmospheric pressure plasma jet with spiral electrodes
12:05 **A. Blech** (191)
Photoelectron circular dichroism in racemic mixtures
12:15 **C. Blondel** (216)
Old recipes to the rescue of modern data on the hyperfine structure of Xe I
12:25 **A. S. Petrovskaya** (223)
Numerical Simulation of Argon Microdischarge for Plasma Deactivation Technology
12:35 **S. Vasudevan** (224)
Photoelectron circular dichroism of heavier chalcogenofenchones using near ultra-violet femtosecond laser pulses

Room 5: Atom-like systems & Fundamental physics
Chair: **Slobodan Milošević**, Institute of Physics, Zagreb, Croatia

10:45 **J. Gębala** (162)
Cold interactions and collisions between helium ions (He^+) and metastable helium atoms (He^*)

Mass spectrometry and ICCD imaging of atmospheric pressure plasma jet with spiral electrodes

N. Selaković[*1], **D. Maletić**[1,2], **G. Malović**[1], **Z. Lj. Petrović**[3]
1. Institute of Physics Belgrade, Pregrevica 118, 11080 Belgrade, Serbia
2. Institute of Physics, Bijenička 46, 10000 Zagreb, Croatia
3. Serbian Academy of Sciences and Arts, Kneza Mihaila 35, 11000 Belgrade Serbia

Here we use spiral electrodes for generating an atmospheric pressure plasma jet APPJ. Their geometry allows the formation of discharges along relatively large source lengths [1]. We use ICCD fast imaging and mass spectrometry to observe discharge propagation as well to determine the chemical composition [2]. A possible application of this type of non-thermal plasma could be in medicine for sterilization of catheters and infusion hoses [3].

In this study, the source that we used was made of a 30 cm long glass tube around which two copper wires were wrapped into a spiral. These two wires did not touch at any point and were set at approximately equal distances of about 10 mm compared to each other. We used 4 slm of helium as a feeding gas during all experiment. One of the wires was powered with sine wave at 70 kHz excitation frequency and the other one was grounded. The applied voltage was generated using signal generator. The signal was amplified with custom made amplifier and transformer before it was applied to the powered electrode. We have used high voltage probe in order to measure the high voltage. The oscilloscope was used to capture signals of current and voltage in order to calculate power delivered to the discharge [4].

A molecular beam mass spectrometer MBMS (HIDEN HPR60) was used to detect neutrals, positive and negative ions mass spectra derived from APPJ discharge. In Fig. 1 one can notice a rich spectrum of negative ions obtained in APPJ's plume dominated by oxygen species such as O^-, OH^-, O_2^- and O_3^-. Also, water clusters $O^- \cdot (H_2O)n$ and $OH^- \cdot (H_2O)n$ can be observed. ICCD and electrical measurement results showed the appearance of a pulsed streamer at the maximum of the positive half-cycle of the voltage signal. In addition, we could notice the appearance of discharge within the glass tube which was following powered electrode during the negative half-cycle and grounded electrode during the positive half-cycle.

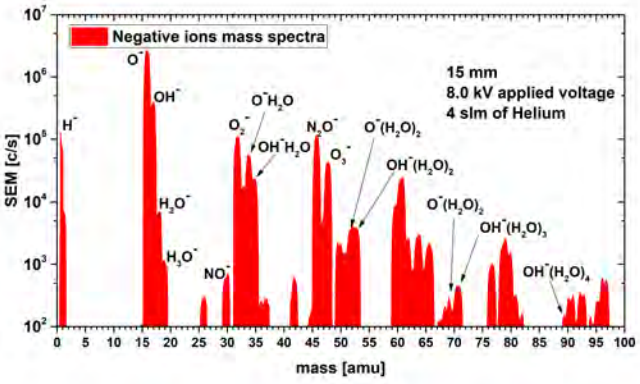

Fig. 1: Negative ions mass spectra 0-100 amu (15 mm distance between APPJ and MBMS, applied voltage 8.0 kV, helium flow rate 4 slm)

Mass spectrometry results showed similar concentrations of positive and negative ions for the same experimental conditions dominated by oxygen and nitrogen species. No water clusters were observed for positive ions. The ICCD acquisition provided insight into the propagation of discharge within the glass tube as well as within the plume which propagates in ambient room.

References

[1] M. Polak, J. Winter, U. Schnabel, J. Ehlbeck and K. D. Weltman, Plasma Processes and Polymers, **9(1)**, 67-76 (2012).
[2] A. Stancampiano., N. Selaković, M. Gherardi, N. Puač, Z. Lj. Petrović and V. Colombo. Journal of Physics D: Applied Physics, **5**1(48), 484004 (2018).
[3] T. Sato, O. Furuya, K. Ikeda and T. Nakatani. Plasma Processes and Polymers, **5**(6), 606-614 (2008).
[4] D. Maletić, N. Puač, G. Malović, A. Djordjević, and Z. LJ. Petrović, Journal of Physics D: Applied Physics, **5**0(14), 145202 (2017).

*Corresponding author: nele@ipb.ac.rs

ПУБЛИКАЦИЈЕ АСТРОНОМСКЕ ОПСЕРВАТОРИЈЕ У БЕОГРАДУ
PUBLICATIONS OF THE ASTRONOMICAL OBSERVATORY OF BELGRADE
Св. 102 No. 102

31st Summer School and International Symposium on the Physics of Ionized Gases

Belgrade, Serbia,
September 5 - 9, 2022

CONTRIBUTED PAPERS

&

ABSTRACTS of INVITED LECTURES, TOPICAL INVITED LECTURES and PROGRESS REPORTS

Editors:
Dragana Ilić, Vladimir Srećković,
Bratislav Obradović and Jovan Cvetić

БЕОГРАД
2022

PUBL. ASTRON. OBS. BELGRADE No. 102, 1 - 302 BELGRADE, AUGUST 2022

31st Summer School and International Symposium on the Physics of Ionized Gases

September 5 – 9, 2022, Belgrade, Serbia

S P I G 2022

CONTRIBUTED PAPERS

&

ABSTRACTS OF INVITED LECTURES,
TOPICAL INVITED LECTURES AND
PROGRESS REPORTS

Editors

Dragana Ilić, Vladimir Srećković,
Bratislav Obradović and Jovan Cvetić

University of Belgrade –
School of Electrical
Engineering

University of Belgrade –
Faculty of Physics

Serbian Academy of
Sciences and Arts

Belgrade, 2022

PUBLICATIONS OF THE ASTRONOMICAL OBSERVATORY OF BELGRADE

FOUNDED IN 1947

All papers in this Publication are peer reviewed.

Director of the Astronomical Observatory: Dr. Gojko Djurašević

Typesetting: Tatjana Milovanov

Internet address http://www.aob.rs

ISSN 0373-3742
ISBN 978-86-82296-02-7

Number of copies / tiraž : 200
Production: Skripta Internacional, Mike Alasa 54, Beograd

CIP - Каталогизација у публикацији - Народна библиотека Србије, Београд

537.56(082)
539.186.2(082)
539.121.7(082)
533.9(082)

SUMMER School and International Symposium on the Physics of Ionized Gases (31 ; 2022 ; Belgrade)

Contributed papers & abstracts of invited lectures, topical invited lectures and progress reports / 31st Summer School and International Symposium on the Physics of Ionized Gases - SPIG 2022, September 5-9, 2022, Belgrade, Serbia ; editors Dragana Ilić ... [et al.]. - Belgrade : Astronomical Observatory, 2022 (Beograd : Skripta Internacional). - 302 str. : ilustr. ; 24 cm. - (Publications of the Astronomical Observatory of Belgrade, ISSN 0373-3742)

Na nasl. str.: University of Belgrade, School of Electrical Engineering; University of Belgrade, Faculty of Physics; Serbian Academy of Sciences and Arts. - Tiraž 200. - Str. 17-18: Preface / editors Dragana Ilić ... [et al.]. - Bibliografija uz svaki rad. - Registar.

ISBN 978-86-82296-02-7

1. Ilić, Dragana, 1978- [уредник] [аутор додатног текста]

а) Јонизовани гасови – Зборници б) Атоми – Интеракција – Зборници в) Плазма – Зборници

COBISS.SR-ID 72751881

SPIG 2022

Progress Reports

Contributed Papers

MASS SPECTROMETRY OF PLASMA JET AND APPLICATION OF ELECTRICAL DISCHARGES OPERATING AT ATMOSPHERIC PRESSURE IN BIOMEDICINE

N. SELAKOVIĆ[1], D. MALETIĆ[1], N. PUAČ[1], G. MALOVIĆ[1] and Z. LJ. PETROVIĆ[2]

[1]*Institute of Physics, University of Belgrade, Pregrevica 118, 11080 Belgrade, Serbia*
E-mail nele@ipb.ac.rs

[2]*Serbian Academy of Sciences and Arts, Kneza Mihaila 35, 11000 Belgrade, Serbia*

Abstract. In the last few decades, the study of plasma jets has been the focus of interest for a large number of scientists especially because of its potential application in biomedicine. The physical phenomenon that characterizes plasma jets is the appearance of a "pulsed atmospheric pressure streamer" (PAPS), a fast ionization front that cannot be detected by a human eye, but its observation is enabled by the use of high-speed ICCD cameras. In order to integrate this type of plasma into biomedical applications it is necessary to perform analysis of the electrical discharge's behavior and its composition. In this work, we present mass spectrometry of three different atmospheric pressure plasma sources (plasma jet, multijet plasma device and dielectric coplanar surface barrier discharge). The results show different mass spectra of neutral, positive and negative ions whose composition and concentration significantly depend on the geometry of the source and the applied parameters: the power delivered to the plasma, the type of working gas and flow rate, humidity, etc. This diagnostic method gave us an insight into the dominant reactive species of oxygen and nitrogen, the so-called RONS, which play a crucial role in biomedical applications. In addition, we have used plasma needle, the atmospheric pressure plasma source, in treatments of bacteria, plant stem cells and cancer cells. and discussed numerous effects obtained by treatment.

References

Stancampiano, A., Selaković, N., Gherardi, M., Puač, N., Petrović, Z. L., and Colombo, V. 2018, *Journal of Physics D: Applied Physics*, *51*(48), 484004.

Puač, N., Živković, S., Selaković, N., Milutinović, M., Boljević, J., Malović, G., and Petrović, Z. Lj. 2014, *Applied Physics Letters*, *104*(21), 214106.

Čech, J., Brablec, A., Černák, M., Puač, N., Selaković, N., and Petrović: Z. Lj. 2017, *The European Physical Journal D*, *71*(2), 1-8.

Twenty-third International Summer School
18 - 22 September 2023
Sozopol, Bulgaria

VEIT
Vacuum Electron Ion Technologies

PROGRAM
ABSTRACTS

TWENTY-THIRD INTERNATIONAL SUMMER SCHOOL ON VACUUM, ELECTRON AND ION TECHNOLOGIES

VEIT 2023

18 - 22 September 2023
SOZOPOL, BULGARIA

Jointly organized by the Institute of Electronics of the Bulgarian Academy of Sciences and the Dutch Institute for Fundamental Energy Research, The Netherlands

Dedicated to the 60th Anniversary of the Bulgarian organizer of the event

TWENTY-THIRD INTERNATIONAL SUMMER SCHOOL ON VACUUM, ELECTRON AND ION TECHNOLOGIES

VEIT 2023

18 - 22 September 2023
SOZOPOL, BULGARIA

PROGRAM
ABSTRACTS

Editors: M. Dimitrova, Ch. Ghelev, B. Georgieva and E. Vasileva

VEIT '23

TWENTY-THIRD INTERNATIONAL SUMMER SCHOOL
ON VACUUM, ELECTRON AND ION TECHNOLOGIES
18 – 22 September 2023, Sozopol, Bulgaria

ORGANIZED BY

INSTITUTE OF ELECTRONICS
BULGARIAN ACADEMY OF SCIENCES, SOFIA, BULGARIA

DUTCH INSTITUTE FOR FUNDAMENTAL ENERGY RESEARCH
EINDHOVEN, THE NETHERLANDS

CO-FINANCED by the: MINISTRY OF EDUCATION AND SCIENCE OF REPUBLIC OF BULGARIA, BULGARIAN NATIONAL SCIENCE FUND,
Project № KP-06-MNF/5/19.05.2023

25 YEARS OF EPJ.org
your physics journal
Young Researcher Attendance Grant

Bulgarian Academy of Sciences

Union of the Physicists in Bulgaria

CHAIRS OF THE SCHOOL

M. Dimitrova, Institute of Electronics, Bulgarian Academy of Sciences, Sofia, Bulgaria
M.C.M. van de Sanden, Dutch Institute for Fundamental Energy Research, Eindhoven, The Netherlands

INTERNATIONAL ADVISORY COMMITTEE

N. Nedyalkov	Bulgarian Academy of Sciences, Sofia, Bulgaria
M. Dimitrova	Czech Academy of Sciences, Prague, Czech Republic
R. Panek	Czech Academy of Sciences, Prague, Czech Republic
Th. Czerwiec	Institut Jean Lamour (IJL), Ecole des Mines de Nancy, Nancy, France
H. Kersten	IEAP University of Kiel, Kiel, Germany
D. Mataras	University of Patras, Patras, Greece
V. Guerra	Instituto Superior Técnico, Lisboa, Portugal
G. Dinescu	National Institute for Laser, Plasma and Radiation Physics, Magurele Bucharest, Romania
Z. Petrovic	Institute of Physics, Belgrade, Serbia
M. Mozetic	"Jozef Stefan" Institute, Ljubljana, Slovenia
I. Katardjiev	Uppsala University, Uppsala, Sweden
M.C.M. (Richard) van de Sanden	Dutch Institute for Fundamental Energy Research (DIFFER), Eindhoven, The Netherlands
G. J. van Rooij	Dutch Institute for Fundamental Energy Research (DIFFER), Eindhoven, The Netherlands
M. Ürgen	Istanbul Technical University, Istanbul, Turkey
A. Ehiasarian	Sheffield Hallam University, Sheffield, UK
I. Petrov	University of Illinois, Urbana, IL, USA

LOCAL ORGANIZING COMMITTEE

Ch. Angelov, I. Balchev, M. Dimitrova (Chair), B. Georgieva, Ch. Ghelev, P. Ivanova, E. Taskova, E. Vasileva

MAIN SCIENTIFIC TOPICS:

- THIN FILMS DEPOSITION
- SURFACES AND THIN FILMS PROCESSING AND ANALYSIS
- COATINGS FOR ADVANCED APPLICATIONS
- NEW MATERIALS
- PLASMA-SURFACE INTERACTION AND PLASMA DIAGNOSTICS
- GREEN TECHNOLOGIES
- MODELING AND COMPUTER SIMULATION

PLENARY AND POSTER SESSIONS:

A: THIN-FILMS DEPOSITION
COATINGS FOR ADVANCED APPLICATIONS

B: NEW MATERIALS. PLASMA-SURFACE INTERACTION AND PLASMA DIAGNOSTICS. GREEN TECHNOLOGIES. MODELING AND COMPUTER SIMULATION

C: SURFACES AND THIN FILMS PROCESSING AND ANALYSIS

ABBREVIATIONS:

TL – TOPIC LECTURE
PR – PROGRESS REPORT
OP – ORAL PRESENTATION
PA – POSTER SESSION A
PB – POSTER SESSION B
PC – POSTER SESSION C

VEIT '23

TWENTY- THIRD INTERNATIONAL SUMMER SCHOOL
ON VACUUM, ELECTRON AND ION TECHNOLOGIES
18 – 22 September 2023, Sozopol, Bulgaria

ABSTRACTS

TOPIC LECTURES

PROGRESS REPORTS

TL–5

PHYSICS OF NON-EQUILIBRIUM COLLISIONAL PLASMAS: KINETIC PHENOMENA AND THEIR EFFECT ON REAL-WORLD APPLICATIONS

Z.Lj. Petrović[1,2], D. Marić[3], S. Dujko[3], N. Selaković[3], J. Marjanović[3], J. Atić[3], D. Bošnjaković[3], I. Simonović[3]

[1]Serbian Academy for Sciences and Arts, Knez Mihailova 35, 11000 Belgrade, Serbia
[2]School of Engineering, Ulster University, Jordanstown, Co. Antrim BT37 0QB, UK
[3]Institute of Physics, University of Belgrade, Pregrevica 118, 11080 Belgrade, Serbia

Low-temperature plasmas have been the basis of a wide range of applications. While thermal plasmas have been the basis of a number of productive and wide-spread applications in the last 150 years, non-equilibrium low-temperature plasmas have become the front of development of the new generations of high-tech applications ranging from nano electronics, micro light sources, to medical plasma applications. The basis of most applications is to employ some set of circumstances that produce a non-equilibrium distribution of plasma constituents favoring specific actions. Such situations may be named kinetic phenomena that have been defined in the physics of non-equilibrium plasmas as the manifestation of their non-equilibrium nature. In this talk, we shall illustrate how several kinetic phenomena may be explained and, based on those explanations, may be optimized and controlled. We shall illustrate the close coupling of fundamental research with subsequent development of new technologies by discussing:

-the reactive ion and fast neutral etching in nano electronics;

-control of the electron energy distribution function by selecting gas mixtures components and the resulting plasma chemical kinetics;

-optimization of gas dielectrics and gas breakdown conditions;

-modelling of positron emission tomography;

-plasma medical applications and applications in agriculture.

Acknowledgements:
This work was supported by Ministry of Science, Technological Development and Innovations of Republic of Serbia grant no. 7749560, project EGWIn. Z.Lj. P. is grateful to SANU F155 project for partial support.

IFPiLM

PLASMA 2023

International Conference
on Research and Application of Plasmas

September 18-22
2023 | Warsaw, Poland

Book of Abstracts

Organized by
Institute of Plasma Physics and Laser Microfusion

Ministry of Education and Science
Republic of Poland

Doskonała Nauka

Projekt dofinansowany ze środków budżetu państwa, przyznanych przez Ministra Edukacji i Nauki w ramach Programu „Doskonała Nauka II - Wsparcie konferencji naukowych: International Conference on Research and Applications of Plasmas - PLASMA 2023”, nr projektu KONF/SN/0198/2023/01.

The project is co-financed by the state budget funds under the program of the Minister of Education and Science called "Excellent science II - support for scientific conferences: International Conference on Research and Applications of Plasmas - PLASMA 2023”, project No. KONF/SN/0198/2023/01.

Sponsors

HAMAMATSU
PHOTON IS OUR BUSINESS

tespol
engineering

Quantum Design
EUROPE

IRtech®

EKSPLA

PRECOPTIC®
THE SCIENCE SUPPORT

KRAJOWY PUNKT KONTAKTOWY
EURATOM IFPiLM

Partners

applied sciences
an Open Access Journal by MDPI

International Scientific Committee

Monika Kubkowska, IPPLM Warsaw, Poland - Chairperson
Dimitri Batani, Université Bordeaux , France
Sebastijan Brezinsek, FZ Juelich, Germany
Maryna Chernyshova, IPPLM Warsaw, Poland
Andreas Dinklage, IPP Greifswald, Germany
Krzysztof Dzierżęga, Jagiellonian University, Poland
Igor Garkusha, IPP Kharkov, Ukraine
Aneta Malinowska, NCBJ, Poland
Didier Mazon, CEA Cadarache, France
Jerzy Mizeraczyk, Gdynia Maritime University, Poland
Ewa Pawelec, Opole University, Poland
Tadeusz Pisarczyk, IPPLM Warsaw, Poland
Svetlana Ratynskaia, KTH Stockholm, Sweden
Marek Rubel, KTH Stockholm, Sweden
Katarzyna Słabkowska, UMK, Torun Poland
Francisco Tabares, CIEMAT Madrid, Spain

Local Organizing Committee

Agata Chomiczewska - Chairperson
Tomasz Fornal
Paweł Gąsior
Wojciech Gromelski
Natalia Wendler

The conference programme includes the following topical sessions:

I. Elementary processes, general plasma physics, dusty plasmas
II. Plasmas in tokamaks and stellarators. Magnetic confinement fusion
III. Plasmas generated by laser beams. Inertial confinement fusion
IV. Space plasmas and laboratory astrophysics
V. Plasma diagnostics. Measurements and data processing, including AI
VI. Plasma medicine, agriculture and environmental applications

Comparison of Two Atmospheric Pressure Plasma Sources for Eradication of Methicillin-resistant Staphylococcus aureus Biofilm

M. Miletić[1], B. Toljić[1], D. Vuković[2], N. Milojević[1], N. Selaković[3], D. Maletić[3], G. Malović[3], N. Škoro[3] and N. Puač[3]

[1] *School of Dental Medicine, University of Belgrade, dr Subotića starijeg 1, Belgrade, Serbia*

[2] *Faculty of Medicine, University of Belgrade, dr Subotića starijeg 1, Belgrade, Serbia*

[3] *Institute of Physics, University of Belgrade, Pregrevica 118, Belgrade, Serbia*

e-mail: maja.miletic@stomf.bg.ac.rs

Abstract

Non-thermal (cold) Atmospheric Pressure Plasmas (APPs) are known to be an efficient tool for various biomedical applications (wound healing, blood coagulation, as a tool in cancer therapy, in stomatology etc.). One of the most widespread application is in inhibition and eradication of bacteria. Here APPs, with its rich chemistry full of Reactive Oxygen and Nitrogen Species (RONS), play an important role, especially in case of strains resistant to antibiotics. Eradication of methicillin-resistant *Staphylococcus Aureus* (MRSA) still presents a challenging task for modern medicine. Due to rapidly evolving mechanisms of resistance MRSA usually skips multimodal antibiotic therapies making it a perfect candidate for novel approach that APPs can offer. The effects of APPs depend on variety of different parameters such as geometry of the plasma source, power deposited to the plasma, exposure time etc. This makes the comparison between different systems highly inconvenient and difficult. We have used two APPs for treatment of MRSA biofilm in order to estimate their efficiency and to identify the most important plasma parameter(s) that can serve as a reference for comparison between plasma sources. Plasma needle operates at atmospheric pressure and it is powered by a sine wave signal @13.56 MHz. In all experiments the working gas was helium and it was kept at 1 slm. For the plasma needle treatments we have varied three experimental parameters: power (2 and 2.5 W), distance from the tip of the plasma source and the surface of the sample (2, 4 and 6 mm) and exposure time (30, 60, 90 and 180 s). In case of atmospheric pressure plasma jet (APPJ) we have used Dielectric Barrier Discharge (DBD) APPJ with two copper electrodes wrapped around the glass tube. The width of the electrodes was 15 mm with 15 mm gap between them. As with plasma needle the working gas was helium with flows of 1 slm and 2 slm. The distance from the samples was 10 mm and treatment times 15 s, 1 min, 2 min, 5 min, 10 min and 15 min. Both plasma sources successfully reduced the viability of bacteria with the increase of the treatment time. Plasma needle was more efficient due to the fact that it reduced the viability to 50% for maximum 3 min while with DBD APPJ treatments needed to be longer than 5 min. The most important parameters for reducing the viability of bacteria in both cases are power deposited to the plasma correlated with treatment time. In case of inhibition zones the results show that with DBD APPJ we can obtain larger zones without bacteria of up to 14 mm compared to maximum of 9 mm obtained for plasma needle. Again, DBD APPJ demands much longer treatment times (15 min) to achieve inhibition zones that are significantly larger than the diameter of the glass tube (6 mm).

This research was supported by the Science Fund of the Republic of Serbia, 7739780*, Atmospheric pressure plasmas operating in wide frequency range – a new tool for production of biologically relevant reactive species for applications in biomedicine - APPerTAin-BIOM*.

References

1. N. Brown, A. L. Goodman, et al. *JAC Antimicrob. Resist.* **2021**, 3, 1-18.
2. M. Vesteergard, D. Frees, et al. *Microbiol. Spectr.* **2019**, 7, 1-23.
3. M. Miletic, D. Vukovic, et al. *Cent. Eur. J. Phys.* **2014**, 12, 160-167.

Treatment of Burkholderia cepacia biofilm by atmospheric pressure plasma jet (APPJ)

D. Vuković[1], B. Toljić[2], M. Miletić[2], N. Milojević[2], N. Selaković[3], D. Maletić[3], G. Malović[3], N. Škoro[3] and N. Puač[3]

[1] Faculty of Medicine, University of Belgrade, dr Subotića starijeg 1, Belgrade, Serbia

[2] School of Dental Medicine, University of Belgrade, dr Subotića starijeg 1, Belgrade, Serbia

[3] Institute of Physics, University of Belgrade, Pregrevica 118, Belgrade, Serbia

e-mail: dragana.vukovic@med.bg.ac.rs

Abstract

Due to its rich chemistry plasma sources are in the last decade deemed as potential novel tool for biomedical applications such as wound healing, cancer therapy and antimicrobial activity. APPJs are simple in construction, easy to use, need low power during treatments and at the same time are rich in Reactive Oxygen and Nitrogen Species (RONS) that are responsible for the plasma efficiency in all these applications [1-2]. One of the challenges that APPJs face is inhibition and eradication of bacteria that already formed a biofilm. Here we will present the results of APPJ treatment of Burkholderia cepacia biofilm. B. cepacia is an opportunistic pathogen causing serious respiratory infections in patients with underlying illnesses, primarily cystic fibrosis (CF), and healthcare-associated infections. Biofilm formation is among the virulence traits contributing to pathogenesis of the infections, while the major host-related risk factor is the use of indwelling medical devices [3]. The B. cepacia strain used in the study was recovered from a respiratory CF sample and identified as a strong biofilm- producer. The APPJ used in this research operates at atmospheric pressure with helium as a working gas. In experiments gas flows were 1 slm and 2 slm. It consists of a Pyrex glass tube (I. D. 4 mm and O. D. 6 mm) and two transparent electrodes. Both electrodes were 15 mm wide and the gap between them was 15 mm. The position of the powered electrode relative to the jet nozzle (edge of the glass tube) was also 15 mm. The power supply of APPJ was a high voltage power supply based on the TDA7293 chip and high voltage transformer. To generate plasma jet we have used sine wave with operating frequency at 80 kHz and the applied voltage was adjusted between 6 kVpp and 8 kVpp. For the APPJ treatment, we used constant distance of 10 mm from the jet nozzle to the surface of the sample. The exposure times were 1 min, 5 min and 10 min. The power was kept constant at 4 W in all treatments. As samples we have used 24 hour old biofilm of *B. cepacia*. After the plasma treatments we have evaluated the biofilm biomass and viability by the crystal violet assay and the MTT assay, respectively. Both the biomass and viability of the bacteria in biofilm reduced with the increase of the treatment time and with the increase of the working gas flow, but no complete eradication was achieved. This can be correlated with the concentration of the RONS delivered to the bacteria forming the biofilm [4]. The maximum viability reduction was 50% due to the fact that bacteria positioned in biofilm matrix at lower layers were shielded from direct contact with RONS.

This research was supported by the Science Fund of the Republic of Serbia, 7739780*, Atmospheric pressure plasmas operating in wide frequency range – a new tool for production of biologically relevant reactive species for applications in biomedicine - APPerTAin-BIOM*.

References

1. S. Duarte, B.H.D Panariello. *Arch. Biochem. Biophys*. **2020**, 30;693:108560.
2. M.J. Nicol, T.R. Brubaker, B.J. Honish, A.N. Simmons, A. Kazemi, M.A. Geissel, C.T. Whalen, C.A. Siedlecki, S.G. Bilen, S.D. Knecht, G.S. Kirimanjeswara. *Sci. Rep.* **2020**, 10, 3066.
3. M. Tavares, M. Kozak, A. Balola, I. Sá-Correiaa. *Clin. Microbiol. Rev.* **2020**, 33:e00139-19.
4. N.H. Alshraiedeh, S. Higginbotham, P.B. Flynn, M.Y. Alkawareek, M.M. Tunney, S.P. Gorman, W.G. Graham, B.F. Gilmore. *Int. J. Antimicrob. Agents.* **2016**, 47, 446-450.

Book of abstracts

4th Workshop on Plasma applications for smart and sustainable agriculture 2024

May 20th-22nd, 2024

COST Action CA19110

Plasma applications for smart and sustainable agriculture - PlAgri

Serbian Academy of Sciences and Arts
Belgrade, Serbia
COST Action PlAgri CA19110

CA19110 Plasma applications for smart and sustainable agriculture

Editors:
Core Group PlAgri CA19110 Action
Acad. Zoran Lj. Petrović, Serbian Academy of Sciences and Arts, Serbia
Dr. Nikola Škoro, Institute of Physics, University of Belgrade, Serbia
Ms. Olivera Jovanović, Institute of Physics, University of Belgrade, Serbia

This publication is based upon work from COST Action CA19110 Plasma applications for smart and sustainable agriculture – PlAgri, supported by COST (European Cooperation in Science and Technology).

COST (European Cooperation in Science and Technology) is a funding agency for research and innovation networks. Our Actions help connect research initiatives across Europe and enable scientists to grow their ideas by sharing them with their peers. This boosts their research, career and innovation.

www.cost.eu

cost
EUROPEAN COOPERATION
IN SCIENCE & TECHNOLOGY

Funded by
the European Union

COMMITEES

ORGANIZING COMMITTEE:

- Acad. Zoran Lj. Petrović, Serbian Academy of Sciences and Arts, Serbia , (Chair)
- Ms. Olivera Jovanović, Institute of Physics Belgrade, Serbia, (Secretary)
- Acad. Dragan Škorić, Serbian Academy of Sciences and Arts, Serbia
- Acad. Slobodan Vukosavić, Serbian Academy of Sciences and Arts, Serbia
- Dr. Nikola Škoro, Institute of Physics Belgrade, Serbia
- Ms. Neda Babucić, Institute of Physics Belgrade, Serbia
- Ms. Anđelija Marković, Institute of Physics Belgrade, Serbia
- Dr. Nenad Selaković, Institute of Physics Belgrade, Serbia
- Ms. Desanka Topalović, Institute of Physics Belgrade, Serbia

INTERNATIONAL PROGRAM COMMITTEE:

- Dr. Nevena Puač, Institute of Physics Belgrade, Serbia (AC)
- Dr. Frantisek Krčma, Brno University of Technology, Faculty of Chemistry, Czech Republic (AVC)
- Dr. Anton Nikiforov, Ghent University, Belgium (WG1)
- Dr. Kinga Kutasi, Wigner Research Centre for Physics, Hungary (WG1)
- Dr. Tomislava Vukušić Pavičić, University of Zagreb, Croatia (WG2)
- Dr. Monica Magureanu, National Institute for Laser, Plasma and Radiation Physics, Romania (WG2)
- Dr. Joanna Pawlat, Lublin University of Technology, Poland (WG3)
- Dr. Henrike Burst, Leibniz Institute for Plasma Science and Technology, Germany (WG3)
- Dr. Zdenko Machala, Comenius University in Bratislava, Slovakia (WG4)
- Dr. Wolfgang Gernjak, ICRA Catalan Institute for Water Research, Spain (WG4)
- Dr. Matteo Gherardi, University of Bologna, Italy (WG5)
- Dr. Oliver Schlüter, Leibniz Institute for Agricultural Engineering and Bioeconomy, Germany (WG5)
- Dr. Gregor Primc, Jozef Stefan Institute, Slovenia (SCM)
- Dr. Augusto Stancampiano, GREMI (SCVM)
- Dr. Jana Šimečkova, Mendel University in Brno, Czech Republic (GAC)
- Dr. Indrek Jõgi, University of Tartu, Estonia (GAVC)

ABSTRACTS

P12

Mass Spectrometry Analysis of Positive Ion Composition in APPJ

N. Selaković[1], N. Puač[1], G. Malović[1] and Z. Lj. Petrović[2,3]
[1]*Institute of physics, University of Belgrade, Pregrevica 118, 11080 Belgrade, Serbia*
[2]*Serbian Academy of Sciences and Arts, Knez Mihailova 35, 11000 Belgrade, Serbia*
[3]*School of Engineering, Ulster University, Jordanstown, Co. Antrim, BT37 0QB UK*
e-mail: nele@ipb.ac.rs

With facing the difficulties in global food security, plasma agriculture provides promise for a sustainable and environmentally friendly farming techniques by utilizing the special characteristics of plasma chemistry, such as the ability to generate reactive species and modify surfaces [1]. Since mass spectrometry (MS) has such high sensitivity and specificity in identifying reactive species, it is one of the best methods for figuring out the complex chemical composition of plasma. In this study, we conducted mass spectrometry measurements of an atmospheric pressure plasma jet (APPJ) with transparent electrodes [2], where we introduced less than 1% water vapor into the working gas (helium in our case) by using a water bubbler.

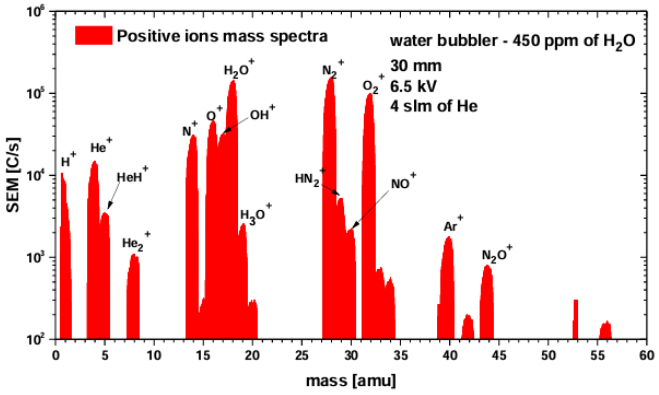

Fig. 1. Positive ions mass spectra of APPJ

In Figure 1, we observe the rich spectrum of positive ions with added water vapor, wherein H_2O^+, N_2^+, O_2^+, N^+ and O^+ emerge as the dominant species. The ions derived from helium such as He^+, HeH^+ and He_2^+ are diminished due to water vapor influence. Experiment showed that minor variations in water vapor content within the working gas led to significant alterations in mass spectra. This has demonstrated MS potential to be of immense significance in tailoring the desired chemical composition of plasma, thereby offering substantial benefits for treatments in agriculture.

Acknowledgment: This work was supported by MSTDI Republic of Serbia grant number 451-03-68/2023-14/200024. Z. Lj. P. is grateful to the SANU Project F155 for partial support.

References

[1] N. Puač et al., Plasma processes and polymers, 15(2), 1700174 (2018).
[2] D. Maletić et al.,, Plasma Sources Science and Technology, 24(2), 025006 (2015).

ESCAMPIG 2024

9- 13 JULY 2024, BRNO, CZECH REPUBLIC

26th Europhysics Conference on Atomic and Molecular Physics of Ionized Gases

BOOK OF ABSTRACTS

MUNI SCI Department of Plasma Physics and Technology

CEPLANT

escampig2024@physics.muni.cz

ESCAMPIG 2024 organized by

Department of Plasma Physics and Technology and CEPLANT

Faculty of Science

Masaryk University

In collaboration with Jednota českých matematiků a fyziků

Local Organizing Committee

Chairman: Zdeněk Bonaventura (MUNI)

Co-chairman: Tomáš Hoder (MUNI)

Bohumila Tesaříková (MUNI)

František Krčma (BUT)

Ondřej Jašek (MUNI)

Pavel Dvořák (MUNI)

Realization/Support

Eliška Vrzalová (MUNI)

Anežka Winklerová (MUNI)

Pavel Kunovský (MUNI)

Monika Stupavská (MUNI)

Tereza Schmidtová (MUNI)

Radka Kunovská (MUNI)

Jan Vondra (JČMF)

International Scientific Committee

Chairman: Carlos Pintassilgo (Portugal)

Ronny Brandenburg (Germany)

Claudiu Costin (Romania)

Aranka Derszi (Hungary)

Anatoly Filippov (Russia)

Victor Herrero (Spain)

Nikola Škoro (Serbia)

Tiberiu Minea (France)

Eugen Stamate (Denmark)

Francesco Taccogna (Italy)

František Krčma (Czech Republic)

Erik Wagenaars (United Kingdom)

Edited by Ondřej Jašek

Postconference edition, Updated 11.9. 2024, Brno

P1-T5-18 A.D. Pajdarova; M. Farahani; **T. Kozak**; J. Capek; *Reverse discharge in bipolar HiPIMS and its dependence on magnetic field geometry*

P1-T5-19 **F.J. Arellano**; M. Kusaba; S. Wu; R. Yoshida; S. Hamaguchi; *Machine learning prediction of the electron density and the electron energy distribution function from the optical emission spectra*

P1-T5-20 **A. Meindl**; C.K. Kiefer; R. Antunes; A. Hecimovic; U. Fantz; *Investigation of Stark broadening in plasma conversion reactors by means of high resolution optical emission spectroscopy*

P1-T5-21 **C. Pascual-Fort**; A. Brisset; N De Oliveira; N. Minesi; C..O Laux; G..D Stancu; *Spatial characterization of N(4S) in a microwave plasma jet at atmospheric pressure by fs-TALIF*

P1-T5-22 M. Krbal; **D. Prokop**; L. Kuthanova; S. Kadlec; T. Hoder; *Breakdown with solid insulation flashover in naturally occurring gases; SF_6; and its alternatives*

P1-T5-23 **D.J. Schreuder**; G. Mattausch; B. Zimmermann; E. von Hauff; *Optical Emission Spectroscopy of an Electron Beam Sustained Hybrid Discharge of Nitrogen at 1 mbar*

P1-T5-24 **D. Maletic**; N. Selakovic; D. Popovic; S. Milosevic; G. Malovic; Z Lj Petrovic; *Mass spectrometry measurements of the capillary single electrode helium plasma jet*

P1-T5-25 **D. Sadi**; E. Baratte; T. Silva ; O. Guaitella; *Ro-vibrational temperatures of CO(X) deduced from emission of third positive and angstrom system of CO in CO_2 glow discharge*

P1-T5-26 **E. Maťaš**; M. Neogrady; L. Moravsky; S. Matejcik; *Quantitative analysis of NO_2 generated in Atmospheric Pressure Plasma Jet using Ion Mobility Spectrometry*

P1-T5-27 **G. F. Alfaro**; M. N.Shneider; A. Gerakis; *Coherent scattering from ponderomotive-driven density perturbations for plasma diagnostics*

P1-T5-28 **G. Kreyder**; D. Stefas; L. Invernizzi; G. Lombardi; K. Gazeli; S. Prasanna; S.M. Starikovskaia; *Nitrogen atoms ps-TALIF in atmospheric pressure*

P1-T5-29 **P. Hartmann**; J. Carmona-Reyes; L.Y. Luo; L. Matthews; T. Hyde; *Mapping the field around a Langmuir probe with charged dust particles*

P1-T5-30 **J. Hnilica**; K. Bernatova; P. Klein; Z. Hubicka; M. Cada; P. Vasina; *Time and energy-resolved mass spectrometry study of the HiPIMS discharge operated in Ar and Ar-N_2 atmospheres*

P1-T5-31 G. Tetard; A. Michau; **S. Prasanna**; P. Brault; K. Hassouni; *Self consistent simulation of dust formation and dynamic in non-equilibrium RF Ar-acetylene plasma*

P1-T5-32 **K. Jurik**; M. Stastny; P. Drexler; K. Mrozek; A. Obrusnik; *Analysis of a radiofrequency-driven resonant plasma source*

P1-T5-33 **K. Sasaki**; K. Fushimi; N. Shirai; *Measurement of negative ion density in streamer discharge in air by transient cavity ringdown spectroscopy*

P1-T6-34 **M. D. Acciarri**; ***C. Moore***; S. D. Baalrud; *Particle in Cell Simulations and Correlation Heating*

P1-T6-35 **H. Akashi**; K. Mizuno; T. Yoshinaga; *Optimization of Null Collision Method in Monte Carlo Model*

Mass spectrometry measurements of the capillary single electrode helium plasma jet

D Maletić(*)[1], N Selaković[1], D Popović[2, 3], S Milošević[2], G Malović[1], Z Lj Petrović[4]

[1]*Institute of Physics, University of Belgrade, Pregrevica 118, 11080 Belgrade, Serbia*

[2]*Institute of Physics, Bijenička 46, 10000 Zagreb, Croatia*

[3]*N2 Applied, Dronning Eufemias gate 20, 0191 Oslo, Norway*

[4]*Serbian Academy of Sciences and Arts, Knez Mihajlova 35, 11000 Belgrade, Serbia*

(*)dejan_maletic@ipb.ac.rs

Plasma jets are simple in construction, but with unique and complex physical and chemical properties that have been in focus of extensive research in the last two decades. These nontermal plasma jets produce complex mixture of reactive species such as ions, radicals, electrons and RONS (reactive oxygen and nitrogen species) and have the potential to revolutionize material processing, biomedicine, agriculture and gas conversion. For example, plasma jets such as micro plasma jet, can be used to etch or deposit thin films on surfaces with high precision, making them useful in the manufacture of microelectronic devices. In biomedicine, plasma jets have been shown to have a range of therapeutic effects, including the ability to kill bacteria and promote wound healing [1]. Plasma jets are streams of highly ionized gas that are generated by an electric discharge. They typically consist of a plasma plume surrounded by a sheath of neutral gas. The electrons can reach high energies while ions and neutral molecules are close to room temperature. Low gas discharge temperatures are crucial in treatment of the thermo sensitive samples such as biological and polymer materials. Some of the recent applications are in production of plasma activated water (PAW) that has been used in sterilization of bacteria and in agriculture to promote plant growth [2]. Many different methods have been used for diagnostics of plasma jets such as optical emission spectroscopy, ICCD imaging, ultra fast imaging, electrical measuremts, mass spectrometry, laser diagnostics [3, 4, 5].

Here, we report mass spectrometry of atmospheric pressure plasma jet. The body of the jet is made of Teflon, the glass capillary (inner diameter of 1 mm and outer diameter 1.5 mm) and electrode copper wire (100 μm), see Fig. 1. The working gas was helium at a constant flow rate of 2 slm. The distance from the mass spectrometer HPR-60 was 15 mm in all measurements. We measure the current and voltage signals at the plasma jet electrode, while changing the output power of the high voltage power

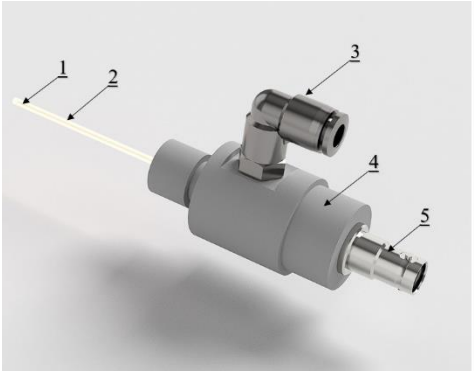

1. Electrode
2. Glass capillary
3. Gas connector
4. Plasma jet body
5. HV connector

Fig. 1: Plasma jet

supply. Mass spectrometer was used to measure the neutrals and ions present in the plasma jet plume. Before each measurement we record ion energy distribution for the most abundant ion present in plasma

N_2^+ to confirm that the discharge is not entering the mass spectrometer. The maximum of the ion energy distribution should be below 5 eV and there should be no additional maxima at higher energies (not shown here).

In figure 2 we presented the yields for the positive ion mass spectra (SIMS+ mode) for the 5.7 Vpp and feeding gas flow rate of 2 slm. From the graph we can see that the plasma jet plume is rich with ion species that are needed in treatment of surfaces for cleaning or sterilization.

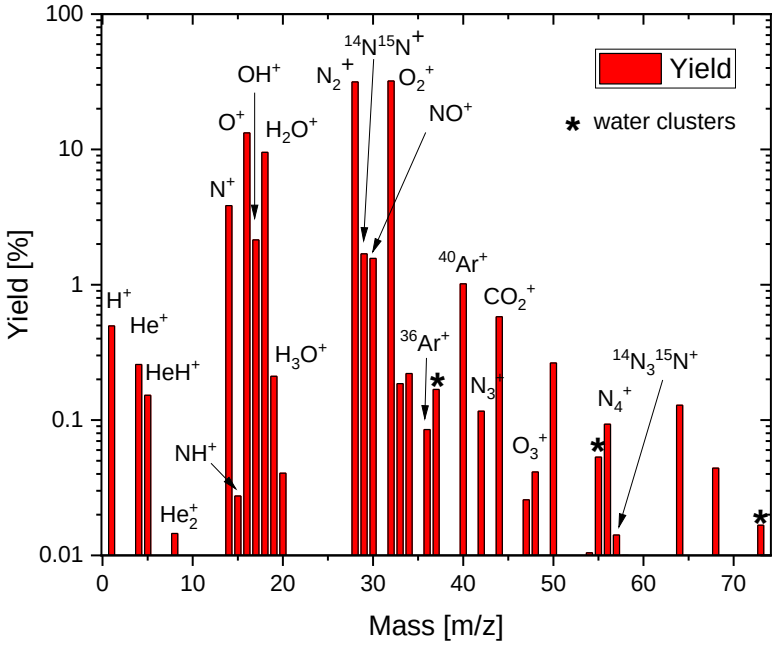

Fig. 2: Yields of the positive ions formed in plasma jet, 5.7 kVpp, 2 slm

In Figure 2 one can see mass spectrum of positive ions where the most abundant species are oxygen and nitrogen. The species formed by ionization of the working gas such as He^+, HeH^+ and He_2^+ are also significant.

Humidity in atmosphere influences production of OH^+, H_2O^+, H_3O^+ and appearance of water clusters $H^+(H_2O)_n$, which are shown in the image with an asterisk. The rich spectrum of positive ions obtained from the plasma jet indicates its potential application. The mass spectrometer technique itself is a powerful tool for monitoring and designing the spectrum itself.

Acknowledgment: This work was supported by MSTDI Republic of Serbia grant number 451-03-68/2023-14/200024. Z. Lj. P. is grateful to the SANU Project F155 for partial support. This work was supported by the project Adaptation of vegetables to new agrometeorological conditions in Slavonia (AVACS), KK.05.1.1.02.0004. The project was financed by the European Union from the European Regional Development Fund.

[1] E. H. Choi et al. *AAPPS Bulletin* **31** (2021) 10.
[2] N. Romanjek Fajdetić et al *Sustainability* **14** (2022) 16237.
[3] D. Maletić et al *Plasma Sources Sci. Technol.* **31** (2022) 025011.
[4] A. Stancampiano et al *J. Phys. D: Appl. Phys.* **51** (2018) 484004.
[5] J. Benedikt et al *Plasma Sources Sci. Technol.* **30** (2021) 033001.

POSTER SESSION 2, Thursday, July 11, 14:30-16:30

P2-T1-01 **S. Kawaguchi**; Y. Iwabe; K. Takahashi; K. Satoh; *Electron collision cross section set of O_2*

P2-T1-02 **V. J. Herrero**; R. J. Pelaez; M. Jimenez-Redondo; I. Tanarro; *Ion chemistry in C_2H_2:N_2:Ar cold plasmas: Anions of astrophysical interest*

P2-T1-03 **W. Graef**; E. Carbone; L. Vialetto; M. Hopkins; L. L. Alves; *The 2024 status report on the LXCat project*

P2-T3-04 **L. Kuijpers**; C.F.A.M van Deursen; E.J. Devid; W.A. Bongers; M.C.M. van de Sanden; *Experimental investigation of the complex chemistry in dry reforming microwave discharges*

P2-T3-05 **N. Babucic**; K.Kutasi; N.Skoro; N.Puac; *Characterization of Microwave Surface-Wave Launchers operating at Atmospheric pressure for Water Treatment*

P2-T3-06 V. Ilbeigi; **P. Kumari**; S. Matejcik; *Study plasma-chemical processes of alkanes in atmospheric pressure corona discharge by ion mobility spectrometry-mass spectrometry (IMS-MS)*

P2-T3-07 S. Lazarova; Ts. Paunska; V. Vasilev; **St. Kolev**; *CO_2 Conversion in a Gliding Arc Discharges with Different Electrode Materials and Magnetic Field Configurations*

P2-T4-08 **F. J. Morales-Calero**; A. Cobos-Luque; J. Munoz; R Rincon; A. M. Raya; J. A. Alcuson; N. Y. Mendoza-Gonzalez; M. D. Calzada; *Fundamental study of atmospheric pressure Ar-N_2 postdischarges and their application for metallic surfaces cleaning and activation*

P2-T4-09 **G. Cartry**; R. MaGee; J. Broude; T. Gans; J. Dedrick; M-A Pinault-Thaury; M. Sasao; Jocelyn Archard; J.M. Layet; *Surface production of negative-ions in hydrogen plasmas: comparative analysis of different surface materials*

P2-T4-10 **L. Zajickova**; M. Janusova; D. Necas; M. Elias; D. Hegemann; P. Navascues; L. Janu; *Insight into plasma polymerization with the significant contribution of ions towards deposition and etching balance*

P2-T4-11 **R. Masheyeva**; P. Hartmann; L.-Y. Luo; K. Dzhumagulova; Y.-X. Liu; J. Schulze; Z. Donko; *On the in-situ determination of the effective secondary electron emission coefficient in low pressure capacitively coupled radio frequency discharges based on the electrical asymmetry effect*

P2-T4-12 **T. Nonaka**; K. Takahashi; A. Uchida; O. Tsuji; *Deposition rates and chemical compositions of C_4F_8 plasma polymerization films on trench sidewalls*

P2-T4-13 **V. Mazankova**; D. Trunec; *Kinetics of ozone production by surface processes*

P2-T4-14 A. Siby; D. Stefas; Y. Agha; L. Invernizzi; C.Y. Duluard; K.. Gazeli; G Lombardi; K. Hassouni; **S. Prasanna**; *Usefulness of ps-TALIF to measure gas temperature and collisional cross-sections*

P2-T4-15 **P. Viegas**; J. Afonso; J. Silveira; T. C. Dias; L.Vialetto; A. S. Morillo-Candas; V. Guerra; *Surface recombination in Pyrex in oxygen DC glow discharges*

P2-T5-16 **N. Selakovic**; D. Maletic; N. Puac; G. Malovic; Z. Lj Petrovic; *Time-resolved images and detection of positive and negative ion species of atmospheric pressure plasma jet with spiral electrodes*

Time-resolved images and detection of positive and negative ion species of atmospheric pressure plasma jet with spiral electrodes

N Selaković(*)[1], D Maletić[1], N Puač[1], G Malović[1] and Z Lj Petrović[2,3]

[1] *Institute of physics, University of Belgrade, Pregrevica 118, 11080 Belgrade, Serbia*

[2] *Serbian Academy of Sciences and Arts, Knez Mihailova 35, 11000 Belgrade, Serbia*

[3]*School of Engineering, Ulster University, Jordanstown, Co. Antrim, BT37 0QB UK*

(*)*nele@ipb.ac.rs*

The potential use of cold atmospheric pressure plasma sources has emerged in recent decades in number of fields, including metalurgy, agriculture, biology, medicine, and more. The use of atmospheric pressure plasma jet (APPJ) with spiral electrodes introduces an interesting approach to plasma generation, offering increased source length and extention of potential applications in medicine [1]. In this study, we explore the experimental setup and diagnostic techniques employed to characterize the APPJ and its chemical composition. Our focus lies on the potential application of non-thermal plasma in sterilization, particularly in sterilizing catheters and infusion hoses [2]. By utilizing spiral electrodes wrapped around a glass tube, we aim to harness the benefits of APPJ for practical applications, while also gaining insights into discharge dynamics and chemical composition through diagnostic techniques such as time resolved ICCD imaging and mass spectrometry [3].

The experimental setup (shown in Fig. 1) consisted of a 30 cm long glass tube wrapped with two isolated copper wires arranged in a spiral configuration (10 mm interelectrode gap), ensuring no contact between them. One wire was powered by a sine wave at 70 kHz excitation frequency and the second wire served as grounded electrode. A signal generator was used to provide a sine voltage of few volts, which was then amplified to the range of kV and applied to the powered electrode. A high voltage probe and oscilloscope were employed to measure voltage and current signals, enabling the calculation of power delivered to the discharge. Helium gas was used as the feeding gas at a rate of 4 slm The discharge appeared inside the glass tube as the ionization front that followed closely the shape of electrodes and then propagated as a plume a few centimeters outside the glass tube.

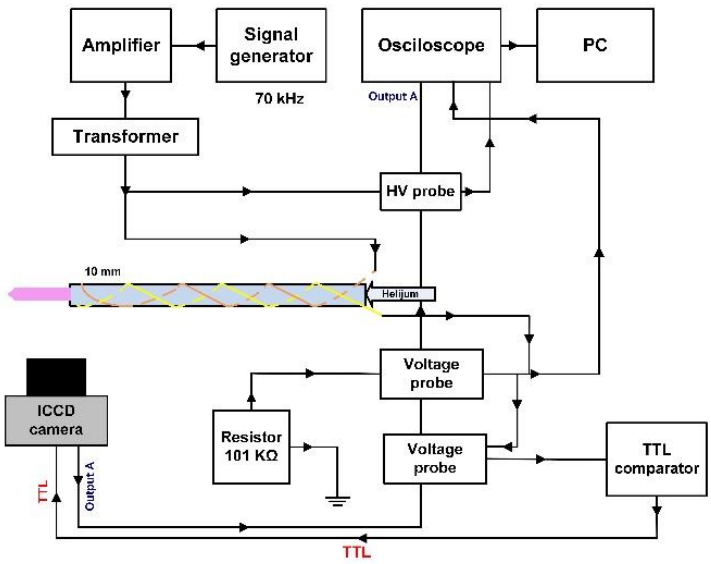

Fig. 1: Experimental setup of APPJ with spiral electrodes

We have performed time resolved ICCD imaging for various applied voltages and used these images to determine the velocity of PAPS (Pulsed Atmospheric Plasma Streamer). A frame of the temporal evolution captured by the ICCD camera is shown in Fig. 2, where the occurrence of PAPS (Pulsed Atmospheric Plasma Streamer) is displayed for the highest voltage value. This demonstrates that the discharge is not continuous but rather it consisted of plasma packages traveling at a velocity far faster than the working gas flow.

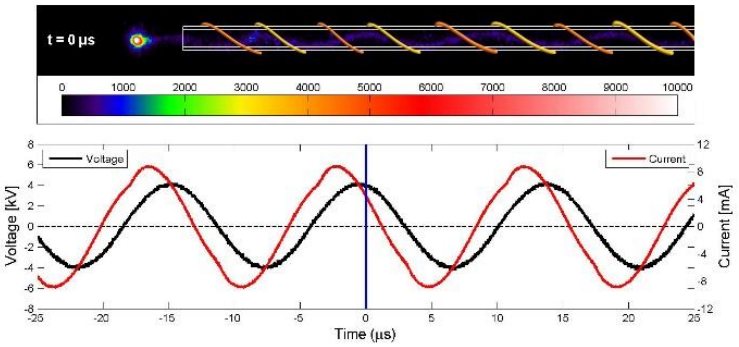

Fig 2.: Time-resolved ICCD frame synced with V-I signals

The positive ion mass spectrum acquired by the Hiden HPR60 MBMS mass spectrometer is shown in Figure 3. The predominant ions of N^+, O^+, N^+, O^+, H_2O^+, H_3O^+, $He^+$and HeH^+ were produced by ionization in a combination of the working gas with atomic and molecular species from the surrounding air, humidity and atmospheric impurities.

Additionally, oxygen species like O^-, OH^-, O_2^-, and O_3^- dominate the mass spectra of negative ions that we have obtained (spectra not shown here). Observations of the $O^- \cdot (H_2O)_n$ and $OH^- \cdot (H_2O)_n$ indicated a potential for water cluster chemistry in the APPJ plume.

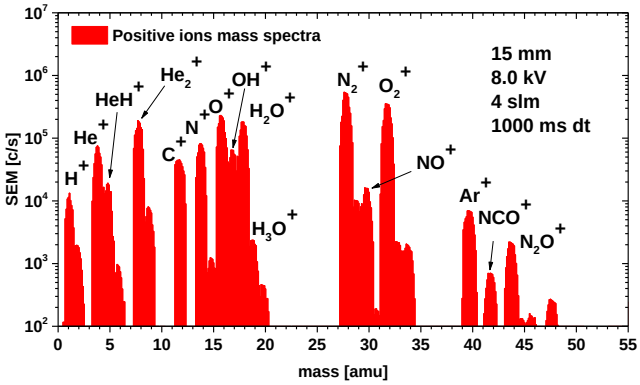

Fig 3.: Positive ions mass spectra

The rich spectrum of positive and negative ions produced in APPJ with spiral electrodes makes this source of non-thermal plasma interesting for potential application in sterilization of long tubes. The appearance of the discharge outside of the glass tube expands the potential application to the other area of interest such as medicine, biotechnologies, agriculture, and more.

Acknowledgment: This work was supported by MSTDI Republic of Serbia grant number 451-03-68/2023-14/200024. Z. Lj. P. is grateful to the SANU Project F155 for partial support. This work was by the Science Fund of the Republic of Serbia, 7739780, Atmospheric pressure plasmas operating in wide frequency range – a new tool for production of biologically relevant reactive species for applications in biomedicine - APPerTAin-BIOM.

[1] M. Polak et al., *Plasma processes and polymers* **9**(1) (2012) 67-76.
[2] T. Sato *et al.*, *Plasma Processes and Polymers*, **5**(6) (2008) 606-614.
[3] A. Stancampiano *et al.*, *Journal of Physics D: Applied Physics*, **51**(48) (2018) 484004.

Detailled Program-Book of abstracts

Contents

Mass spectrometry of plasma reactive species produced by a surface DBD source

N. Škoro[1], N. Selaković[1] and N. Puač[1]

[1] *Institute of Physics, University of Belgrade, Pregrevica 118, 11080 Belgrade, Serbia*

In this study a Molecular Beam Mass Spectrometer was used to investigate production of reactive species by a DBD source. The source was operated at different powers and frequencies, in air and gas mixtures and measurements were conducted at different distances from the electrode. The analysis revealed dependence of concentrations of reactive species on operating parameters of the discharge.

1 Introduction

As non-thermal plasmas at atmospheric pressure can be generated in ambient air or gas mixture, they have been studied extensively for different applications, including recently established applications in agrifood field [1]. Dielectric barrier discharge (DBD) sources are particularly convenient, with respect to other atmospheric pressure sources, as they can create large effective surfaces of active plasma region. So, plasma treatments with DBD source can be utilized for effective decontamination of molds, mycotoxins and other pathogens from food products [2]. In these processes ratio between concentrations of reactive short-lived and long-lived species plays a key role. Formation of reactive species depends on several parameters, e.g. input power, driving signal frequency, gas mixture etc. Mass spectrometry is a plasma diagnostic technique that can provide immediate information on created neutral and ionic species in the interaction volume which presents a crucial input parameter for studying interaction processes and revealing plasma mechanisms in plasma treatment [3].

2 Experimental setup

In this study mass spectrometry was used to investigate production of reactive species by a DBD source. The source was operated at different powers and frequencies, in air and gas mixtures and measurements were conducted at different distances from the electrode. The analysis of reactive species was performed using HIDEN Molecular Beam Mass Spectrometer (MBMS) HPR60 device.

For detection of neutral reactive species, the Residual Gas Analyzer (RGA) mode of the MBMS was employed in two operational ways. In the MID scan mode, a real-time monitoring of radical evolution under both active and inactive discharge conditions was performed. A shutter in the inner side of the sampling orifice (SL) allowed to measure the sum of foreground and backgound (SL open) and the background signal (SL closed).

3 Results and conclusion

In Fig.1 we show measurement of O_3 concentration at 2 distances from the source. There is a significant peak at the moment of plasma inception (6 minutes after start of the recording) when there was a gradual increase in input voltage from 0 V to 200 V.

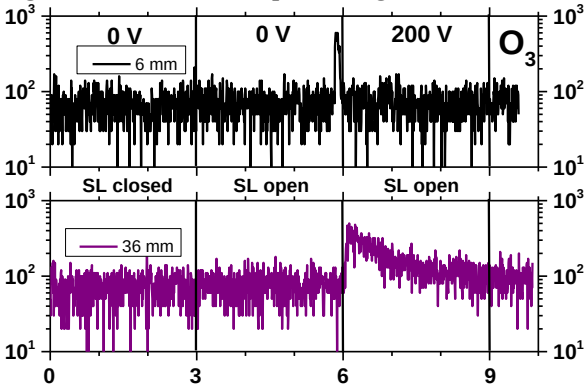

Figure 1. O3 time evolution in case of plasma off (0 V) and on (200 V) conditions for different distances (6 mm and 36 mm) from the plasma source to the mass spectrometer sampling orifice.

This behaviour suggests that ozone formation is initially enhanced at lower plasma power, while increasing voltage up to 200 V leads to a stabilization effect.

Acknowledgments: *This work was supported by the MSTDI Republic of Serbia grant no. 451-03-66/2024-03/200024.*

References

[1] Bilea, F. et al. Non-Thermal Plasma as Environmentally-Friendly Technology for Agriculture: A Review and Roadmap. *Critical Reviews in Plant Sciences* **43**, 428–486 (2024).

[2] Janić Hajnal, E. et al. Effect of Atmospheric Cold Plasma Treatments on Reduction of Alternaria Toxins Content in Wheat Flour. *Toxins* **11**, 704 (2019).

[3] Maletić, D. et al. Detection of atomic oxygen and nitrogen created in a radio-frequency-driven micro-scale atmospheric pressure plasma jet using mass spectrometry. *Plasma Phys. Control. Fusion* **54**, 124046 (2012).

Investigation of reactive species formation in surface dielectric barrier discharge with liquid electrodes

O. Galmiz[1], R. Cimerman[1], M. Janda[1], N. Selaković[2], N. Puač[2] and Z. Machala[1]

[1]*Division of Environmental Physics, Faculty of Mathematics, Physics and Informatics, Comenius University Bratislava, Slovakia*
[2]*Institute of Physics, University of Belgrade, Pregrevica 118, 11080 Belgrade, Serbia*

This study focuses on the characterization and quantification of reactive species produced by cold plasma generated using liquid electrodes in a surface dielectric barrier discharge system. By varying experimental conditions, the production of reactive oxygen and nitrogen species in both gas and liquid phases was systematically analysed. Several analytical techniques were employed to assess the chemical composition of the plasma-treated medium.

1 General

The typical surface dielectric barrier discharge (SDBD) systems, produce plasma along a thin dielectric layer and are not capable of direct interaction with liquids. This limitation restricts the formation of short-lived, highly reactive species, such as hydroxyl (·OH) and oxide (·O) radicals and their transport to liquids. To overcome this challenge, we use a liquid electrode SDBD system, where plasma is ignited directly from the liquid surface [1,2]. This approach significantly enhances plasma-liquid interactions, making the system more versatile for applications such as water activation, material surface treatment, and biomedical sterilization.

Liquids that are plasma-treated and contain a mixture of various reactive oxygen and nitrogen species (RONS) are typically referred to as plasma-activated liquids (PAL). Key reactive species such as ·OH, O_3 , NO, NO_2 , and H_2O_2 play crucial roles in plasma-driven surface modifications and decontamination processes [3,4]. The interaction of these species with target surfaces during plasma treatment significantly influences the reaction pathways and outcomes.

This study presents an investigation of the electrical discharge properties of a cold plasma that is created using liquid electrodes. The chemical species that are created during the discharge and subsequently transferred into the liquid are systematically characterized and quantified.

To characterize the reactive species formed in the gas phase, Fourier-transform infrared (FTIR) spectroscopy was used to quantify gas-phase species, such as NO, NO_2 , N_2 O, and O_3 . The concentration of nitrogen-containing species showed fluctuations with increased discharge power, peaking at approximately 50 ppm. Meanwhile, O_3 concentrations reached up to 150 ppm, varying based on reactor type and discharge power.

In addition, the analysis of these species, as well as the detailed composition of the plasma were studied by using mass spectroscopy. The spatial evolution of O_3 within the liquid phase was further analyzed using in-situ UV-VIS spectroscopy.

In parallel, absorption spectroscopy was employed to quantify key plasma-induced species in the plasma-treated liquid, with concentrations measured in the mM range.

Acknowledgment
This work was funded by the EU NextGenerationEU through the Recovery and Resilience Plan for Slovakia under the project No.09I03-03-V04-00094, the Marie S. Curie Action Postdoctoral Fellowship under Horizon Europe with grant agreement number 101066764, and Slovak Research and Development Agency grants APVV SK-SRB-23-0043.

References

[1] Galmiz, O. et al. Hydrophilization of outer and inner surfaces of Poly(vinyl chloride) tubes using surface dielectric barrier discharges generated in ambient air plasma. *Plasma Process. Polym*. **14**, 1600220 (2017).
[2] Galmiz, O. et al. Production of reactive species by using surface dielectric barrier discharge in direct contact with water. *Plasma Sources Sci. Technol.* **34** 025011 (2025).
[3] Brandenburg, R. et al. Antimicrobial Treatment of Heat Sensitive Materials by Means of Atmospheric Pressure Rf-Driven Plasma Jet. *Contrib. Plasma Phys*. **47**, 72 (2007).
[4] Machala, Z. et al. Plasma agents in bio-decontamination by dc discharges in atmospheric air. *J. Phys. D: Appl. Phys*. **43,** 222001 (2010).

AAPPS DPP

KYUSHU UNIVERSITY

9th Asia-Pacific Conference on Plasma Physics

AAPPS-DPP2025 Program Book

September 21-26, 2025
Fukuoka International Congress Center
Fukuoka, JAPAN

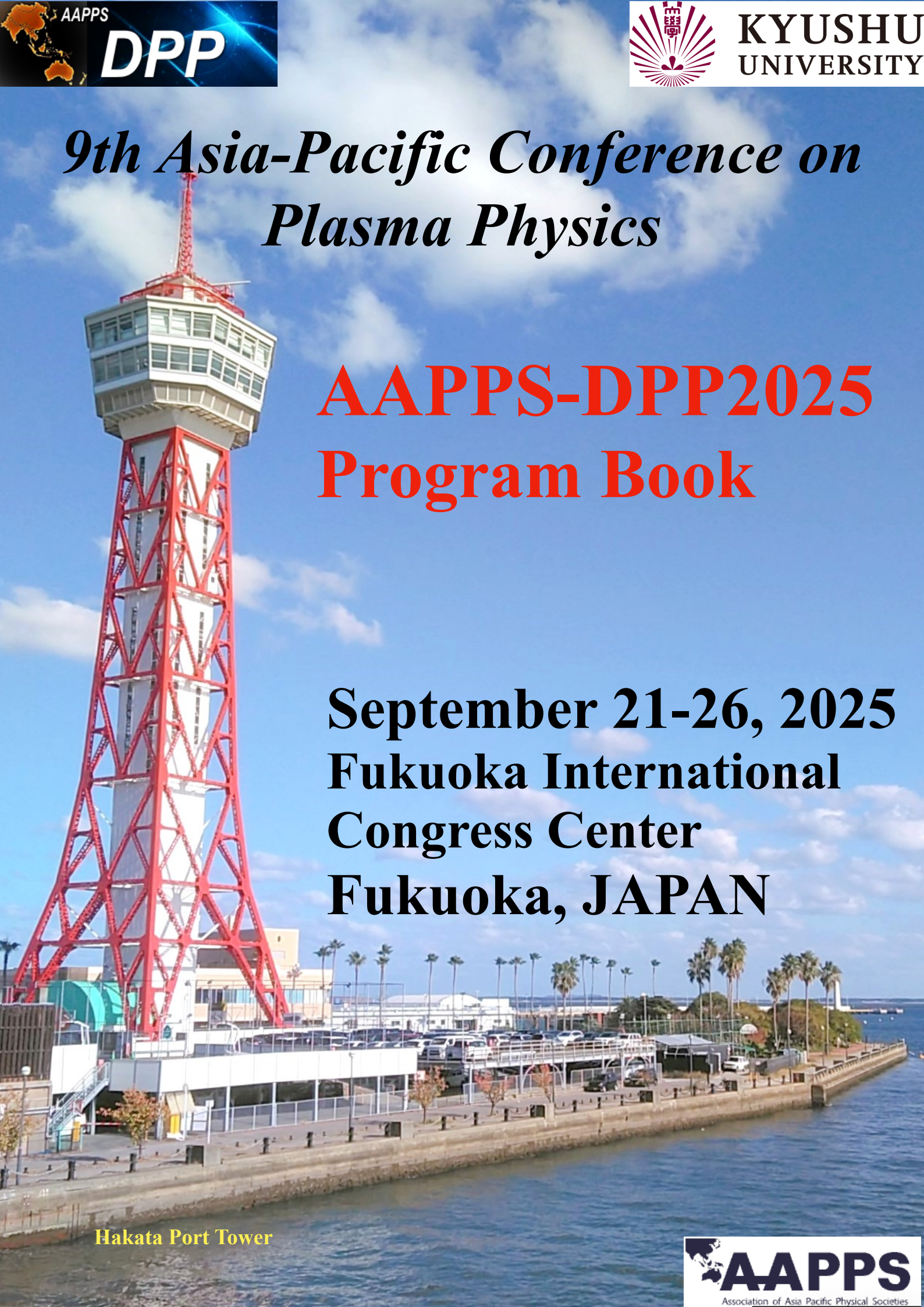

Hakata Port Tower

AAPPS
Association of Asia Pacific Physical Societies

9th Asia-Pacific Conference on Plasma Physics

(AAPPS-DPP2025) September 21-26, 2025 https://www.aappsdpp.org/DPP2025/

Fukuoka International Congress Center, Fukuoka, Japan

Organized by AAPPS-DPP

Issued September 17, 2025

The Division of Plasma Physics of the Association of Asia Pacific Physics Societies (AAPPS-DPP) has been successfully organizing annual conferences on plasma physics in the Asia Pacific region for the past 8 years. The 1st Asia-Pacific Conference on Plasma Physics (AAPPS-DPP2017) was held during September 18-23, 2017 in Chengdu, China (http://aappsdpp.org/DPP2017rogramlatest/index.html) followed by AAPPS-DPP2018 during November 12-17, 2018 in Kanazawa, Japan (http://aappsdpp.org/DPP2018/index.html), and AAPPS-DPP2019 during November 4-8, 2019 in Hefei, China (http://aappsdpp.org/DPP2019/index.html). The subsequent three conferences AAPPS-DPP2020 (http://aappsdpp.org/DPP2020/index.html), AAPPS-DPP2021 (http://aappsdpp.org/DPP2021/index.html) and AAPPS-DPP2022 (http://aappsdpp.org/DPP2022/index.html) were held as online conferences using the Zoom platform. We returned to an in-person format in the 7th Asia-Pacific Conference on Plasma Physics (AAPPS-DPP2023) which was held from Nov. 12-17, 2023 in Port Messe Nagoya, Japan (https://www.aappsdpp.org/DPP2023/index.html). 8th Asia-Pacific Conference on Plasma Physics (AAPPS-DPP2024) was held in Grand Swiss-Bel Hotel, Malacca, Malaysia during Nov. 3-8, 2024, co-organized by Malaysian Institute of Physics (MIP) (https://www.aappsdpp.org/DPP2024/index.html).

[1] Scope of the AAPPS-DPP2025:

AAPPS-DPP2025 is a plasma physics conference under the authority of AAPPS-DPP for scientific discussions on plasma physics. This conference provides interdisciplinary and in-depth discussions among and in various fields of plasma physics and applications.

[2] Organization:

AAPPS-DPP (http://aappsdpp.org/AAPPSDPPF/) is organizing body of this conference. Kyushu University is co-organizer.

AAPPS-DPP chair
&2025 IOC chair
Rajdeep S Rawat

AAPPS-DPP CEO
& 2025 General PC chair
Mitsuru Kikuchi

LOC chair, AAPPS-DPP BoD
Senior Vice President of Kyushu U.
Masaharu Shiratani

[3] Program Overview

Conference run from Sunday to Friday. We have A. Hasegawa memorial session on Sunday, who is Maxwell and Alfven prize winner as well as DPP's I-HAC member. Due to large number of talks, F, A1 and A2 topical session starts from Sunday. We have reception on Sunday 15:00-17:00. Monday to Friday are standard conference days where morning sessions are plenary talks dedicated for interdisciplinary discussion and in-depth discussion in specific fields in the afternoon session.

9th Asia-Pacific Conference on Plasma Physics (AAPPS-DPP 2025) ***Fukuoka International Congress Center 21-26, September, 2025*** *[ver. 9-17]*

Sunday (2025.09.21)		Monday (2025.09.22)		Tuesday (2025.09.23)		Wednesday (2025.09.24)		Thursday (2025.09.25)		Friday (2025.09.26)
		Registration: 7:30~		Registration : 8:00~		Registration : 8:00~		Registration : 8:00~		Registration : 8:00~
		8:30-10:10:Opening(Chair:Kazunori Koga) O-1 M. Shiratani Opening remark 10min O-2 R. Rawat DPP Chair's address 5min O-3 M. Kikuchi DPP CEO remark 5min O-4 S. Bhattacharjee/IPE U30 ceremony 15min O-5 H. Suk U40 ceremony 15min O-6 Se Youn Moon PIP ceremony 15min O-7 Lou C. Lee Chandra ceremony 15min O-8 Y. Kishimoto About Kuniaki Mima 5min O-9 Liu Chen About Akira Hasegawa 5min O-10SiWoo Yoon AAPPS-DPP2026 10min O-11 Wonho Choe IUPAP award 5min		**8:30-10:30:Plenary 2 Chairs:R. Matsumoto, P.Diamond, Yu Lin, Y.Kuramitsu** 8:30-9:00: PL-5 Hiroya Yamaguchi(SA) 9:00-9:30: PL-6 Vladimir Rosenhaus(CD) 9:30-10:00:PL-7 Anna Tenerani(F) 10:00-10:30:PL-8 Gianluca Gregori(L2)		**8:30-10:30:Plenary 4 Chairs: CK Huang, TS Hahm, Pisin Chen, F. Zonca,** 8:30-9:00:PL-13 Yan Feng(B2) 9:00-9:30:PL-14 Ting Long(CD) 9:30-10:00:PL-15 James Rosenzweg(L2) 10:00-10:30:PL-16 Mahendra Verma(F)		**8:30-10:30:Plenary 6 Chairs: T. Johzaki, Feng Chen, Liu Chen, SK Tiwari** 8:30-9:00:PL-21 Alexey Arefiev(L1) 9:00-9:30:PL-22 Ying Li(SA) 9:30-10:00:PL-23 Colin Roach(F) 10:00-10:30:PL-24 Edward Thomas(B2)		**8:30-10:30:Plenary 8 Chairs: X.Zhang, Y. Yamanishi, X. Garbet, L. Xu** 8:30-9:00:PL-29 Wei Chen(MF1) 9:00-9:30:PL-30 K. Sankaranarayanan (A2) 9:30-10:00:PL-31 Julian Mak(CD) 10:00-10:30:PL-32 Lorin Matthews(B2)
	[3]9:30-16:35: A. Hasegawa memorial symposium (410) Morning session 5 x 25min invited talks Lunch break Afternoon session 5 x 25min invited talks	**10:10-11:00: Photo & Coffee Break**		**10:30-11:00: Coffee break**		**10:30-11:00: Coffee break**		**10:30-11:00: Coffee break**		**10:30-11:00: Coffee break**
		11:00-13:00: Plenary1 Chairs: LC Lee, SY Moon, ZX Wang, P. Yoon		**11:00-13:00:Plenary3 Chairs: D. Batani, T. Tokuzawa, Won-Ha Ko, H. Tanaka**		**11:00-13:00:Plenary 5 Chairs: XZ Zhao, S. Zenitani, Kai Zhao, Thomas Bosman**		**11:00-13:00:Plenary 7 Chairs: QZ Zhang, S. Benkadda, H. Kurita, T. Hada**		**11:00-13:00:Plenary 9 Chairs: S.Toko, Y. Omura, Jack Lovell, S.Jacquemot**
		11:00-11:30: PL-1 Qu-Gang Zong (Chandra)		11:00-11:30:PL-9 Tobias Dornheim(L1)		11:00-11:30:PL-17 Mark Cheung(SA)		11:00-11:30:PL-25 Ramses Snoeckx(A1)		11:00-11:30:PL-33 Erik Wagenaars(A1)
		11:30-12:00: PL-2 Keishi Sakamoto (PIP)		11:30-12:00:PL-10 Haiqing Liu(B1)		11:30-12:00:PL-18 Takahiro Miyoshi(B1)		11:30-12:00:PL-26 Brendan Lyons(B1)		11:30-12:00:PL-34 Xinlin Li(SG)
	[4] 12:00-16:10	12:00-12:30: PL-3 Felix Warmer(MF1)		12:00-12:30:PL-11 Y. Ono(MF1)		12:00-12:30:PL-19 Ya Zhang(A1)		12:00-12:30:PL-27 Joanna Pawlat(A2)		12:00-12:30:PL-35 GianMario Polli (MF2)
		12:30-13:00: PL-4 Linghua Wang(SG)		12:30-13:00:PL-12 Bornali Sarma(A2)		12:30-13:00:PL-20 A. Kirschner(MF2)		12:30-13:00:PL-28 NS Saini(SG)		12:30-13:00:PL-36 Natsumi Iwata(L1)
	F-1(414)									
	A1-1(402+403)	**13:00-14:00: Lunch** **13:05-14:05: WIPP WS(1) room 203+204**		**13:00-14:00: Lunch** **13:05-14:05: WIPP WS(2) room 203+204**		**13:00-14:00: Lunch** **13:00-14:00: BoD [404]**		**13:00-14:00: Lunch** **13:00-14:00: I-HAC [404]**		**13:00-14:00: Lunch**
[1] 13:00-17:00 : Registration **[2]15:00-17:00: Reception at 5th Floor**	A2-1(405+406)	**14:00-16:10: Topical 1**	**14:00-16:00** Poster session 1 201+202	**14:00-16:10: Topical 3**	**14:00-16:10** Poster session 3 201+202	**14:00-16:10: Topical 5**	**14:00-16:10** Poster session 5 201+202	**14:00-16:10:Topical 7**	**14:00-16:10** Poster session 7 201+202	**14:00-16:10:Topical 9**
	F-2(414)				Poster core time L1,L2				Poster core time F, A1,A2	
	A1-1(402+403)	CD-1(401)		CD-3(401)		CD-5(401)		CD-7(401)		CD-9(401)
	A2-2(405+406)	F-3(414)		F-5(414)		F-7(414)		B1-10(413)		F-11(414)
		B1-1(413)		B1-5(413)		B1-8(413)		B2-7 (504+505)		B1-12(413)
	RMPP Editor meeting (410) 17:00-18:00	B1-2(404)		B1-6(404)		B2-5(504+505)		L1-7(411)		B2-9(504+505)
		B2-1(504+505)		B2-3(504+505)		A1-6(402+403)		L2-7(412)		A1-11(402+403)
		A1-2(402+403)		A1-4(402+403)		A2-7(405+406)		SG-7 (503)		A2-10(405+406)
		A2-3(405+406)		A2-5(405+406)		L1-5(411)		SA-7(502)		L1-9 (411)
		L1-1(411)		SG-3(503)		L2-5(412)		MF1-7(409)		L2-9 (412)
		L2-1(412)		SA-3(502)		SG-5(503)		MF1-11(402+403)		SG-9 (503)
		SG-1(503)		MF1-3 (409)		SA-5(502)		MF2-7(410)		SA-9 (502)
		SA-1(502)		MF1-10(412)		MF1-5(409)				MF1-9(409)
		MF1-1(409)		MF2-3 (410)		MF2-5(410)				MF2-9(410)
		MF2-1(410)								HEDP-2 (404)
		16:10-16:30: Coffee Break		**16:10-16:30: Coffee Break**		**16:10-16:30: Coffee Break**		**16:10-16:30: Coffee Break**		**16:10-16:30: Coffee Break**
		16:30-18:40 Topical 2	**16:30-18:40** Poster session 2 201+202	**16:30-18:40 Topical 4**	**16:30-18:40** Poster session 4 201+202	**16:30-18:40 Topical 6**	**16:30-18:40** Poster session 6 201+202	**16:30-18:40 Topical 8**	**16:30-18:40** Poster session 8 201+201	**16:40-18:30:Plenary 10 Chairs: Y. Ghim, H. Suk, R. Rawat, M. Kikuchi**
		CD-2(401)		CD-4(401)		CD-6(401)		CD-8(401)		16:30-17:00: PL-37 Felix Parra(MF2)
		F-4(414)		F-6(414)		F-8(414)		F-10(414)		17:00-17:30: PL-38 Min Chen(L2)
		B1-3(413)		B1-7(413)		B1-9(413)	Poster core time CD, SG, SA, MF1,MF2	A1-9(402+403)	Poster core time B1, B2	17:30-18:00: PL-39 Poster Prizes
		B1-4(404)		B2-4(504+505)		B2-6(504+505)		A1-10(404)		18:00-18:30: PL-40 Closing W. Choe
		B2-2(504+505)		A1-5(402+403)		A1-7(402+403)		A2-10(405+406)		
		A1-3(402+403)		A2-6(405+406)		A2-8(405+406)		L1-8(411)		
		A2-4(405+406)		L1-4(411)		L1-6(411)		L2-8(412)		
		L1-2(411)		L2-4(412)		L2-6(412)		SG-8(503)		
		L2-2(412)		SG-4(503)		MF1-6(409)		SA-8(502)		
		SG-2(503)		SA-4(502)		P-B fusion(410)		MF1-8(409)		
		SA-2(502)		MF1-4(409)		HEDP-1 (404)		MF2-8(410)		
		MF1-2 (409)		MF2-4(410)						
		MF2-2 (410)		MF2-10(404)						
		19:30 ~: Reception for VIP		**18:50-19:50: EV-2 (410)** **8th General Assembly**				**20:00-23:00: Conference Dinner at Izakaya restaurant**		

Table 1 Program Overview

[9] Scientific Program

9.1 Scientific Program

9th Asia-Pacific conference on Plasma Physics will cover following sub-disciplines of plasma physics.

1.	CD	: Cross-disciplinary (Focused Topics related turbulence and structure formation)	:PC chair ;Patrick Diamond
2.	F	: Fundamental disciplines in plasma physics	:PC chair ; Fulvio Zonca
3.	B1	: Plasma Simulation, Diagnostics and Data Science	:PC chair ; T-H Watanabe
4.	B2	: Quantum/Dusty plasma, Plasma Source, Basic Experiments, A&M	:PC chair ; Yan Feng
5.	A1	: Plasma Materials and Processing	:PC chair ; Se Young Moon
6.	A2	: Plasma Life Science	:PC chair ; Masafumi Jinno
7.	L1	: ICF, HEDS, Laboratory Astro Physics	:PC chair ; Yasuhiko Sentoku
8.	L2	: LWFA/PWFA, Photon beam Science	:PC chair ; Min Chen
9.	SG	: Space plasma & Geomagnetism	: PC chair ;Yoshiharu Omura
10.	SA	: Solar &Astro plasma	: PC chair ;Peng-Fei Chen
11.	MF1	: Magnetic Fusion plasma (Core)	: PC chair ;Zheng-Xiong Wang
12.	MF2	: Magnetic Fusion plasma (Edge)	: PC chair ; Young-chul Ghim

CD(Cross-Disciplinary) covers cross-disciplinary focused topics related to turbulence and structure formation
F(Fundamental disciplines in plasma physics) covers 1. Mathematical plasma physics, 2. MHD and Reconnection, 3. Kinetic MHD, 4. Plasma turbulence, 5. Gyro kinetics, 6. Collisional transport, 7. Turbulent transport, 8. Phase space dynamics, 9. Relativistic plasma physic
B1 (Basic 1) covers 1. Plasma simulation and computational method, 2. Plasma diagnostics and techniques, 3. Data Science
B2 (Basic 2) covers 1. Quantum and Dusty plasmas, 2. Plasma Sources, 3. Basic experiments and emerging topics, 4. Atomic& Molecular physics in plasma,
A1 (Applied 1) covers Plasma Materials and Processing
A2 (Applied 2) covers Plasma Life Science
L1 (Laser 1) covers Inertial Confinement Fusion, High Energy Density Science, and Laboratory Astro Physics
L2 (Laser 2) covers Laser and plasma wakefield acceleration, and Photon beam Science
SG(Space&Geomagnetism) covers space and geomagnetic plasma physics program covers
SA(Solar/Astro) covers solar plasma physics and astro plasma physics
MF1 (Magnetic fusion (Core)) covers magnetic confinement fusion plasma (core)
MF2 (Magnetic fusion (Edge)) covers magnetic confinement fusion plasma, edge, SOL, divertor and PMI)

9.2 Satellite Meeting : symposium, mini-workshops

There are several symposiums, mini-workshops, special sessions.

1. Akira Hasegawa memorial symposium

Our distinguished professor Akira Hasegawa (I-HAC member) passed on June 22. Zensho Yoshida (U. Tokyo) and Liu Chen (UCI, JZU, Acad. Sinica) are organizing memorial symposium on his scientific achievements such as Kinetic Alfven wave, Hasegawa-Mima equation, Dipole plasma confinement, Self-organization and formation of thermal barrier (Hasegawa-Wakatani equation), Optical Soliton.

2. Special Session in honor of 2024 S. Chandrasekhar Prize Laureate Pisin Chen

In Laser plasma sessions (L2), special session on Prof. Pisin Chen's scientific achievements on Plasma Wakefield Acceleration and Laboratory Astro Plasma Physics will be organized by Pisin Chen.

3. K. Mima Memorial Session

Memorial session (L1-4) will honor the scientific achievements and legacy of Prof. Kunioki Mima, who was a great academic in the field of theoretical and computational plasma physics. Organizers are Y. Kishimoto and N. Iwata.

4. Mini Workshop on Woman in Plasma Physics

Mini Workshop for Women in Plasma Physics (WIPP) started from AAPPS-DPP2023 and continued to AAPPS-DPP2024. 2025 WIPP WS will be held 13:05-14:05 on Monday 22th and Tuesday 23th of September 2025. Organizers are Anisa Qamar and A.B. Murphy.

5. Mini Symposium: Advancements in Hydrogen-Boron Fusion

This symposium covers the landscape of hydrogen-boron research with both magnetic confinement and laser-driven approaches. Organizers are Dimitri Batani and Martin Peng.

6. EPS-AAPPS joint session

L1-5 session is EPS-AAPPS session organized by Dimitri Batani to strengthen this cooperation.

Plenary talks: Morning sessions will be plenary talks with 30 minutes long including Q&A. Plenary speakers should gave short general introduction in the beginning and should not use Jargon in your sub-field since the audience is not expert in your sub-field.

A1-6 plasma processing and simulation/diagnostics [Chair: Peter Bruggeman] 14:00-16:20, Sep. 24 [402+403]

A1-6-I1 20min	Kai Zhao(Dalian university of technology) Parameter dependences of charged particle dynamics and electron power absorption mode in dual-frequency capacitively coupled argon discharges
A1-6-I2 20min	Bocong Zheng(Beijing Institute of Technology) Transport analysis in capacitively coupled plasmas
A1-6-I3 20min	Masaya Shigeta(Tohoku University) The Difficulty and Charm of Computational Plasma Fluid Mechanics
A1-6-I4 20min	Ho Jun Kim(Hanyang University) Analysis of stagnation point flow within an inductively coupled plasma reactor for the enhancement of deposition methodologies
A1-6-I5 20min	Sanghoo Park(Korea Advanced Institute of Science and Technology (KAIST)) Practical issues in tomographic reconstruction of semiconductor processing plasmas
A1-6-I6 20min	Haruka Suzuki(Nagoya University) Reconstruction of three-dimensional structure of plasma emission using multi-directional imaging

A1-7 Plasma catalyst/surface interaction [Chair: Ho Jun Kim] 16:20-18:50, Sep. 24 [402+403]

A1-7-I1 20min	Sirui Li(Eindhoven University of TEchnology) Integrated Process for Carbon Valorization Using Plasma-Sorbent Systems
A1-7-I2 20min	Peter Bruggeman(University of Minnesota) Plasma Interactions at the Interface with Liquids, Nanoparticles and Catalytic Surfaces
A1-7-I3 20min	Liguang Dou(Institute of Electrical Engineering, Chinese Academy of Sciences) Synergistic promotion of vibrant H radicals and targeted Cu/MgAlO interface for CO2 hydrogenation by non-thermal plasma
A1-7-I4 20min	Zheng Yang(School of Physics, Dalian University of Technology) High efficiency NOx synthesis and regulation using dielectric barrier discharge in the needle array packed bed reactor
A1-7-O1 15min	Pedro Viegas(Instituto Superior Técnico - Universidade de Lisboa) Oxygen loss frequency and recombination probability in oxygen-containing plasmas
A1-7-O2 15min	Monika Verma(Delhi Technological University) Effect of Plasma Process Parameters on the Electrical Characteristics of Dual-Gate Graphene Field-Effect Transistors
A1-7-O3 15min	Abhijit Mishra(Indian Institute of Technology Jodhpur) Variations in Discharge Characteristics of Bipolar Pulsed Cold Atmospheric Plasma Jets Induced by Liquid Conductivity

A1-9 Plasma catalyst/Liquid interaction [Chair: Yangyang Fu] 16:20-18:50, Sep. 25 [402+403]

A1-9-I1 20min	Hang Wang(Institute of Electrical Engineering Chinese Academy of Sciences) Microsecond pulse discharge in oil: electrohydraulic effect, gas generation and mechanics
A1-9-I2 20min	Quan-Zhi Zhang(Dalian University of Technolgoy) Plasma streamer propagation dynamics in gas phase DBD, catalyst pores and SDBD
A1-9-I3 20min	Nikola Skoro(Institute of Physics Belgrade) Measurement of reactive species in atmospheric pressure plasma systems used for creation of plasma activated liquids
A1-9-I4 20min	Susumu Toko(University of Osaka) Sorption enhanced methanation with plasma catalysis using various types of zeolites
A1-9-I5 20min	Keigo Takeda(Meijo University) Surface reactions of reactive species in low temperature plasma
A1-9-O1 15min	Shikha Pandey(Indian Institute of Technology Jodhpur) Environmental Friendly Wastewater Treatment through Non-Thermal Plasma: Mechanistic Insights into Dye Degradation
A1-9-O2 15min	Chun Li(Beijing University of Chemical Technology) Atmospheric Pressure Air Plasma for Efficient Degradation of Aging-related Body Odors

A1-10 Thermal plasma/Nano-energy material [Chair: Sanghoo Park] 16:20-18:50, Sep. 25 [404]

A1-10-I1 20min	Xiaolei Fan(The University of Manchester) On the role of sheath layer in nonthermal plasma catalysis

9th Asia-Pacific Conference on Plasma Physics, 21-26 Sep, 2025 at Fukuoka

Measurement of reactive species in atmospheric pressure plasma systems used for creation of plasma activated liquids

Nikola Škoro[1], Nenad Selaković[1], Neda Babucić[1], Desanka Topalović[1], Nevena Puač[1]
[1] Institute of Physics, University of Belgrade, Belgrade, Serbia
e-mail (speaker): nskoro@ipb.ac.rs

In recent years the topics of many different studies were focused on investigating the ability of Cold Atmospheric Plasma (CAP) treatments to produce Plasma Activated Liquids (PAL) that can be further used in different applications [1, 2]. During CAP treatments short-lived and long-lived reactive species generated in the plasma interact with the liquid target and after the treatment long-lived species are deposited and preserved in the samples. Physicochemical properties and concentrations of the reactive species produced in PAL depend not only on type of plasma source, type of discharge, but also significantly on CAP operating parameters, liquid target properties, amount of liquid etc. On the other side, for medical and agricultural applications tailoring PAL properties presents a crucial step as small charges in the RONS concentrations may induce different effects to biological systems. Therefore, an important step in investigation of plasma reactivity used in these applications is to obtain the link between plasma properties, concentrations of reactive species in the plasma and those in the produced PAL.
To illustrate potential variations in PAL properties, in Fig.1 we present results of measurements of Reactive Oxygen and Nitrogen Species (RONS) after treatment by using Microwave (MW) launcher with Ar as working gas. The results showed that increasing the flow of Ar as the working gas caused considerable differences in RONS concentrations and the changes did not follow the same trend during the flow increase.

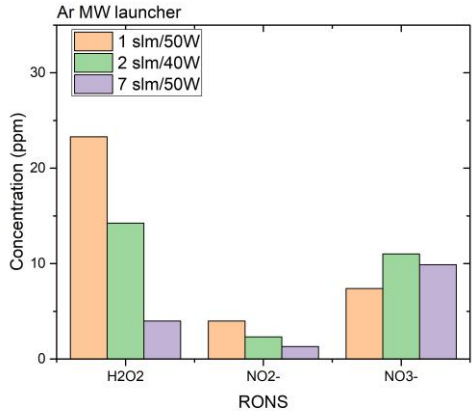

Figure 1. Measurements of RONS concentrations in PAW obtained from dH_2O for 3 treatment conditions (the gas flow and forwarded power). The treatment time was 10 minutes. Plasma was formed in Ar as working gas. Plasma plume was touching the liquid surface.

In this work we aim to establish dependence between reactive species measured in the plasma region and PALs properties. We will present results of PAL creation by using two types of plasma sources operating at atmospheric pressure to treat water and cell medium – MW launcher operating with Ar and Dielectric Barrier Discharge (DBD) source operating with addition of He. MW launcher was powered from a solid-state power supply at 2.45GHz and operated with different gas flows. The DBD source was operated at different powers and frequencies in kHz range, in air and He gas mixtures. Different plasma diagnostics was employed to obtain data on reactive species in the plasma – optical emission spectroscopy (OES) and mass spectrometry (MS). The MS analysis of reactive species was performed using HIDEN Molecular Beam Mass Spectrometer (MBMS) HPR60 device that can sample directly from ambient pressure. The device was employed in two operational modes: scan of complete mass spectrum and MID scan mode. In this mode, a real-time sensitive monitoring of radical evolution under both active and inactive discharge conditions was performed. To perform reliable measurements of long-lived reactive species in PAL we employed colorimetric methods in both water and cell medium and measured pH after the treatment.
OES of the MW discharge provided the information on the most prominent excited species formed: OH radical, N_2, N_2^+ and O atoms. Intensity of the emission lines was changing with input power and the gas flow. MS of DBD enabled to monitor production of NO, N_2O, NO_2 and O_3 depending on the operating conditions. We were able to select the operating parameters that supported the more intensive creation of O_3 or NO_x. Optical spectrometry provided information on the most intensive emission of excited species depending on the working gas.
In both systems we performed measurement of RONS concentrations in PAL by employing different colorimetric methods with respect to the liquid used. In the case of the cell medium, the existing colour of the liquid can prevent proper establishment of adsorbance and hence determination of RONS concentrations. So, we assessed the available colorimetric methods and selected the most reliable for specific liquid.

Acknowledgement: MSTDI of Republic of Serbia grant no. 451-03-68/2025-01/200024, and the Science Fund of the Republic of Serbia, grant no. 7739780 - APPerTAin-BIOM.

References

[1] A. Kumar, N. Škoro, W. Gernjak, N. Puač, Cold atmospheric plasma technology for removal of organic micropollutants from wastewater-a review, Eur. Phys. J. D 75 (2021) 283
[2] N. Puač and N. Škoro, Plasma–Liquid Interaction for Agriculture-A Focused Review, Plasma Proc. Polym. 22 (2025) e2400208

SAPP XXV

25th Symposium on Application of Plasma Processes
and
14th EU-Japan Joint Symposium on Plasma Processing

Book of Contributed Papers

Štrbské Pleso, Slovakia

31 Jan - 5 Feb, 2025

Edited by G. D. Megersa, E. Maťaš, J. Országh, P. Papp, Š. Matejčík

Book of Contributed Papers: 25th Symposium on Application of Plasma Processes and 14th EU-Japan Joint Symposium on Plasma Processing, Štrbské Pleso, Slovakia, 31 January – 5 February 2025.

Symposium organised by Department of Experimental Physics, Faculty of Mathematics, Physics and Informatics, Comenius University in Bratislava and Society for Plasma Research and Applications in hotel SOREA TRIGAN***.

Editors: G. D. Megersa, E. Maťaš, J. Országh, P. Papp, Š. Matejčík

Publisher: Society for Plasma Research and Applications, Bratislava, Slovakia

Issued: January 2025, Bratislava, first issue

ISBN: 978-80-972179-5-2

URL: https://neon.dpp.fmph.uniba.sk/sapp/

ON MECHANISM OF REACTIVE NITROGEN SPECIES FORMATION IN NEGATIVE POLARITY HIGH PRESSURE GLOW DISCHARGE

Mário Janda[1], Nenad Selaković[2], Olivera Jovanović[2], Neda Babucić[2], Nikola Škoro[2], Oleksandr Galmiz[1], Nevena Puač[2]

[1]*Faculty of mathematics, physics and informatics, Comenius University in Bratislava, Slovakia*
[2]*Institute of Physics, University of Belgrade, Belgrade, Serbia*
E-mail: janda1@uniba.sk

Mass spectroscopy (MS) was used for detection of oxygen and nitrogen species produced by negative polarity high pressure glow discharge (HPGD). Atomic O and N species as well as nitrogen oxides NO and NO_2 were detected. It was not possible to detect ions generated in the discharge directly. As shown by chemical kinetic model, concentration of negative ions is negligible in HPGD because of elevated temperature. Chemical kinetic model was also used to study formation pathways of species detected by MS.

1. Introduction

Electrical discharges can generate chemically active non-equilibrium plasmas, where electrons have significantly higher energy than ions and neutral particles. Among the many types of electrical discharges, low-pressure glow discharges are one of the most common and fundamental, often used for illumination [1]. While less common and well-known than their low-pressure counterparts, high pressure glow discharges (HPGD) offer the possibility of removing organic pollutants from exhaust gases [2]. Furthermore, their stability and efficiency in generating nitric oxide from air make them useful for nitrogen fixation [3].

HPGD can be ignited between a high-voltage metal electrode and a water surface, with the second electrode submerged [4]. This configuration, in combination with the generation of nitrogen oxides in the gas phase, makes HPGD suitable for generating plasma-activated water [5].

Plasma-activated water (PAW) is water that has been exposed to plasma. This exposure infuses the water with reactive oxygen and nitrogen species (RONS), such as hydrogen peroxide, nitrates, and nitrites, which temporarily alter the water's chemical properties and make it useful in many applications in food, agriculture, and biomedicine [6, 7]. These possibilities have made PAW a hot topic in the low-temperature plasma community in recent years.

Despite many studies and obtained results, further research is crucial for a better understanding of the formation mechanisms of reactive species, such as nitrogen oxides, and for assessing the role of different gas-phase species in the formation of aqueous RONS in PAW. From a practical point of view, this knowledge will allow for increased energy efficiency and selectivity with respect to the desired products when generating PAW. For this reason, the formation of RONS by HPGD is studied in this paper, using mass spectrometry (MS) and chemical kinetic modelling. For MS measurements we used molecular beam mass spectrometer (MBMS) that can sample from atmospheric pressure enabling to directly access chemical species created in the plasma. In principle the MBMS can detect both neutral and ionic species but in this study we focused to neutrals.

2. Experimental setup

A schematic diagram of the experimental apparatus is shown in Figure 1. The high pressure glow discharge was generated by a DC high voltage (HV) power supply (Glassmann PSIWH 20R25) with negative polarity output, capable of delivering up to 20 kV. The power supply was connected to the cathode via a 1 MΩ series resistor (R) to limit current. This power supply can also operate as a stabilized current source, providing up to 30 mA.

The cathode consisted of a stainless steel needle with a flat tip and an outer diameter of 0.7 mm. The discharges were generated in dry air from the pressure cylinder (purity 5.0), flowing along the cathode

towards the anode with the gas flow rate of 0.3-0.45 slm, controlled by mass controller (Bronkhorst F201-EV).
For diagnostics of neutral species, a grounded steel ring with an inner diameter of about 4 mm and an outer diameter of about 8 mm served as the anode. This ring was positioned 5 mm in front of the entrance to the mass spectrometer, which had an orifice diameter of 100 µm. For the measurements the mass spectrometer front plate with the orifice was grounded. The cathode-anode gap distance was maintained at 3 mm.
The electrical potential between the cathode and ground was measured using a high voltage probe (Tektronix P6015A) connected to a digital oscilloscope (Keysight MSOX 3024T).
The MBMS used for measurements (Hiden Analytical HPR 60) was operating in two modes- RGA (Residual Gas Analyzer) mode, that provides data on the mass spectra of neutrals in the range 0–100 amu; and MID scan, when the device is set to monitor the temporal changes of selected species. In both cases, for the detection of neutral species a ionization chamber was active with the electron energy set to 70 eV. The MBMS has an internal shutter – Swagelok that allows recording of the background signal coming from the gas phase inside the device.

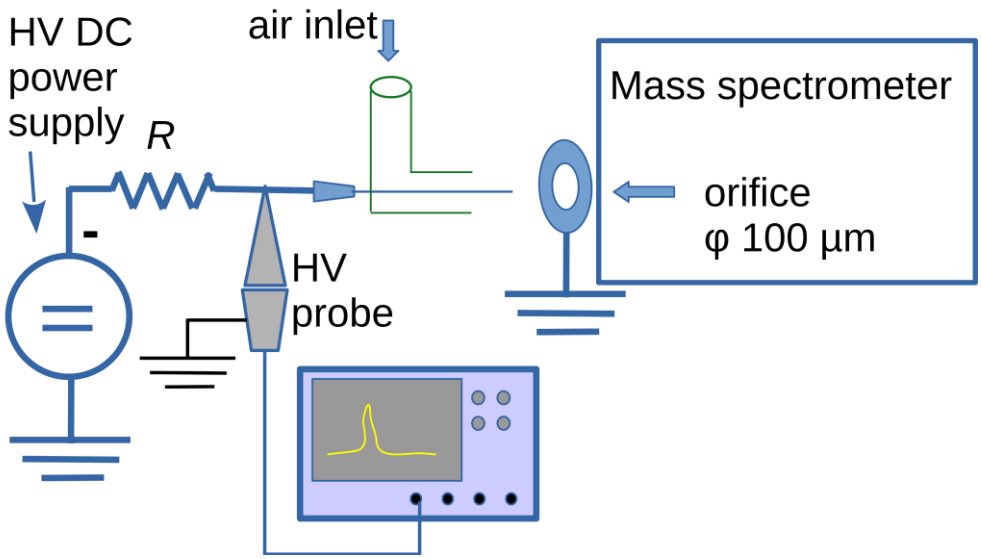

Fig. 1. A schematic diagram of the experimental apparatus.

3. Chemical kinetic model

The aim of the chemical kinetic model is to calculate density evolution of studied species interacting via defined set of chemical reactions. For this purpose we used ZDPlasKin module [8] that includes a Fortran 90 version of the VODE solver for numerical solution of system of ordinary differential equations [9]. Authors of ZDPlasKin also provide a ready-to-use list of plasma chemical processes in nitrogen-oxygen mixtures with all necessary rate coefficients [10]. This set of reactions (version 1.03) includes ~650 chemical reactions among 53 species.
The rate constants of reactions between heavy species from this list are calculated from the thermodynamic gas temperature T_g. The rate constant for electron impact reactions must be calculated from electron energy distribution function (EEDF) obtained by solving the Boltzmann equation for free electrons. The ZDPlasKin package includes a Bolsig+ solver [11] for this purpose. A set of required electron scattering cross sections was taken from the LXCat project database [12].
Finally, ZDPlasKin module requires use of additional subroutines written by user for comprehensive control of simulation conditions, e.g., changes in the gas temperature, pressure and reduced electric field. Our physical model has two parts, glow discharge and afterglow. The afterglow part has to be included because in some experiments, the gas from the discharge did not enter the mass spectrometer directly, but there was a 5 mm gap between the grounded ring electrode and orifice.

For modeling of GD we used constant temperature T_g = 2000 K, constant pressure of 1 atmosphere and constant reduced electric field strength E_n = 60 Td. We also used constant electron density n_e = 10^{12} cm^{-3}. These values were estimated based on previous experimental observations of HPGD [13]. In order to take into account diffusion of species our of the discharge plasma channel and mixing with the surrounding ambient air, we included a primitive diffusion model in our code. After each calculation step with duration Δt, concentration of each heavy particle n_i is decreased by Δn_i calculated as

$$\Delta n_i = -\alpha_{diff} n_i \Delta t, \quad (1)$$

where α_{diff} is coefficient representing diffusion of particles out of the plasma channel. To keep constant pressure (total density of particles), the removed particles were replaced by N_2 and O_2 molecules (ratio 4:1). This simulates mixing with the ambient air.

In the second part of the model, an afterglow period of 0.2 s, the reduced electric field strength decreased exponentially to 3 Td with a time constant of 20 ns. Electrons concentration was calculated dynamically along with the densities of all other species, rather than being held constant. Mixing with the surrounding air continued during the afterglow phase, leading to a calculated decrease in gas temperature. Electron diffusion was also incorporated, with a diffusion coefficient ten times higher than that of the heavy particles.

4. Results and Discussion

HPGD was generated with discharge current of either 2.1 mA, or 3 mA. The applied voltage was -3 kV and -4 kV, respectively. The discharge voltage (across the gap) decreased from ~1.3 kV to ~1.15 kV when the HPGD current increased from 2.1 mA to 3 mA. Mass spectra of produced neutral species were measured for both discharge currents. The obtained spectra had the same species visible for both currents so in Figure 2 we present the data recorded for 3 mA.

The data shows only species created in the plasma as the background signal, recorded in plasma off conditions, was subtracted. The most abundant species created in the discharge were atoms of H,N and O and reactive species OH, H_3O, NO, H_2O_2 and N_2O.

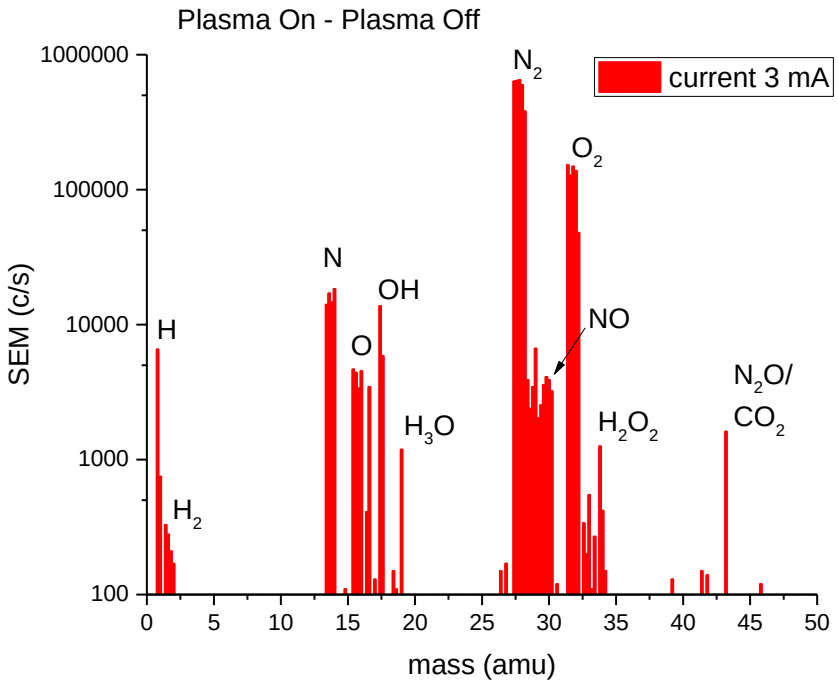

Fig. 2. Mass spectra of neutral species measured for current 3 mA.

In the MID scan mode, we monitored temporal changes in the nitrogen species NO, N_2O and NO_2 important for PAW generation. In Figure 3 we show recorded signals for these species with respect to different measurements conditions. Measurements were conducted with Swagelok open and with Swagelok closed. Swagelok open represents the sum of foreground and background species, while Swagelok closed corresponds to background species only. For the first 6 minutes of recording the discharge was off so variations in the signal is only due to processes inside the device. Once the discharge is ignited, increase in NO and NO_2 signals was due to the species created in the discharge. Obviously, creation of N_2O species was not large so the signal did not change after discharge inception.

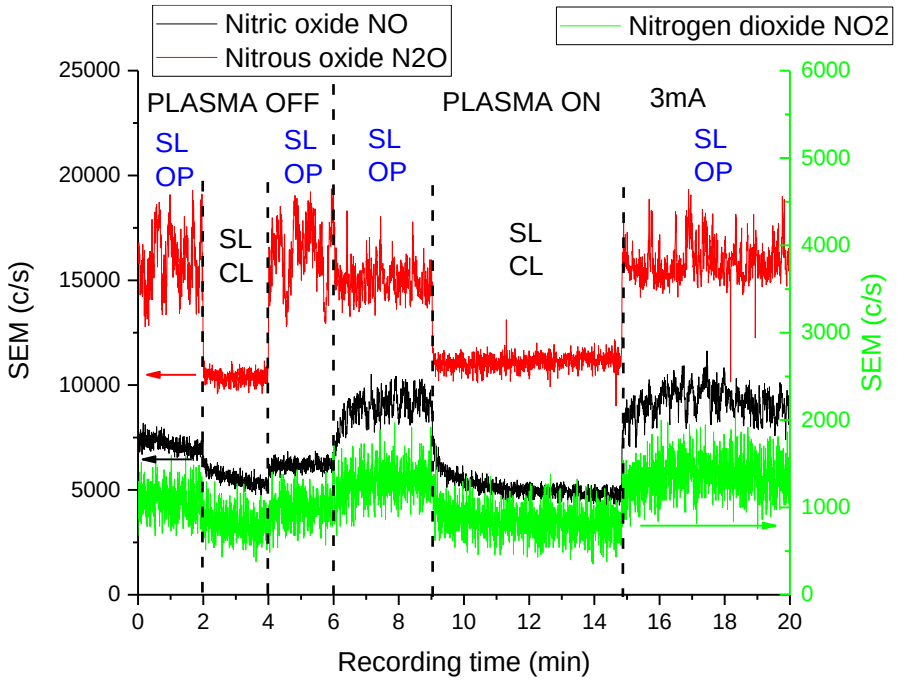

Fig. 3. MID-scan of NO, NO_2 and N_2O species without and with the discharge operating in front of the MS orifice with addition of synthetic air. Discharge current was 3 mA. Measurements were perforemed with Swagelok closed (SL CL) and open (SW OP).

In summary, the experimental data confirmed generation of N, O, NO and NO_2 by HPGD. Chemical kinetic model using ZDPlasKin module was used to explain their formation. As for example, Figure 4 shows time evolution of N, O, NO, NO_2 and O_3 species concentrations in the glow discharge. This calculation was performed with $\alpha_{diff} = 2\ s^{-1}$.

Our model incorporates diffusion, but the employed calculation approach is simplified, and the exact value of the diffusion coefficient remains unknown. Instead, we utilize a parameter, α_{diff}, to represent the diffusion rate. We performed several calculations with α_{diff} ranging from 0.1 to 10 s^{-1}. Since α_{diff} influences the calculated steady-state concentrations of species in the plasma, we cannot definitively determine the actual concentrations of the studied species in the HPGD. However, we observed that α_{diff} in studied range does not significantly affect the ratio of concentrations of various RONS or their production pathways.

Figure 4 demonstrates that the concentrations of all studied RONS reach a steady state after approximately 0.2 ms, remaining constant thereafter. This steady state arises from a balance between production (through chemical reactions) and removal (via chemical reactions and diffusion). Consequently, we analyzed the reaction pathways separately for the initial phase of the simulation and for the subsequent steady state.

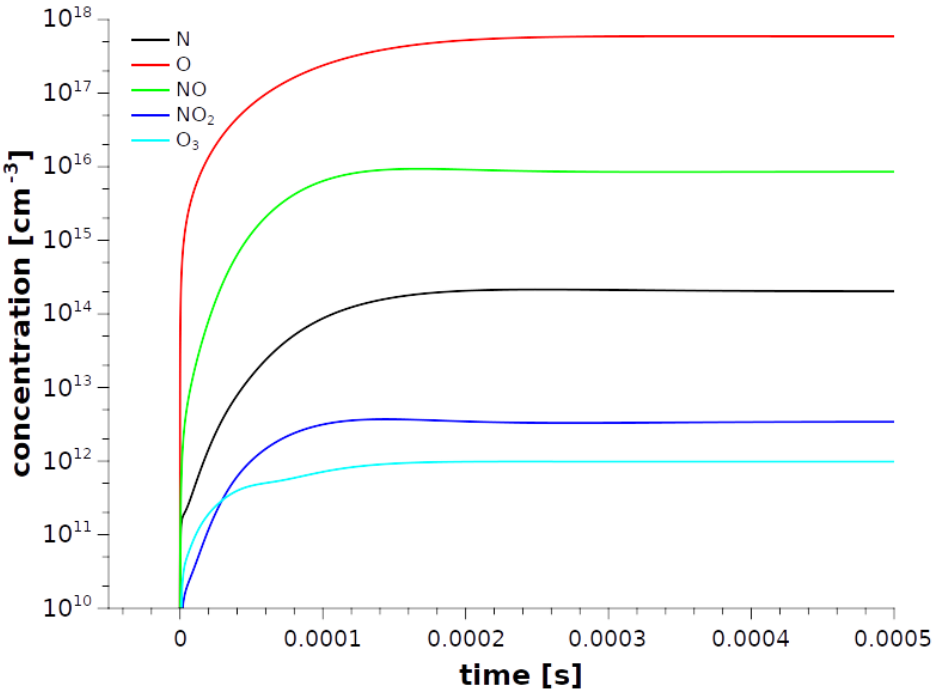

Fig. 4. Time evolution of N, O, NO, NO_2 and O_3 species concentration; calculated with $\alpha_{diff} = 2\ s^{-1}$.

In the initial phase (Figure 5), O atoms are mainly produced by reactions of O_2 with electronically excited molecular nitrogen species N_2* (the most important being $N_2(B^3\Sigma)$, and by electron impact dissociation of O_2 molecules:

$N_2^* + O_2 \rightarrow N_2 + O + O,$ (2)
$e + O_2 \rightarrow e + O + O.$ (3)

Contribution of other reactions, such as

$N + O_2 \rightarrow O + NO$ (4)

on O atoms production is already quite small.
In the later steady state phase, the production reactions (2-4) are compensated by O atoms recombination reactions

$O + O + M\ (M = O, O_2, N_2) \rightarrow O_2 + M.$ (5)

In this simplified O production/removal mechanism we omitted reactions between O, $O(^1D)$ and $O(^1S)$ species. An equilibrium between these species is achieved quickly, with O representing more than 99.9% of them.
N atoms are produced mostly by these two reactions:

$O(^1D) + NO \rightarrow O_2 + N,$ (6)
$N_2(a`^1) + NO \rightarrow N_2 + N + O.$ (7)

There is also a third important reaction producing N atoms, electron impact dissociacion of N_2, but it plays an important role at the very beginning of the simulation ($t < 50\ \mu s$), when there is still not enough NO molecules for N generation by equations (6) and (7).

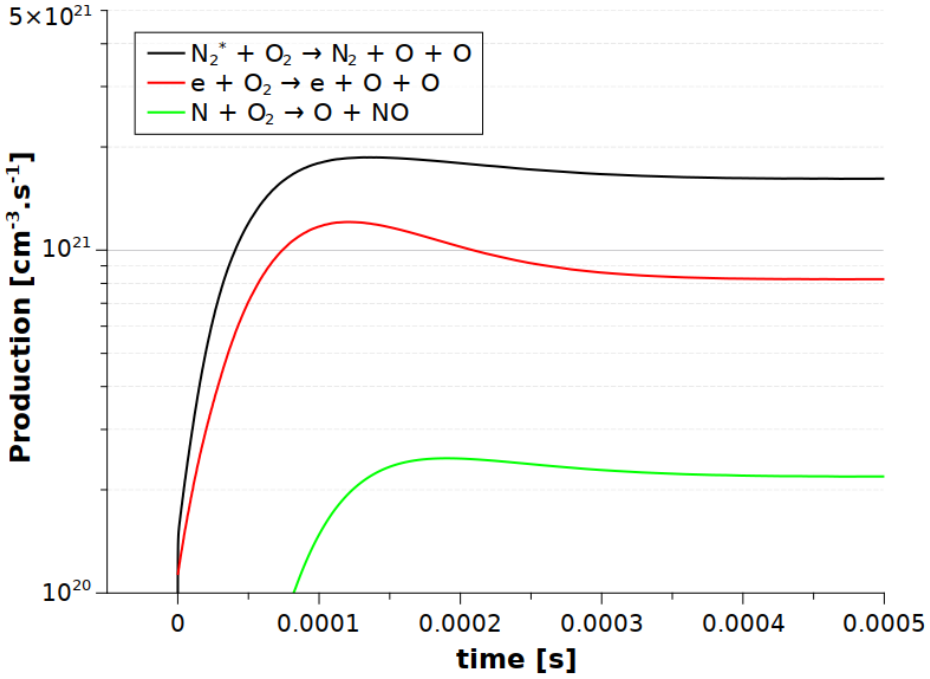

Fig. 5. Production of O atoms during the initial phase of the simulation; calculated with α_{diff} = 2 s^{-1}.

In steady state, the removal of NO molecules by N (equations (6) and (7)) is compensated by NO production via reaction

$N + O_2 \rightarrow O + NO.$ (8)

Reactions (6-8) all involve NO, they are crucial not only for N production and losses, but they also influence the density of NO. Reaction (8) is actually the most important for NO production (Figure 6). The other two important reactions are

$N_2(A^3) + O \rightarrow NO + N(^2D),$ (9)
$N(^2D) + O_2 \rightarrow NO + N.$ (10)

In the steady state, the production of NO is compensated by its removal (Figure 7) via reactions (6), (7), (11) and (12)

$NO + N(^2D) \rightarrow N_2 + O,$ (11)
$NO + N \rightarrow N_2 + O.$ (12)

NO_2 is produced almost eclusively by reaction (13) and removed by reaction (14)

$O + NO + M \rightarrow NO_2 + M\ (N_2, O_2),$ (13)
$O + NO_2 \rightarrow NO + O_2.$ (14)

Steady state NO_2 concentration $[NO_2]$ can be therefore easily calculated as $[NO_2] = k_{13}.[NO]/k_{14}$, assuming balance between NO_2 production and destruction by reactions (13) and (14). In this formula, [NO] is steady state concentration of NO, k_{13} and k_{14} are rate coefficients of reactions (13) and (14), respectively. At 2000 K, the ratio of these two rate coefficients is 7.3×10^{-4} and it explains why the steady state concentration of NO_2 is much lower than the concentration of NO (Figure 4).

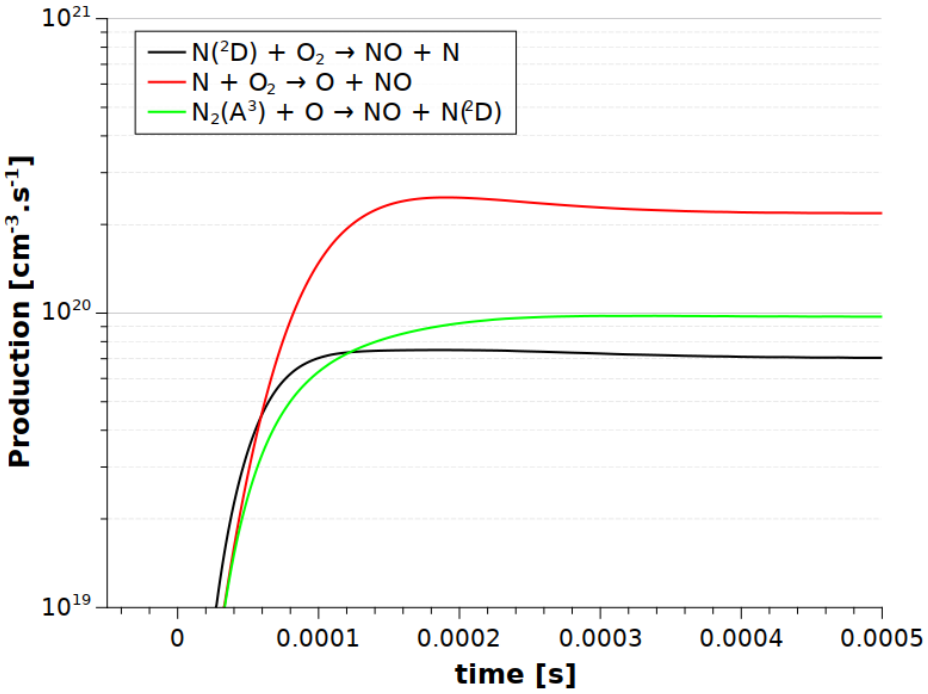

Fig. 6. Main reactions responsible for production of NO molecules; calculated with α_{diff} = 2 s^{-1}.

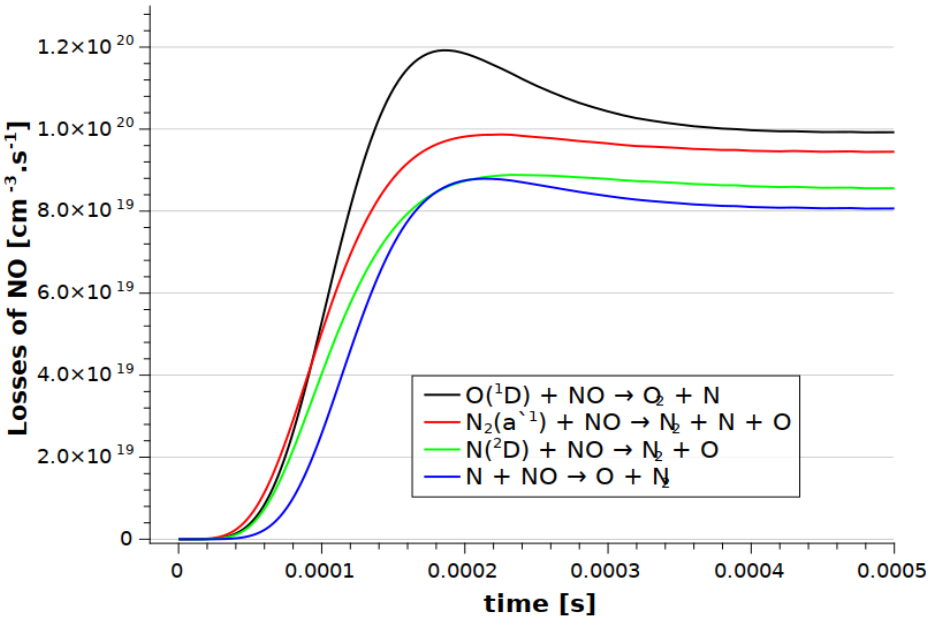

Fig. 7. Main reactions responsible for losses of NO molecules; calculated with α_{diff} = 2 s^{-1}.

Based o *ex-situ* measurements of the gas after treatment by glow discharge, the concentration of NO is higher than the concentration of NO_2, but the difference is not so significant [3]. Final NO and NO_2 concentration is mainly determined by reactions in the gas after leaving the discharge zone (afterglow). Figure 8 shows time evolution of gas temperature and N, O, NO and NO_2 species concentrations in the discharge afterglow, calculated with α_{diff} = 10 s^{-1}. The concentration of atomic species (N and O) decreases rapidly. While the NO concentration decreases slowly, the NO_2 concentration increases, despite mixing with the ambient air. Consequently, the difference between NO and NO_2 concentrations decreases in the discharge afterglow.

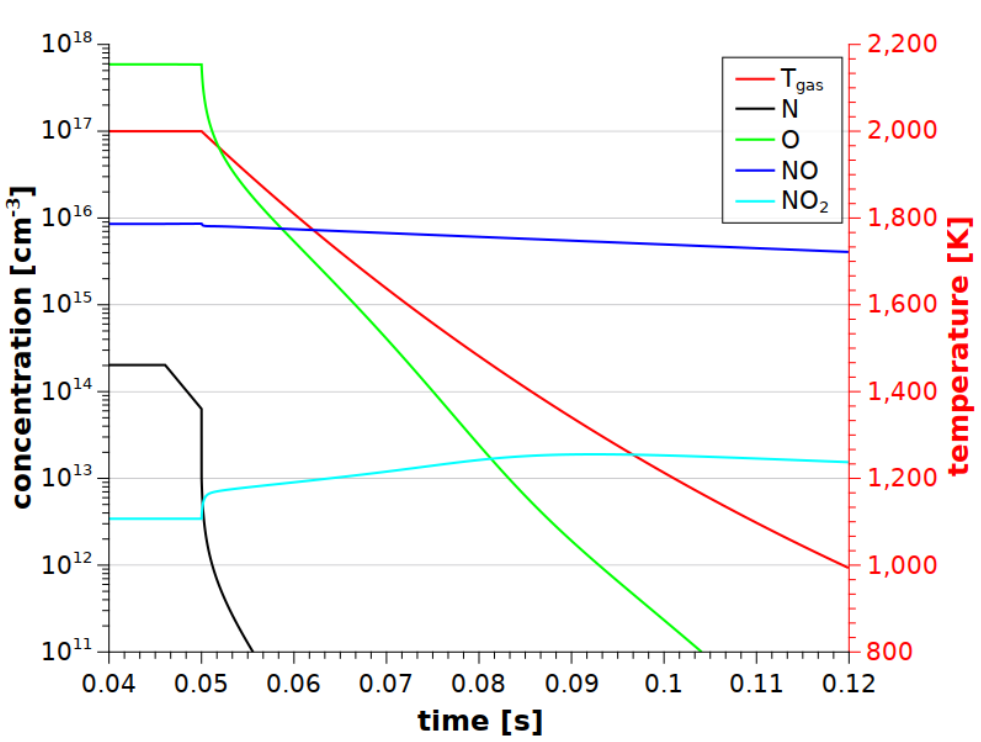

Fig. 8. Time evolution the gas temperature and N, O, NO and NO_2 species concentrations; calculated with α_{diff} = 10 s^{-1}.

A stable signal from ions directly generated by the HPGD was not detected by mass spectrometry. This can be attributed to two main factors. Firstly, the HPGD migrated on the surface of the orifice plate that served as anode, making its position relative to the spectrometer's gas entrance (a 100 µm orifice) highly variable. A stable ion signal could only be observed if the HPGD was positioned directly above this orifice, which occurred only randomly and occasionally. Secondly, even with the discharge positioned stably above the orifice, ion detection remains challenging. Positive ions are repelled from the anode, and the concentration of negative ions within the HPGD is relatively low, according to the kinetic model. The dominant negative ion, O^-, has a concentration of approximately 10^{10} cm^{-3}, two orders of magnitude lower than the electron concentration. This low negative ion concentration may be due to the elevated gas temperature in the HPGD plasma channel.

5. Conclusions

Fixation of nitrogen from the air, converting it into reactive compounds, remains a significant challenge and a hot topic within the low-temperature plasma community. High-pressure glow discharges offer a stable and efficient means to generate nitrogen oxides, key precursors for nitrogen fixation. This study investigates the mechanisms of nitrogen oxide generation in an HPGD using a combined approach of mass spectrometry and chemical kinetic modeling.

Mass spectrometry provided insights into the types of reactive oxygen and nitrogen species produced, while the kinetic model simulated the complex chemical reactions within the plasma. Our findings shed light on the dominant reaction pathways on nitrogen oxide formation. However, further research is crucial to refine our understanding. Future experimental work should focus on improving the detection and quantification of reactive species, particularly ions. Model enhancements are also necessary, including a more accurate representation of diffusion processes and the discharge afterglow phase. Furthermore, incorporating additional chemical reactions involving water molecules will enable us to explore the crucial role of humidity in the generation of nitrogen oxides, nitric acid, and nitrous acid. This comprehensive approach promises to advance our knowledge of nitrogen fixation using HPGD

and pave the way for the development of efficient and sustainable plasma-based technologies for fertilizer production and other applications.

Acknowledgement: Supported by the project of bilateral cooperation between Republic of Serbia and Republic of Slovakia 2024-2025 (project no. 337-00-3/2024-05/07 and APVV SK-SRB-23-0043); grant of the Ministry of Science, Technological Development and Innovations no. 451-03-68/2024-14/200024; and VEGA project No. 1/0596/22.

6. References

[1] Claude G 1913 *The Engineering Magazine* **115** 271–274.
[2] Machala Z, Laux C O and Kruger C H 2005 *IEEE Trans. Plasma Sci. - Special Issue on Plasma Images* **33** 320-321.
[3] Janda M, Hensel K, Machala Z and Field T A 2023 *J. Phys. D Appl. Phys.* **56** 485202
[4] Janda M, Machala Z, Morvová M, and Morva I 2008 *Orig. Life Evol. Biosph.* **38** 23-35
[5] Pai D Z 2021 *Journal of Physics D: Applied Physics* **54** 355201
[6] Rathore V, Tiwari B S and Nema S K 2021 Plasma Chem Plasma Process. **42** 109-129
[7] Chen Z, Xu R-G, Chen P and Wang Q 2020 *IEEE Trans. Plasma Sci.* **48** 3455–3471.
[8] Pancheshnyi S et al. 2008 Computer Code ZDPlasKin, Univ. Toulouse, Toulouse, LAPLACE, CNRS-UPS-INP, France. [Online]. Available: https://www.zdplaskin.laplace.univ-tlse.fr
[9] Brown P N, Byrne G D and Hindmarsh A C 1989 *SIAM J. Sci. Stat. Comput.* **10** 1038–1051
[10] kinet_N2_O2_v1.03 2015 [Online]. Available: http://www.zdplaskin.laplace.univ-tlse.fr/wp-content/uploads/2015/08/kinet_N2_O2_v1.03.inp
[11] Hagelaar G J M and Pitchford L C 2005 Plasma Sources Sci. Technol. **14** 722-733
[12] Pancheshnyi S et al. 2012 *Chem. Phys.* **398** 148–153.
[13] Machala Z et al. 2007 *J. Molec. Spectrosc.* **243** 194-201.

MASS SPECTROMETRY OF DIELECTRIC BARIER DISCHARGE WITH WATER ELECTRODE

Neda Babucić[1], Nenad Selaković[1], Oleksandr Galmiz[2], Mário Janda[2], Olivera Jovanović[1], Nevena Puač[1], Nikola Škoro[1]

[1]*Institute of Physics, University of Belgrade, Pregrevica 118, 11080 Belgrade, Serbia*
[2]*Division of Environmental Physics, Faculty of Mathematics, Physics and Informatics, Comenius University in Bratislava, Mlynská dolina, 842 48 Bratislava, Slovakia*
E-mail: nedab@ipb.ac.rs

This paper presents the results of an investigation into the generation of reactive species in two setups of a dielectric barrier discharge (DBD) plasma source, using a water target with different vessels. By analyzing both neutral mass spectra and MID-scan spectra, we explore the concentrations of reactive oxygen and nitrogen species (NO, NO_2 and O_3) under varying plasma conditions and mass spectrometer configurations.

1. Introduction

In the past decade, a lot of interest has been drawn to atmospheric pressure plasmas (APPs) because of their unique properties and wide range of applications in fields such as material processing, agriculture, food industry and biomedicine [1, 2, 3, 4]. Since they do not require costly vacuum systems and operate at atmospheric pressure, APPs have the advantage of being accessible and versatile. Lately, atmospheric pressure plasma in contact with water has attracted significant interest due to its potential to generate reactive species and drive advanced chemical processes for various applications.

The behaviour and chemistry of APPs are greatly affected when they come into contact with water, either as an electrode or as a target. Reactive oxygen, nitrogen and hydrogen species are found in water and are essential for a variety of processes, such as biomedical treatments, sterilization, and water purification. Water forms a dynamic interface where plasma-induced reactions take place, producing reactive species like ozone (O_3), hydrogen peroxide (H_2O_2), hydroxyl radicals (OH), nitrates (NO_3^-), nitrites (NO_2^-) etc. These species play an essential role in enhancing the efficacy of plasma-based processes [5].

Also, higher humidity introduced in feeding gas of APPs has been demonstrated to increase the generation of reactive species, such as OH radicals, which are necessary for surface modification and decontamination [6]. The interaction, however, is complex and depends upon a number of variables, including ambient circumstances, water composition, and plasma characteristics. To optimize plasma processes and customize them for particular applications, it is essential to comprehend these interactions.

Dielectric barrier discharges (DBDs) are widely used for surface activation in atmospheric-pressure plasma applications. However, treating sensitive materials like polymers can be challenging because high-density plasma may cause damage, such as pin-holing. This issue often occurs in volume barrier discharges or coronas, where the plasma moves perpendicular to the treated surface. A practical solution is to generate plasma that travels parallel to the surface. This approach minimizes the risk of damage while maintaining effective treatment. One promising method is the surface dielectric barrier discharge (SDBD), where the plasma spreads along the surface of a dielectric plate. This setup not only protects the material but also improves the efficiency of the process.
In our earlier work [7, 8, 9] we introduced a novel plasma discharge reactor for efficiently activating polymers at the gas/liquid interface. This design uses liquid electrodes to ignite the SDBD directly from the liquid surface. Although the plasma-water interaction is limited to the edge of the dielectric tube, the system is both scalable and flexible, making it suitable for a wide range of applications.

Mass spectrometry is an analytical technique that measures the mass-to-charge ratio of ions to identify and quantify molecules in a sample. Primary advantage of atmospheric pressure mass spectrometry lies in its ability to rapidly and accurately analyse a wide range of chemical species [10]. These instruments are equipped with specialized pumping systems that create a pressure gradient, enabling the effective intake of gases from atmospheric plasmas. For neutral species, the mass spectrometer incorporates an ionization chamber that converts neutrals into ions, enabling their detection and analysis. The mass analyser which filters and detects neutral species or positive and negative ions, generating detailed mass spectra for all components. The technique provides real-time measurements of reactive species, ions, and neutral molecules, which are essential for understanding plasma processes and optimizing plasma-based applications.

When it comes to plasma in contact with water, due to technical challenges, mass spectrometric analysis of the plasma has so far been conducted by introducing water vapour into the working gas [11]. In this paper, we tackled the technical challenge and developed a setup where the mass spectrometer inlet was positioned in close proximity to the plasma-water interface, allowing us to successfully record mass spectra.

In this paper, we will present the results of our investigation into the reactive species generated by the dielectric barrier discharge (DBD) setup, but with two different water vessel configurations. The analysis includes both neutral mass spectra and MID-scan spectra, offering insights into the concentrations of key reactive oxygen and nitrogen species, such as NO, NO_2, CO_2 and O_3, as well as the detailed composition of the plasma obtained under these conditions.

2. Experimental set up

The schematic of the DBD at atmospheric pressure and HIDEN HPR60 mass-energy spectrometer is given in Figure 1. The DBD device is in the triple-phase interface (plasma-liquid-solid) plasma system consisting of a thin glass test tube with a 10 mm diameter and a 0.5 mm wall thickness was used. The liquid inside the test tube served as the high-voltage electrode and was connected to a power supply generating a sinusoidal voltage waveform. The Petri dish bath, which grounded the system, completed the circuit. Tap water with an electrical conductivity of approximately 0.3 mS/cm was used as the liquid electrode. The water was electrically insulated both inside and outside the test tube to ensure stability. The discharge operated in ambient air at atmospheric pressure. The high-voltage sine waveform had an amplitude range of 0 to 20 kV and could be adjusted to frequencies between 23 and 30 kHz. Power was delivered to the liquid electrodes through a high-voltage resonance generator (Lifetech-300W) paired with a function generator (FY3200S-24M).

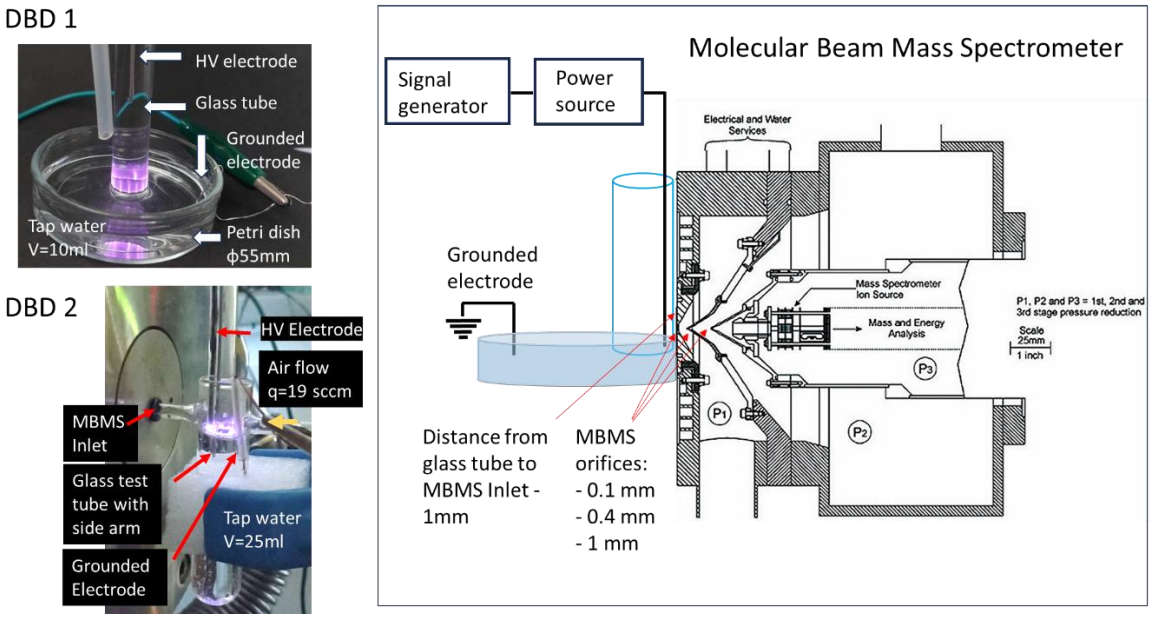

Fig. 1. DBD device in two configurations (DBD1 and DBD2) with a schematic representation of mass spectrometry measurements. In DBD1 setting, the device was immersed in 10ml of tap water placed in a Petri dish (ϕ55mm). In DBD2 setting, the device was placed in a glass test tube filled with 25ml of tap water, equipped with a side arm for gas sampling and a hole for synthetic air intake (q = 19 sccm).

Mass spectrometry measurements were performed by using MBMS (Molecular Beam Mass Spectrometer) HIDEN HPR60. To ensure the formation of a molecular beam, the geometry of the MBMS HPR60 system consists of a centralized combination of the orifice, cone1, and cone2 (P1 vacuum section is formed between the orifice and cone1, P2 vacuum section is formed between cone1 and cone2, and P3 vacuum section is formed after cone2 in the region of the mass analyzer). The orifice had an opening diameter of ⌀0.1 mm, cone1 ⌀0.4 mm, and cone2 ⌀1 mm, accompanied by the following voltages for DBD setups (the orifice was grounded, Vcone1 = 0 Vand Vcone2 =0 V).

During all experiments for DBD setups, the regions within the vacuum section of the mass spectrometer responsible for generating the pressure gradient had the following pressure values: $P_1 = 3.3 \cdot 10^{-1}$ Torr, $P_2 = 7.5 \cdot 10^{-6}$ Torr, and $P_3 = 2.4 \cdot 10^{-7}$ Torr. To identify the species of interest, we first recorded the mass spectra of neutrals (0–100 amu) using the RGA (Residual Gas Analyzer) mode, during which the ionization chamber was active. Within the ionization chamber, the electron emission current from the filament was for DBD1 = 5 µA and for DBD2 =10 µA. In both cases, the electron energy was 70 eV.

After that, we used MID-scan to monitor the temporal changes of selected species for different formation conditions: without plasma, with plasma at specific applied powers for DBD1 (5W and 15W) and DBD2 (15W), with Swagelok open, and with swagelok closed. Swagelok open represents the sum of foreground and background species, while swagelok closed corresponds to background species only.

3. Results and discussion

In this study, we have measured the neutrals mass spectra by using a mass spectrometer for two different configurations of Dielectric Barrier Discharge (DBD) system. In both configurations, titled DBD1 and DBD2, discharge was in contact with water during mass spectrometry measurements. The analysis of neutral species was performed in two different measurement modes of HPR60: RGA mode for neutral mass spectra and MID-scan mode for track in time changes of specific neutral species. These modes provide a comprehensive overview of the ionization processes and chemical compositions

present in the plasma generated by each DBD system. The neutral mass spectra revealed the types and relative concentrations of neutral species, the MID-scan measurement provided insight into the temporal evolution of these species.

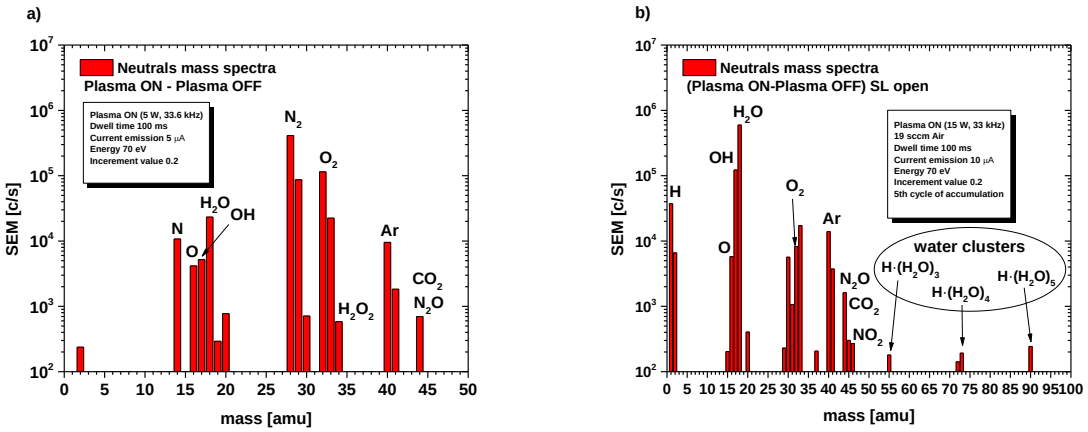

Fig. 2. Neutral mass spectra for a) DBD1 setting and b) DBD2 setting at an operating frequency of 33.6kHz. In the case of the DBD2, an airflow of 19sccm was added. The graphs were obtained by passing the raw results through a MatLab script to integrate the obtained lines for specific mass number.

Figure 2(a) and (b) present Neutral mass spectra for configurations DBD1 and DBD2, respectively. The presented spectra show the difference of Plasma ON mass spectra and Plasma OFF mass spectra. Plasma ON/OFF mass spectra represent the foreground signal i.e. the difference of total signal (swagelok open) and background signal (swagelok closed). The spectra in Figure 2 clearly show that the dominant species in the discharge are nitrogen and oxygen compounds (N, O_2, H_2O_2, N_2O, H, H_2O) which is to be expected because it is a discharge at atmospheric pressure where the target is water. Atomic nitrogen and atomic oxygen are present as a result of plasma reactions, along with the NO radical. The OH radical is also present, resulting from both plasma reactions and water dissociation in the MBMS. In Figure 2(b), water clusters can also be observed at mass numbers 53, 73 and 91, which appear in neutral mass spectra due to water vapor from the bottle containing the discharge. The high humidity in the DBD2 configuration and the plasma conditions promote cluster formation unlike in the case of DBD1 configuration where we did not detect any water clusters of mass above 50 amu.

While the mass spectra results provided an overall view of the main species present in the discharge chamber, nitrogen oxides and ozone can impact the industrial environment even at much lower concentrations (below the detection limit of the mass spectra used). Therefore, more sensitive measurements were conducted specifically for the important species NO, NO_2, N_2O, and O_3, as represented here. It was recorded for different conditions, Plasma ON and OFF with background only (BG), as well as Plasma ON and OFF with foreground and background (FG+BG). Unlike the case of BG, where only the inner part of the MS is considered in the measurement, in the case of FG+BG, the mass spectrometer is open so outside ambient air is also evaluated.

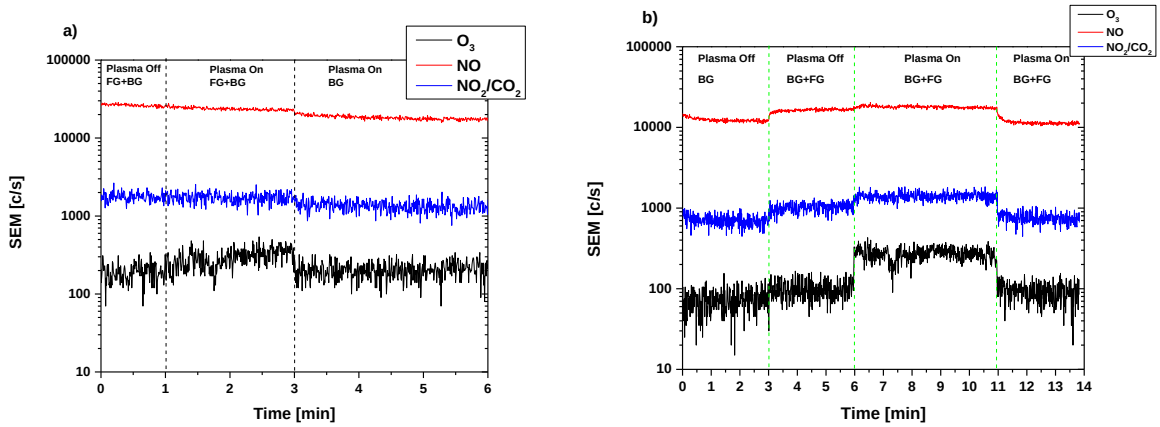

Fig. 3. The mid-scan provides constant tracking of selected species, with different stages of the experiment marked by labels: plasma on and off, foreground (FG) and background (BG); (a) DBD1 Setup, ionization filament current set to 5 µA at 70 eV, and (b) DBD2 Setup, ionization filament current set to 50 µA at 70 eV.

The MID-scan for DBD1 setup (Figure 3(a) starts with Plasma OFF and swagelock open (1st minute), both the foreground (outside the spectrometer) and background are measured. The discharge is ignited in minute 1 and swagelok is open. Here we can see that NO continues to decrease slightly, NO_2 remains constant, and O_3 increases, indicating plasma-driven production of O_3. After the 3rd minute, with the plasma still on but swagelock closed, all species (NO, NO_2, and O_3) decrease as expected (only background inside device is measured).

The Figure 3(b) shows MID-scan spectra for DBD2 configuration. In the first three minutes, with the plasma off and the swagelock closed, only the background signal is measured. After opening of the swagelok (3-6 minutes), the increase in NO and NO_2 suggests the influence of ambient air, while O_3 remains unchanged. Between 6 and 11 minutes, with the plasma on and the swagelok open, NO and NO_2 rise slightly, but O_3 increases significantly, indicating plasma-driven O_3 production. Finally, from 11th minute, with the plasma on and the swagelok closed, all species decrease due to limited external interaction (only background is measured).

4. Conclusion

Mass spectrometry analysis of two setups of a DBD source with a water electrode, generated at atmospheric pressure was performed. Despite the difference in the water vessel used in each setup, in both setups similar trends in the behavior of reactive species were shown, indicating strong influence of plasma on water target. In both cases, plasma activation leads to the generation of reactive oxygen and nitrogen species, such as NO, NO_2, CO_2, and O_3, with notable increases in O_3 concentration when the plasma is on. Differences in the water vessel may affect the plasma's efficiency in producing reactive species, but both setups demonstrate that the plasma's interaction with the water is crucial for modulating the levels of reactive species. These findings highlight the importance of the plasma-water system in applications such as water treatment and agriculture, where reactive species generated in plasma-activated water could have significant biological and chemical effects.

Acknowledgments: The research was supported by the project of bilateral cooperation between Republic of Serbia and Republic of Slovakia 2024-2025 (project no. 337-00-3/2024-05/07), grant of the Ministry of Science, Technological Development and Innovations no. 451-03-68/2024-14/200024 and by the EU NextGenerationEU through the Recovery and Resilience Plan for Slovakia under the project No. 09I03-03-V04-00094.

5. References

[1] Penkov, O. V., et al. "A Review of Recent Applications of Atmospheric Pressure Plasma Jets for Materials Processing."*Journal of Coatings Technology and Research*, vol. 12, 2015, pp. 225-235.

[2] Puač, N., et al. "Plasma Agriculture: A Rapidly Emerging Field." *Plasma Processes and Polymers*, vol. 15, no. 2, 2018, p. 1700174.

[3] Bilea, F., et al. "Non-Thermal Plasma as Environmentally-Friendly Technology for Agriculture: A Review and Roadmap." *Critical Reviews in Plant Sciences*, vol. 43, no. 6, 2024, pp. 428-486.

[4] Machala, Z., et al. "Emission Spectroscopy of Atmospheric Pressure Plasmas for Bio-Medical and Environmental Applications." *Journal of Molecular Spectroscopy*, vol. 243, no. 2, 2007, pp. 194-201.

[5] Machala, Z., et al. "Chemical and Antibacterial Effects of Plasma Activated Water: Correlation with Gaseous and Aqueous Reactive Oxygen and Nitrogen Species, Plasma Sources and Air Flow Conditions." *Journal of Physics D: Applied Physics*, vol. 52, no. 3, 2018, p. 034002.

[6] Sainct, F. P., et al. "Temporal Evolution of Temperature and OH Density Produced by Nanosecond Repetitively Pulsed Discharges in Water Vapour at Atmospheric Pressure." *Journal of Physics D: Applied Physics*, vol. 47, no. 7, 2014, p. 075204.

[7] Galmiz, O., et al. "Study of Surface Dielectric Barrier Discharge Generated Using Liquid Electrodes in Different Gases." *Journal of Physics D: Applied Physics*, vol. 49, no. 6, 2016, p. 065201. https://doi.org/10.1088/0022-3727/49/6/065201.

[8] Galmiz, O., et al. "Hydrophilization of Outer and Inner Surfaces of Poly(vinyl Chloride) Tubes Using Surface Dielectric Barrier Discharges Generated in Ambient Air Plasma." *Plasma Processes and Polymers*, vol. 14, no. 9, 2017. https://doi.org/10.1002/ppap.201600220.

[9] Galmiz, O., et al. "Plasma Treatment of Polyethylene Tubes in Continuous Regime Using Surface Dielectric Barrier Discharge with Water Electrodes." *Journal of Physics D: Applied Physics*, vol. 51, no. 19, 2018. https://doi.org/10.1088/1361-6463/aabb49.

[10] Rees, J. A., et al. "Mass and Energy Spectrometry of Atmospheric Pressure Plasmas." *Plasma Processes and Polymers*, vol. 7, no. 2, 2010, pp. 92-101.

[11] Willems, G., et al. "Absolutely Calibrated Mass Spectrometry Measurement of Reactive and Stable Plasma Chemistry Products in the Effluent of a He/H2O Atmospheric Plasma." *Journal of Physics D: Applied Physics*, vol. 50, no. 33, 2017, p. 335204.

ACKNOWLEDGEMENT

31st SUMMER SCHOOL AND INTERNATIONAL
SYMPOSIUM ON THE PHYSICS OF IONIZED GASES

is organized by

University of Belgrade – School of Electrical Engineering

University of Belgrade – Faculty of Physics

Serbian Academy of Sciences and Arts

University of Belgrade,
School of Electrical Engineering

University of Belgrade,
Faculty of Physics

Serbian Academy
of Sciences and Arts

and

with the support of the

**Ministry of Education, Science and Technological Development,
Republic of Serbia**

Republic of Serbia
Ministry of Education,
Science and Technological
Development

sponsored by

EPJ D
Atomic, Molecular,
Optical and Plasma
Physics

SOLEIL
SYNCHROTRON

RoentDek
Handels GmbH
Supersonic Gas Jets
Detection Techniques
Data Acquisition Systems
Multifragment Imaging Systems

SPECS™

technical organizer

PANACOMP - Zemlja čuda d.o.o.